Multi-scale identification of composite materials

Shaojuan Huang

Par **Shaojuan HUANG**

Multi-scale identification of composite materials

Thèse présentée
pour l'obtention du grade
de Docteur de l'UTC

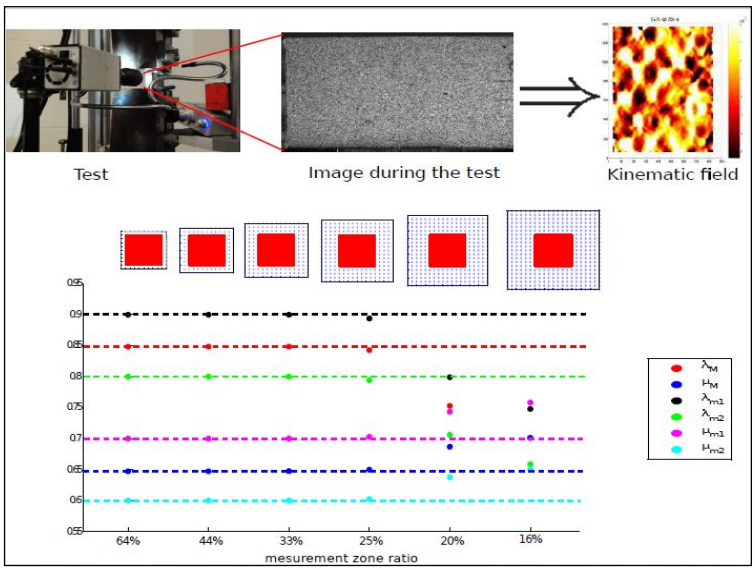

Soutenue le 4 janvier 2016
Spécialité : Mécanique Avancée : Unité de recherche en Mécanique - Laboratoire Roberval (UMR-7337)

D2244

Multi-scale identification of composite materials

Shaojuan HUANG

Spécialité : Mécanique Avancée

Thesis defended on the before the jury :

Reviewers :

Eric FLORENTIN	*Jean-Noël PERIE*
Professeur	Maître de conférences (HDR)
INSA Centre Val de Loire	Institut Clément Ader

Examiners :

Olivier ALLIX	*Franck DELVARE*	*Zoheir ABOURA*
Professeur	Professeur	Professeur
ENS de Cachan	Université de Caen	Université de Technologie de Compiègne

Supervisors :

Pierre VILLON	*Pierre FEISSEL*
Professeur	Maître de conférences (HDR)
Université de Technologie de Compiègne	Université de Technologie de Compiègne

---

Sorbonne Universités

Université de Technologie de Compiègne

Laboratoire Roberval UMR CNRS 7337

04 - 01 - 2016

Abstract

Composite materials are more and more important in the industry community. For the identification of the heterogeneous and anisotropic mechanical behavior of some composite, the full-field measurements are widespread in the mechanics community, because they can offer a very rich information of displacement or strain to exploit heterogeneous tests. During last thirty years, some specific inverse identification strategies have been proposed but most of these methods consider the identification problem only on the measured area and would usually need boundary conditions to be performed. However, the boundary conditions are not always completely known and might not be on the measurement zone. There is hence a need of identification methods allowing both the identification over the whole specimen and the dealing of missing boundary conditions. The Modified Constitutive Relation Error (M-CRE) allows dealing with such situations through the taking into account of the whole available information from a theoretical and experimental point of view without additional assumption.

For the identification of elastic properties, a first mono-scale strategy has been proposed and actually used to process different types of boundary conditions as well as their absence. Considering the identification of heterogeneous elastic properties, the lack of information outside the measurement zone prevents from identifying heterogeneous properties in this area. It leads us to propose a multi-scale approach where micro heterogeneous properties are sought at the measurement level and macro homogeneous ones at the specimen level.

Key Words : *Inverse identification, Modified Constitutive Relation Error, Multi-scale, Composites.*

Resumé

Les matériaux composites sont de plus en plus important dans la communauté de l'industrie. Pour l'identification du comportement mécanique anisotrope et hétérogène de certains composite, les mesures de champs cinématiques sont répandues dans la communauté mécanique, parce qu'elles offrent de riches informations en déplacement ou déformation permettant d'exploiter des essais hétérogènes. Dans les dernières années, certaines identification inverses spécifiques ont été proposées, mais certains de ces méthodes ne considèrent le problème d'identification que sur la zone de mesure ou ont généralement besoin de conditions limites pour être mises en oeuvre. Cependant, mener l'identification sur l'ensemble de l'éprouvette (au-delà de la zone de mesure) offre la possibilité de tenir compte d'information de conditions limites supplémentaire, même si dans le même temps, cela amène à traiter d'autres bords sous conditions limites. L'Erreur en Relation de Comportement Modifiée (ERC-M) permet de traiter ce type de cas en prendant en compte l'ensemble des informations disponibles d'un point de vue théorique et expérimental sans hypothèse supplémentaire.

Pour l'identification des propriétés élastiques, une première stratégie mono-échelle a été proposée et permet effectivement de traiter les differents types de conditions limites ainsi que leur absence. Pour un matériau hétérogène, les mesures ne sont pas assez riches pour permettre l'identification des propriétés élastiques hétérogènes en dehors de la zone de mesure. Une approche multi-échelle est donc proposée permettant de tenir compte de toute l'éprouvette, dans laquelle des propriétes micros hétérogènes sont recherchées sur la zone de mesure et des propriétes macros homogènes sur l'ensemble du domaine.

Mots Clés : *Identification inverse, Erreur en Relation de Comportement Modifiée, Multi-échelle, Composites.*

Contents

List of figures

List of tables

Introduction

Contents

1.1 Background and Purpose

Composite materials have been used since several hundred years before Christ. Not only natural composites are used directly, like wood, bamboo, organic materials, tissue and minerals, but also man-made composites are applied, for example, ancient Pharaohs made their slaves use bricks with straw to enhance the structural integrity of their buildings. During the last few decades, new composites have rapidly spread from glass fiber for automobile bodies to more specific composites for aerospace and a range of other applications. The main impetus for the growth of composite materials is that the properties are superior to those of the individual components in some specific respects. Sometimes, in order to introduce the high stiffness and strength in some direction where it is really required, we need highly anisotropic and heterogeneous composites. Moreover, composites can form the heterogeneous structures which meet the requirements of specific design and function. Thus, composite materials enter more and more into the composition of mechanical parts, and they are now used for critical structures parts (e.g., A350, wind turbine blade, lifeboat, automotive, etc.), so they require efficient and effective methodology for characterization. Therefore, their characterization takes a great deal of interest in the mechanics community.

In the field of materials characterization, experimental tests are necessary in three main aspects: validate the theoretical behavior models; explore the material response under various stress states; detect the material response in critical operating ranges. In practice, most of the mechanical parts are subjected to heterogeneous stress fields during their life cycle. Firstly, they may be subjected to a complex

loading. Secondly, it may be introduced by their geometry, necessary for the assembly of a structure. Such complex heterogeneous loadings or geometries will introduce many difficulties in the characterization process. For example, in the simple case of static, not only will there be the stress concentration phenomena, but also the knowledge of stress distribution will be imperfect. It is therefore necessary to improve knowledge of these composite materials, in particular under the service loading status.

We should note that "heterogeneity" of certain materials will depend on the desired scale of observation and is more pronounced when the scale decreases. In the specific conditions of use, we would like to identify the property fields which reflect the space-dependent appearance of these materials, rather than the homogenized modules. The need to access to detailed data stimulates the use of appropriate measurement means and the development of suitable characterization techniques. This is the case of contact-less tracking technologies, such as full-field measurements [5], which open up new prospects for the identification of mechanical properties.

Taking advantage of full-field measurements, it also implies to develop or adapt new identification strategies. The overall goal is to optimally exploit a large amount of measurement data to identify constitutive parameters. Such approach is often referred as inverse approach. Some specific methods of inverse approach dedicated to full-field measurements have been proposed during the last thirty years [42], but most of these methods consider the identification problem only on the measured area or would usually need boundary conditions to be performed. However, the boundary conditions are not always completely known. Furthermore, even if they are known (e.g. free edge), they might not be on the boundary of the measurement zone. There is hence a need of identification methods allowing both the identification over the whole specimen, and the dealing of missing boundary condition. The Modified Constitutive Relation Error (M-CRE) as proposed in this dissertation is a good method to identify static elastic properties, which allows to deal with such situations through the taking into account of the whole available information from a theoretical and experimental point of view.

Furthermore, considering the identification of heterogeneous elastic properties, the lack of information outside the measurement zone prevents from identifying heterogeneous properties in this area. However, in the usual experiment cases, the measurement zone is only a sub-part of the specimen. If we use the mono-scale approach, we can only identify the local heterogeneous properties of the measurement zone. It is obvious that the scale of description of behavior needs to be compatible not only with the measurement means, but also with the computing means. Hence, a multi-scale approach is proposed to account for any specimen where

micro heterogeneous properties are sought at the measurement level and macro homogeneous ones at the specimen level. The M-CRE is a suitable framework to achieve such a multi-scale identification.

1.2 Structure

The work is presented according to the following organization:

- The second chapter presents the general context of the study. The significance of our work is explained by introducing the need of identification of heterogeneous and anisotropic composite materials. Various full-field measurements techniques and inverse approaches for identification are presented and compared to illustrate the reasons for selecting M-CRE.
- An identification strategy is introduced in the third chapter, which is dedicated to full-field displacement measurements based on the M-CRE developed in our work. A theoretical presentation of the mono-scale approach in the context of static elasticity is explained in detail. The formulations with various boundary conditions are also presented.
- In the forth chapter, the mono-scale approach is tested and validated on different numerical examples with disturbed measurements. The illustrating examples also show how to balance between the various possible experimental information so that the inverse problem is well-posed. The results confirm the effectiveness and robustness of the proposed strategy.
- The fifth chapter introduces a multi-scale identification strategy based on the M-CRE. Two coupling schemes are proposed to combine the displacement and stress fields at both the micro and the macro scales. The details of how to identify the global homogeneous properties of the whole specimen and the local heterogeneous properties of the sub-part measurement zone are discussed in this chapter.
- Some numerical applications of the multi-scale approach are presented in the sixth chapter. Two steps of validation of this method are clearly illustrated by the examples. Different types of loading experiments are considered to show the wide use of our method.
- Some conclusions are given in the seventh chapter.

Identification of composite materials

Contents

2.1 Definition and classification of composite materials

Composite material is a material made from several different substances in general. However, there is no really adequate definition of a composite material. In order to use in structural applications here, an acceptable composite material should include the following two main points in the definition:

(1) It consists of two or more physically distinct and mechanically separable materials;

(2) The properties are superior to the properties of the individual components, and possibly unique in some specific respects.

The second point provides the main motive power to develop the composite material. For example, fibers have very high strength and modulus but they are usually very brittle. Plastics have low strength but they may be ductile and have considerable resistance to some chemical environments. By combining fibers and plastics, it can produce a new material with a strength and stiffness close to that of the fibers and with the chemical resistance of the plastic. Moreover, it is possible to obtain an ability to absorb energy during deformation or some resistance to crack

propagation [1]. In this example, the fiber is denoted as reinforcement, and the plastic is denoted as matrix.

Composite materials have been classified in many ways depending on the ideas and concepts that need to be identified. One of the common classifications includes three large families: natural composite materials, micro-composite materials and macro-composite engineering products. Since the purpose of our identification is concerned primarily with micro-composite materials, a more relevant classification (Table 2.1) is based on the size, shape, and distribution of the two or more phases in the composite [1].

	Shape	Distribution
(1)	continuous fibers	aligned, random
(2)	short fibers	aligned, random
(3)	particulates	random
(4)	dispersion strengthened with particle size $< 10^{-8}$	random
(5)	lamellar structures	aligned
(6)	skeletal or interpenetrating networks	multi-distribution
(7)	multi-component, fibers, particles	multi-distribution

Table 2.1: Classification of micro-composite materials

There has been a rapid development in the use of fiber reinforced materials in various kinds of applications. For example, for automotive, fiber reinforced materials can be used in body parts, front-end panels, drive shafts, bumpers and so on. Another application is in aircraft, such materials can be used in fuselages, wings, landing gear, helicopter blades and so on. The composite materials described in this dissertation are concerned primarily with fiber reinforced materials.

Material	Density (Mg m^{-3})	Young's modulus (GN m^{-2})	Tensile strength (MN m^{-2})	Specific Young's modulus (N m)/Kg	Specific tensile strength (N m)/g
High strength Al-Zn-Mg alloy	2.80	72	503	25.7	180
Quenched and tempered low alloy steel	7.85	207	2050-600	26.4	261-76
Carbon fiber-epoxy resin unidirectional laminae (V_f=0.60)					
(i) parallel to fibers	1.62	220	1400	135	865
(ii) perpendicular to fibers	1.62	7	38	4.32	23.46
Glass fiber-polyester resin unidirectional laminae (V_f=0.50)					
(i) parallel to fibers	1.93	38	750	19.7	390
(ii) perpendicular to fibers	1.93	10	22	5.18	11.40
Glass fiber-polyester resin planar random fibers (V_f=0.20)	1.55	8.5	110	5.5	71

Table 2.2: Comparison of some typical values of the properties of engineering materials at 20 ^0C (V_f is the volume fraction of fibers) [1]

From Table 2.2, we can find that if fiber reinforced composite materials are compared to the traditional metals, they do not have a clear advantage on the

basis of strength and stiffness alone. Their main advantages are considered on the modulus per unit weight (specific modulus) and the strength per unit weight (specific strength). The higher specific modulus and specific strength means that the weight of components can be reduced. Reduction of weight means greater efficiency and energy saving. That is why the rapid growth of composite materials application focuses on the moving components, especially in all forms of transport.

On the other hand, Table 2.2 shows that there is a great difference of properties between different fiber directions (parallel or perpendicular). Since some of the fiber reinforced composite materials are highly anisotropic and heterogeneous, it may be either a serious limitation in some application, or a source of outstanding advantages, because it can introduce a product in specific direction where the high stiffness and strength is really required.

From the above remarks, the properties of composite materials are very complex. The components own properties, the volume fractions of components, the directions of reinforcement, the interfaces properties and the manufacturing route and processes have their effects on the final properties of composite materials because of the microstructure and internal stress. In order to apply the composite materials to engineering and structural products, it is very important to identify their final properties.

2.2 Measurement and identification

2.2.1 Conventional techniques

Because the composite materials properties depend on many factors, it is generally difficult to find these exact properties in tables or databases. Sometimes reasonable values can be found using micro-mechanical models or using the data given by composite materials suppliers, but generally the safest way to establish the properties is to measure them experimentally on test specimens [2]. This is more challenging for fiber reinforced materials because unlike homogeneous (independent of position) and isotropic (the same in every direction) metals and ceramics the material properties change from specimen to specimen. Heterogeneous and anisotropic properties of composite materials add another difficulty in the measurement technique, since heterogeneity and anisotropy increase the number of independent material constants.

For the anisotropic elastic properties, a mature laminate theory has been developed. This theory is used to calculate the elastic properties of laminates from the properties, orientation and distribution of individual laminae. Full descriptions

of this theory can be found in many books. One of the most straightforward accounts is given by R.M. Jones [3] which makes extensive use of an earlier book by Ashton, Halpin and Petit [4]. It is useful for the simple case of composite laminates, such as unidirectional lamina. However, the calculation becomes more complex and time-consuming with complex-directional laminates. Another limitation is the assumption of homogeneity. Only the averaged apparent mechanical properties are obtained.

In the other conventional technique using strain gauge, the unknown parameters are provided directly by a simple relationship between applied load and local strain measurements. However, it is difficult to acquire such pure states of stress and strain in composite materials due to their anisotropy and heterogeneity at different scales. On the other side, the final mechanical properties of composite are effected by the manufacturing conditions, but we cannot take out test samples from large industrial structures. These are the reasons why an increasing interest is found in methods which allow the identification of constitutive parameters from heterogeneous stress/strain fields. There are two main problems: firstly, how to get rich measurement information, and secondly, how to treat the indirect relationship between rich measurement information and unknown parameters. The solutions of these two problems are introduced and described in the following sections.

2.2.2 Full-field measurements

In the middle of the 20^{th} century, experimental methods in solid mechanics focused on point-wise measurements for quantitative data. The lack of information between measurement points, led to a measured response representing an averaged overall material response. In this case, the identification of the material behavior was usually limited to homogeneous materials undergoing uniform strain or at least well controlled strain. In the late 20^{th} century, the development of full-field measurements, a field record of a quantity (displacement, strain, density, temperature), offered a rich information allowing to take into consideration heterogeneous tests in terms of stress for the characterization of material behavior. The source of heterogeneity of the test can come from the material itself, the geometry of the specimen or the loading. Since the features of composites are heterogeneous at different scales, full-field measurements are very attractive to composites material characterization.

Grédiac reviews different kinds of full-field techniques which are proposed and used in composite material characterization in [5]. Most of the techniques are for displacement field measurements. Here, two main categories are introduced: (1)

Non-interferometric methods—the measurand is encoded in the spatial variation of light intensity, for example, speckle [6], grid method [7] and image correlation [8]); (2) Interferometric methods—the nature of interference is a beat phenomenon between two periodic signals of same frequency, which is useful to obtain phase variation information, such as speckle interferometry [9] and moiré interferometry [10]). The main features and applications are discussed below.

The self interference of many random coherent waves scattered from a rough object surface or propagated through a medium of random refractive index fluctuations results in a granular structure known as speckle pattern [11]. Speckle patterns carry information about the surface under investigation, because the position and the irradiance of pattern will be changed when the surface undergoes changes. We call the technique which monitors the positional changes of the speckle patterns as speckle photography. The attractiveness of speckle photography lies in the ability to measure large and out-of-plane displacements [5], and also in the simplicity of the optical setups. However, it needs coherent light produced by laser or specific optical device, which requires highly stable environment.

The grid method has a very simple basic principle [12]: a geometric grid is affixed to a substrate, and the local displacements will modulate the phase of the grid acting as a periodic carrier. It is useful to measure the in-plane displacement. This particular techniques is relatively easy to implement and the quality of phase detection algorithms provides an excellent measurement resolution [13]. Its main drawback is the required surface preparation.

Compared to speckle photography, when the deformations are smaller than the speckle size, speckle interferometry is a suitable measurement technique. Speckle interferometry can be defined as the set of techniques that aim to create, record and take advantage of a two-beam interference pattern involving at least one speckle wave [14]. The displacement field is obtained by correlation of two speckle patterns: before and after object displacement. Neither grating nor smooth surface are necessary, because this method needs surface to scatter light. The advantage of speckle interferometry is the increase of sensitivity. However, due to its high sensitivity, the method is susceptible to environmental disturbances.

Geometric moiré is an effect superimposed over the grid technique, modifying the spectral information delivered by the technique. It is the nonlinear effect of beating between two patterns whose spatial frequencies are close to each other [15]. Based on the same physical phenomenon as the above geometric moiré, moiré interferometry can observe much greater grating frequency, so that the moiré method is extended to submicron level [10]. Moiré interferometry can also measure out-of-plane displacement [16].

However, all of the above methods have two major limitation [17]: firstly, they have varying stability requirements, especially limit the interferometric methods applicability to research environments; secondly, the data processing required to reduce the fringe patterns and thereby obtain the desired data is laborious and time consuming for the above methods. At the same time, the rapid growth of computer technology that spurred continued growth of computational methods also provided the foundation for the explosion of growth in vision-based full-field experimental measurement method. Digital image correlation (DIC), which appeared in the early 1980s [18][19], is one of the new vision-based full-field measurement. The details of DIC are discussed in the following section.

2.2.3 Digital Image Correlation

Different from the above methods, DIC is popular thanks to its relative simplicity: (1) Neither laser nor specific optical device are required, because it use incoherent white light; (2) It is rather simple to prepare the surface of the specimen; (3) By matching different zones of two images captured before and after loading, the displacements are easily obtained. This straightforward measurement method is well suited to analyze the specific mechanical properties of composite materials because of their anisotropic and heterogeneous nature.

In the early 1980s, Peter and Ranson started the correlation method of digital images. They proposed an approach for conversion of digitized ultra-sound images into estimates for local surface displacements by employing continuum-based matching principles [20]. In the following years, several improvements have been made, such as, the sub-pixel detection algorithm based on interpolation of the movement [8], and non-linear least squares approaches using first-order gradients in a matching function to obtain local displacements. Later, Chu presented several experiments to demonstrate the viability of the correlation method in experimental mechanics [17]. He used a DAGE MTI analog camera to record images of a speckle pattern and demonstrated conclusively that the method could be used to measure deformations. In order to extend the DIC technique to calculate the displacement gradient terms, Bruck developed a method which can determine displacements and gradients using the Newton-Raphson method of partial corrections [21]. More and more applications of DIC were proposed, for instant, Chen combined the Fast Fourier Transform (FFT) to determine the movements proved fast and accurate for small planar deformation [22]. On the other hand, for the analysis of very large deformations, Hild presented the work of an evolution of image processing by the correlation analysis using a new multi-scale approach [23]. At the same time, the

vision system of DIC has been developed to stereo-vision system. Luo verified the ability of stereo-vision system to make local strain and deformation measurements in cracked material [24]. Three years later, Helm demonstrated a robust stereo-vision system could be used on full-scale aero-structures as well as on laboratory-scale specimens [25]. Finally, Bay extended 2D and 3D methods to volumetric images. He performed DIC on volumetric elements on the interior of a material [26].

The general scheme of DIC is that a video camera observes an object and the image is digitized and sent to a computer. Within the computer, numerical schemes utilize the basic theory of deformation as a mapping [8]. There are three main kinds of DIC: 2D-DIC [27, 28] and planar loading and surfaces, 3D-DIC for general motion and deformation of curved or planar surface [29], and V-DIC or Digital Volume Correlation for interior deformation measurements in opaque solids [30].

Here, we only introduce the basic concepts of 2D-DIC. After simple surface preparation, the specimen has a random pattern on its surface. A single Charge-Coupled Device (CCD) camera is positioned perpendicular to object surface during the mechanical test, and records the undeformed image and deformed images. Full-field displacement data is obtained by using the subset-based approach: match small subsets of an undeformed image to locations in an image of the surface after deformation. 2D-DIC has several advantages [31]: it is relatively simple to use under both laboratory and field conditions; data acquisition and data analysis procedures are well established; since data analyzed at least 15000 subsets per second, it is near real time analysis; variability are commonly obtained less than 0.01 pixels in displacement on a point-to-point basis.

With development of 2D-DIC, several variants of approaches are divided into "local" approaches and "global" approaches. In traditional local image correlation techniques, the transformation is decomposed into a multitude of independent and local transformations, or shape functions, which parameterized by the coefficients of their local expansion near centers and used in the neighborhood of these centers [32]. Conversely, in a global approach, it is possible to choose a continuous transformation basis, which can be defined over the whole ROI. One of the reasons investigators opted to link full-field measurements with numerical simulations was to make the comparisons easier, possibly seamless, for identification and validation purposes [33]. For example, one of the limitation of local approaches comes from the assumption that the displacement field is continuous [34]. It means that discontinuity can lead to large errors in determining the displacement. However, for the global approaches, specific finite element can then be considered with enriched kinematics, as in the extended finite element method (X-FEM) framework [35] to add discontinuities to a given mesh. Finally, the fact that discretization of the displacement field are shared

with numerical modeling makes the coupling direct and seamless between image correlation.

2.3 Inverse approach of identification

2.3.1 Inverse approach

The previous sections show that full-field measurements can offer rich measurement information, a key point is then to develop or adapt identification strategies based on full field measurements. The overall goal is to optimally exploit a large amount of measurement data to identify constitutive parameters. In particular, the goal is to estimate as many parameters as possible using as few experiments as possible. Such approach is often referred as *inverse approach* in the literature. It is compared with *direct approach* (Figure 2.1) which is the determination of output response (stress, strain, displacement, etc.) when the input excitation (forces, initial stress, sources, etc.) and the system (geometry, constitutive equations, physical characteristics, kinematic constraints, etc.) are known. The *inverse approach* usually corresponds to situation where the system is at least partially unknown because of incomplete available information such as the geometry of the system, constitutive materials and initial conditions. To compensate for, and reconstruct, the missing information on the system parameters, supplementary (possibly partial) information about the output response must be sought in addition to the known input excitation [36].

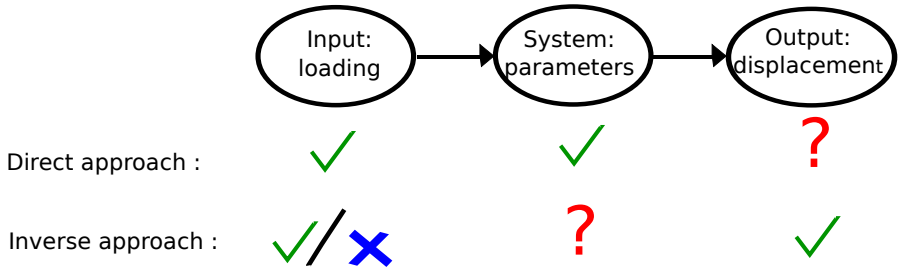

Figure 2.1: Direct approach and inverse approach

Hadamard proposed a definition of well-posed problems [37]: (1) a solution to the problem exists; (2) this solution is unique; (3) the solution depends continuously on data. Inverse problems are often ill-posed in that at least one of the above well-posedness conditions is violated. The origins of ill-posed character are multiple. One of the ill-posed source is the measurement uncertainty, which can cause several solutions or instability of the solution, depending on the nature of the problem. It

means that a weak disturbance of data can lead to a serious disturbance of solution, in other words, the solution is highly sensitive to experimental errors. Another ill-posed source is the indirectly measured boundary condition. If only a global load of boundary is known, the assumption of traction distribution will introduce a modeling error.

In order to solve an ill-posed inverse problem, we must turn it into a well-posed problem. Several regularization methods are possible [38]:

(1) Existence: expand all parameters; reformulate the problem as a minimization problem.

(2) Uniqueness: if several solutions exist: set up a criterion of choice; regularize the problem by adding *prior information* to experimental data [39]; accept the existence of several solutions, and adopt a probabilistic viewpoint to model prior information and various uncertainties by constructing an *a posteriori* probability density function on solution within a Bayesian framework [40].

(3) Continuity with data: reduce the size of the parameter space; add a term of minimization energy for discriminating oscillations, or a term of distance from a reference value to the research physical quantities [41].

However, in the case of using inverse approach to identify the parameters of a model selected *a priori* for its relevance, the parameter identification problems are less sensitive to experimental uncertainties. It means they do not always require regularization.

2.3.2 Inverse approach specifically designed for full-field measurements

Some specific methods designed for full-field measurements have been proposed to extract constitutive parameters in the past years, and a review can be found in [42]. These inverse approaches can be grouped into two large families [38]:

(1) approaches by auxiliary fields: based on the weak form of equilibrium, specific choices for the test field lead to a direct identification of the sought parameters. Among these, we can cite the *Virtual Fields Method (VFM)* [43] and the *Reciprocity Gap Method (RGM)* [44] for full-field data.

(2) approaches by minimization: from the overdetermined set of equation traducing the available information, some equations will be verified exactly through imposed constraints, while the other equations will simply be better verified through the minimization of a gap to these equations. The following methods have been applied to full-field displacement data: the *Finite Element Model Updating method (FEMU)* [45], the *Equilibrium Gap Method (EGM)* [46] and the *Constitutive Relation*

Error method (CRE) [47].

The principles, the advantages and the limitations of the above strategies will be discussed in details below.

2.3.2.1 Virtual Fields Method

This method was first proposed by Grédiac [43] in the framework of static linear anisotropic elasticity. This approach is applicable to situation with experimental availability of the strain field, where the strain field is obtained from full-field measurement (possibly via the approximate differentiation of a measured displacement field). The loading conditions are assumed to be known. The basic idea of VFM consists in writing the global equilibrium of the tested specimen with the principle of virtual work with different and independent virtual fields. This leads to a system of equations in which the constitutive parameters are unknown. The key point is to choose the appropriate virtual fields, because each possible choice of virtual field yields a scalar equation that must be verified by the constitutive model that predicts the stress value for given strain and constitutive parameters [36].

Many applications of the VFM have been studied and some are in various cases of composite materials characterization. For example, in [48] a new approach to the Iosipescu in-plane shear test is presented by using VFM and it is validated by a finite element simulation for different composite materials. The other paper [49] deals with the direct identification of the in-plane elastic properties of orthotropic composite plates (T-shaped specimen) from heterogeneous strain fields. It overcomes the difficulty of no available exact analytical solution for a geometry such as T-shaped specimen. In order to extend the composite applications in naval and ground transportation fields, the thickness of composite is to be increased to fulfill the structural function. Pierron et al. [50] therefore proposed a method based on VFM to determine the four through-thickness stiffnesses of thick laminated composite. There are also other researches about nonlinear model [51] and damage model [52] using VFM.

Its directness is the main advantages of VFM. Moreover, Avril and Pierron [53] showed that the stationarity conditions for cost functional associated with FEMU, CRE or EGM can be interpreted in terms of the virtual fields method for specific suitably chosen virtual fields.

2.3.2.2 Reciprocity Gap Method

The RGM is primarily suitable to the situations where mechanical field measurements are available on the boundary. It relies on a simple idea of *reciprocity*

property: when a solid is subject to two different loads P_1, P_2 and presents two different corresponding responses R_1, R_2, the work of the P_1 load in the R_1 response is equal to the work of the P_2 load in the R_2 response. The reciprocity gap is defined through the reciprocity relation between the actual field in the real solid that provided the measurements and a fictitious solution field in a fictitious solid in the absence of the unknown elements (cracks, inclusions, sources) [54]. Obviously, the property of reciprocity is not verified when comparing the two fields, but the difference of the scalar value will enable the identification of the absence of the unknown elements.

The RGM is introduced by the work of Bui [44], and then used in the work of Andrieux and Abda [55] to determine planar cracks with overspecified boundary data. A series of identification of planar cracks for different families of auxiliary fields has been studied in the following years. For instance, in elastostatics field, [56] identifies 2D cracks by the mean of elastic boundary measurements with the search of the unique zero of the reciprocity gap functional; in elastodynamics field, the work of [57] shows that a unique family of planar shear waves permits the identification of the normal, position and a convex hull of a linear crack through simple interpretations of the instantaneous reciprocity gap; in thermoelasticity field, [58] considers a 3D homogeneous isotropic elastic solid containing a family of planar cracks submitted to a time-dependant thermal loading; in viscoelasticity field, the paper of [59] studies the identification of a planar crack for Zener type linear viscoelastic solids under the condition of low frequency.

The main advantage of RGM is its simplicity. It can be considered as a variation on the VFM where kinematical fields are known only on the boundary. However, there is two limitations of RGM: (1) it is necessity of knowing the measured fields over the complete outer boundary of the body; (2) it applies only to the case of linear behavior laws.

2.3.2.3 Finite Element Model Updating method

Since the finite element method [60] can provide displacement, strain or stress fields in almost any case of specimen geometry, loading conditions and constitutive equations, it is the most popular numerical method for the direct approach. For the inverse problem, the FEMU consists of updating the parameters of a finite element model in order to minimize the difference between measured and simulated fields [61]. Its principle is shown in Figure 2.2 which is presented in [62].

The process can be described by the following steps:

(1) Perform a first calculation with an initial set of constitutive parameters θ^0;

(2) Collect the data from the finite element model prediction, and then compare with the experimental measurement;

(3) Formulate an objective function depending on the sought parameters, and which is often the sum of the square gap between the measured and numerical data;

(4) Implement the optimization method to minimize this objective function;

(5) Stop the procedure when the objective function is lower than a given threshold value and obtain the identified parameters θ.

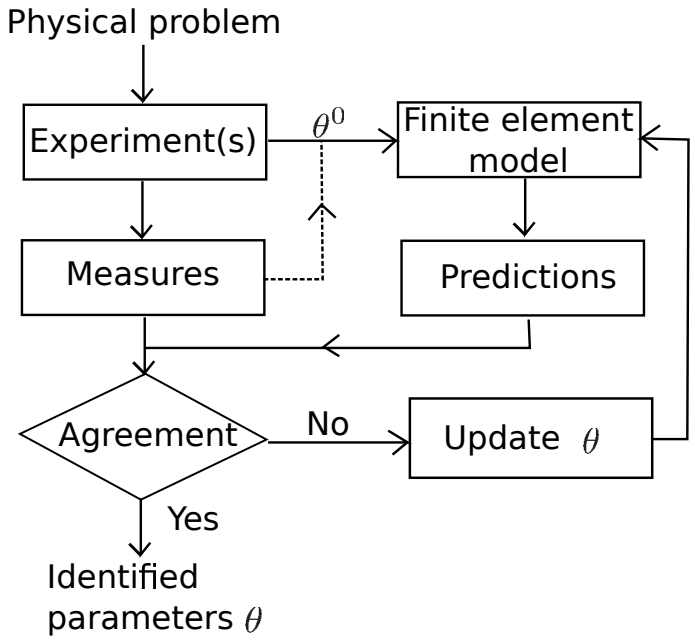

Figure 2.2: Schematic view of FEUM identification [62]

Applications of FEMU to constitutive parameter identification are the subject of many investigations, a detailed presentation of the application on composites follows [63]. There are several examples of identification of the in-plane elastic properties of different kinds of composite, such as eight-ply woven composite laminate [64] and orthotropic composite which is subjected to a biaxial loading [65]. Recently identification of in-situ mechanical parameters has been studied. Kang et al. [66] proposed to identify fiber-matrix interface elastic properties of a metal matrix composite by matching numerical and experimentally observed interface failure modes. Later Wang et al. [67] developed this strategy to identify viscoelastic adhesive interfacial properties. At the same time, other researches focused on the determination of damage constitutive laws by FEMU. Anghileri et al. [68] analyzed the identification of model parameters defining damage and failure mechanisms in composite materials based on a multi-objective optimization. Sztefek and Olsson studied both the tensile stiffness distribution [69] and nonlinear compressive stiffness

[70] in impacted composite laminates determined by FEMU. Leclerc et al. [71] presented a new method to study the elastic properties of composite based Integrated Digital Image Correlation (I-DIC), which conciliated the best of DIC and FEMU. In this method, two stages (image correlation and mechanical identification) are coupled to minimize information losses, while avoiding most of intermediate steps.

Although above approaches have been successfully applied, there are three main drawbacks of FEMU: (1) the computing time since iterative calculations are required; (2) the accuracy of identified parameters with real noisy measured data will greatly depend on the number of local minimal in the objective function [63]; (3) boundary conditions in terms of traction must often be known to perform the calculations [5].

2.3.2.4 Equilibrium Gap Method

The method of Equilibrium Gap aims at allowing for the identification of a distribution of elastic properties and its evolution during the test (damage) based on measured displacement [46]. The basic idea is to find the distributed elastic properties, with fixed displacement measurements, to verify at best the internal balance within the material. Assuming quasi-static conditions and no body forces, the local equilibrium equation could be written as $div\ \sigma[\overline{\varepsilon};\theta] = 0$. At any point of the sample where $\overline{\varepsilon}$ is known, an equality that must be satisfied by any constitutive model predicting σ for known $\overline{\varepsilon}$. Thus, parameters associated with a model, or some spatial distribution of heterogeneous properties, could be identified by enforcing satisfaction of local equilibrium. However, measurement or modeling errors generally implying the unfeasibility of exact equilibrium satisfaction. Instead, it achieves the balance equation by minimizing the local residual stress on the finite element nodes [72].

A first attempt to use full-field data to feed an identification procedure for a damage law has been proposed by Claire et al. [46]. At first, isotropic materials are consisted in formulating the equilibrium gap on the common middle nodes of the adjacent Q8 elements [73]. The method was then extended to other types of elements such as Q4 elements [74] [75]. In the following steps, it is proposed to extend the approach to orthotropic materials. Instead of using the finite element formulation of the problem, [76] uses the finite difference formulation, because this choice is compatible with the way the information is assessed and treated in the usual DIC software. At the same time, Périé et al. [77] proposed a two-step approach to go from DIC to an anisotropic damage law based on biaxial test of composite material.

The EGM has the advantage of being directly applicable as a post-treatment for any displacement field measurement. A specific feature of this method is the

need to solve the balance problem on the measurement area. However, there are two main limitations of EGM: (1) it can be considered as equivalent to the VFM employed with some piecewise particular fields, each of them being defined by a non-zero virtual displacement of one of the mid-side nodes of the mesh, so the EGM has the same limitations as the VFM which need field measurements over domain [42]; (2) considering the EGM based on finite difference implementation, numerical differentiation of sampled data unfortunately often causes signification amplification of the original measurement errors [36]. Hence, the approaches with precondition have been proposed.

2.3.2.5 Constitutive relation error

The CRE measures the distance between a given stress field $\underline{\underline{\sigma}}$ and another stress field computed through a constitutive model from a given displacement field $\underline{u}$. It can be defined by the form of cost function in its simplest form (small-strain hypothesis, equilibrium, linear elastic behavior):

$$\mathcal{J}(\underline{u}, \underline{\underline{\sigma}}, \mathcal{C}) = \frac{1}{2} \int_{\Omega} (\underline{\underline{\sigma}} - \mathcal{C} : \varepsilon(\underline{u})) \mathcal{C}^{-1} (\underline{\underline{\sigma}} - \mathcal{C} : \varepsilon(\underline{u})) d\Omega$$

where the elasticity tensor $\mathcal{C}$ is allowed to be homogeneous or heterogeneous.

This method was proposed by Ladevèze for error estimation in the finite element method in the early 1980s [47]. Its principle is based on the model error detection within the structure. The idea is assumed that the constitutive relation could be inaccurate, which leads to the constitutive relation error. This error can be calculated locally on the structure, which allows us to detect the regions which are not modeled correctly. Almost at the same time, equivalent concepts have been proposed in other contexts for solving inverse problems. For example, the electrostatic energy functional of Kohn-Vogelius [78]. The CRE then turned out to be very useful for model updating in vibration dynamics, based on modal analysis with experimental data on natural frequencies and modal displacements [79], and also adapted to the forced vibration problems [80]. In the late 1990s and early 2000s, the CRE has been theoretically extended to a wide range of problems. For example, it can incorporate either the damping or the non-linearity due to both materials and contacts [81]; it can deal with application of a model reduction method to the updating of models of industrial structures with many degrees of freedom [82]. From 2002, quantitative identification of a behavior model from mechanical test by CRE has been studied [83][84][85]. The method of CRE measures the distance between an admissible stress and an admissible displacement [86]. This distance is quantified by an energy norm, which will be minimized in the identification procedure.

Three important characteristics of CRE are: (1) its strong and clear physical meaning; (2) its additive character with respect to the structure, allowing the definition of local error indicators over substructures [87]; (3) it is in principle applicable to any identification problem where overdetermined data is available, that is which does not specifically require full-field measurements. On the other hand, the CRE framework accommodates full-field measurements in a very natural way [42].

2.3.3 Modified constitutive relation error

Each inverse approach has its own advantage to use in specific application. However, there are two common problems: 1. Not all information is available. For example, in many cases, the full-field measurement is only on a sub-part of the specimen or boundary conditions may be unknown or not completely known. It leads to a lack of information outside the measurement zone or on the boundary of the specimen. Therefore, EGM which needs measurements over the whole domain, and FEMU/RGM which needs boundary conditions to be performed, may have leave apart some of the available information or add supplementary hypothesis (e.g. on boundary conditions). 2. Not all the available information is reliable. For example, there are measurement uncertainties in experimental study and model errors in numerical analysis, which may lead to a loss of accuracy of a FEMU approach.

There is hence a need for identification methods allowing both the identification over the whole specimen, and the dealing of missing boundary condition. **The Modified Constitutive Relation Error (M-CRE)** as proposed here is a suitable method to identify static elastic properties, which allows to deal with such situations through the taking into account of the whole available information from a theoretical and experimental point of view [88]. Its principle consists in dividing the relations which characterize the problem into a reliable set and an uncertain set. The latter is dealt with only approximately throughout the strategy. The M-CRE was first developed for model updating in dynamics [80] [89], and then extended to transient dynamics for linear [90] and non-linear [91] behavior. In this framework, Banerjee et al.[92] presented the formulation and implementation of M-CRE suitable for large-scale inverse identification of linear elastic material properties in the context of steady-state elastodynamics. Considering its application to full-field displacement measurement, it was first proposed in [84], then several works focused on standard CRE [93] [86]. In [94], a M-CRE formulation was proposed, allowing the taking into account of free-edge boundary condition as well as of the lack of boundary condition, while the measurement zone could be a sub-part of the whole domain. A

comparison between the M-CRE and the FEMU methods was performed on some numerical examples where realistic perturbations were added and the result showed that the M-CRE was more robust.

2.4 Multi-scale approach

After choosing the suitable inverse approach, the next key issue is how to achieve multi-scale identification. Various multi-scale strategies for direct approach and inverse approach are separately introduced in the following sections.

2.4.1 Multi-scale strategies for direct approach

There are many multi-scale modeling strategies discussed in the applied mechanics communities for direct approach, which involve models of different nature at different scales. Coupling macro and micro models is aimed to take advantage of both the simplicity and efficiency of the macro models, as well as the accuracy of the micro models. Weinan E et al.[95] presented a review of Heterogeneous Multiscale Methods (HMM) and classify many multi-scale methods in a general setting. The classical multi-scale techniques include Multigrid Method [96], Domain Decomposition [97], Wavelet-based Methods [98], Adaptive Mesh Refinement [99], Fast Multipole Method [100] and Conjugate Gradient Method [101]. They are general purpose solvers for the micro scale problem. Conversely, there are some modern multi-scale techniques focusing on further reducing the computational cost to capture the macro scale behavior of the system, such as Car-Parrinello Method [102], Quasi-continuum Method [103], Optimal Prediction [104], Heterogeneous Multiscale Method [105], Gap-Tooth Scheme [106], Adaptive Model Refinement [107] and FE^2 Approach [108].

Among these multi-scale modeling, two types of coupling are applied: concurrent coupling and serial coupling. The former links the micro scale and the macro scale models together as the computation goes on [109], and the latter determines an effective macro scale model from the micro scale model in a pre-processing step and use the resulted macro scale model in further applications. Yet, two types of coupling can be combined to yield optimal efficiency: the results of a concurrent simulation can be used to suggest the functional form for the constitutive relation, which can then be used in a serial coupling method.

2.4.2 Multi-scale strategies for inverse approach

For the inverse identification problem, besides the previous multi-scale numerical simulation strategies, we also need to consider the multi-scale measurement methods. For example, Johann Rannou et al. proposed a 3D dimensional experimental and numerical multi-scale analysis of a fatigue crack [110]. At first, X-Ray Computed Micro Tomography is used to get 3D pictures of *in situ* test for the morphology of cracked surface. And then Digital Volume Correlation is applied to measure macro displacement fields of cracked samples. In a third step, the combination of the two previous measurement is completed with a level-set modeling and multi-grid X-FEM simulation to improve the understanding of 3D crack growth laws. Finally the estimation of stress intensity factors is obtained.

Another example for multi-scale identification is developed by Jean-Charles Passieux et al.[111]. A nearfield/ farfield multi-scale approach to FE-DIC is proposed to overcome the tricky and well-known compromise between spatial resolution and uncertainty, because the level of uncertainty associated with the identified parameters depends on the quality of the kinematic measurement. At first, two cameras are used to acquire images with two different image resolutions: farfield images capture the full specimen at the scale of the structure, while nearfield images zoom on a structural detail where the displacement field is particularly sensitive to the identified parameters. Then an automatic and accurate image registration process is proposed to bridge precisely the measurement performed at both scales. In a second step, an inverse multi-scale identification method based on the FEMU is presented. Identification results in [111] show that the multiscale approach greatly improves the uncertainty of both the measured displacement and the identified material parameters.

2.5 Conclusion

In this first chapter, we explained the significance of our work by introducing the need of identification of the heterogeneous and anisotropic composite materials. Several standard identification procedures based on full-field measurements and classical multi-scale approaches were presented. However, the two limitations of measurement/model uncertainty and imperfect boundary conditions are not always discussed and solved by these standard methods. The following study seeks to provide solutions. At first, we will present the identification strategy based on Modified Constitutive Relation Error and the applications of identifying heterogeneous elastic properties on mono-scale. And then, we will propose a multi-

scale identification strategy to solve the more complex problems and validate it through applications.

Mono-scale identification

Contents

3.1 Introduction

This chapter presents the identification strategy based on the principles of the Modified Constitutive Relation Error. The basic idea is to construct mechanical fields and material parameters that are a trade-off between all the available information but with no further hypothesis. It is applied to the identification of elastic properties from DIC data and allows to deal with problems with different kinds of boundary conditions (known or unknown).

3.2 Framework: direct problem and measurements

The identification framework is the one of a mechanical test on a given specimen in order to identify its elastic properties based on DIC data. The specimen is hence modeled as a $2D$ domain Ω, in plane stress. The load is measured over $\partial_f\Omega$ as well as the displacement field on one part of the specimen surface Ω_m (Figure 3.1). We can also assume a part of the edge of the specimen $\partial_d\Omega$ is free of load and the remaining boundary denoted $\partial_\emptyset\Omega$ corresponds to a lack of knowledge on the boundary conditions. The elastic properties of the specimen, collected in the

vector $\underline{\theta}$, can be sought as homogeneous or heterogeneous, isotropic or not. Hence, the sought unknowns are the elastic parameters, but the stress and displacement fields are also unknown and are to be determined in order to get $\underline{\theta}$. This can lead to the following model and equations describing the available information, both experimental and theoretical, verified by the stress $\underline{\underline{\sigma}}$, the displacement $\underline{u}$ and the parameters $\underline{\theta}$:

- On Ω,
  - ◇ Equilibrium: $\underline{div}\ \underline{\underline{\sigma}} = \underline{0}$
  - ◇ Constitutive relation: $\underline{\underline{\sigma}} = \mathcal{C}(\underline{\theta}) : \underline{\underline{\varepsilon}}$
  - ◇ Kinematic compatibility: $\underline{\underline{\varepsilon}} = \frac{1}{2}(\underline{\underline{\nabla}}\ \underline{u} + \underline{\underline{\nabla}}^T \underline{u})$
- On Ω_m,
  - ◇ Displacement measurement: $\underline{u} = \underline{\tilde{u}}$
- On $\partial_d\Omega$,
  - ◇ Free edge boundary condition: $\underline{\underline{\sigma}} \cdot \underline{n} = \underline{0}$
- On $\partial_f\Omega$, two cases can be considered depending on the available data:
  - ◇ Measured traction boundary condition: $\underline{\underline{\sigma}} \cdot \underline{n} = \underline{f}$, on $\partial_f\Omega$

  or
  - ◇ Measured global load F_0 along a given direction $\underline{N}_0$:

    $\int_{\partial\Omega_f} \underline{\underline{\sigma}} \cdot \underline{n} dS \cdot \underline{N}_0 = F_0$
- On $\partial_\emptyset\Omega = \partial\Omega \backslash (\partial_d\Omega \cup \partial_f\Omega)$, unknown boundary condition

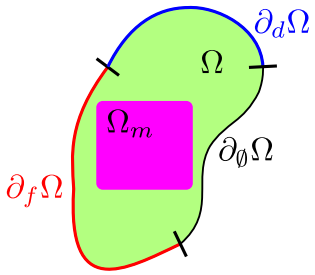

Figure 3.1: Direct problem for mono-scale

3.3 Splitting of the equations

The goal of the identification is to take advantage of the redundant information described by the equations listed in Section 3.2 in order to deduce the material parameters. Since the equations are redundant, they cannot all be verified exactly by $(\underline{u}, \underline{\underline{\sigma}}, \underline{\theta})$ and some of them hence have to be relaxed. In the following, the equations to be relaxed are chosen based on the the principle of the Modified Constitutive Relation Error and will yield the mechanical fields (displacement and stress) and

material properties that are a trade-off of all the available information [82]. The trade-off is built so that the reliable information should be exactly verified and the less reliable information only verified at best by minimizing a functional. To that purpose, the various equations of the identification problem are split into three groups:

- the group of reliable equations: the equilibrium equation and the kinematic compatibility on Ω, the free edge boundary condition on $\partial_d\Omega$;
- the group of less reliable equations: the constitutive relation on Ω (whose parameters are sought), the equality to the measured displacement $\underline{\tilde{u}}$ on Ω_m (with some uncertainties);
- the group of equations whose reliability depends on the study case: the boundary condition of traction distribution or global load on $\partial_f\Omega$.

3.4 Identification strategy

3.4.1 Admissible sets and functionals

In order to identify the properties of the material, the triplet $(\underline{u}, \underline{\underline{\sigma}}, \underline{\theta})$ is sought as the solution of a minimization problem where the reliable equations are considered as constraints and the less reliable equations are defined as a function that is to be minimized. Based on the splitting of the equations proposed in Section 3.3, we therefore introduce:

- the space associated with the constraints on the displacement field:

$$\mathcal{U}_{Ad} = \{\underline{u} \in H^1(\Omega)\} \tag{3.1}$$

- the spaces associated with the possible constraints on the stress field:
  - ◇ equilibrium and free edge:

$$\mathcal{S}^0_{Ad} = \{\underline{\underline{\sigma}} \in H_{div}(\Omega)/\underline{div}\ \underline{\underline{\sigma}} = \underline{0}\ on\ \Omega, \underline{\underline{\sigma}} \cdot \underline{n} = \underline{0}\ on\ \partial_d\Omega\} \tag{3.2}$$

  - ◇ traction distribution on $\partial_f\Omega$:

$$\mathcal{S}^f_{Ad} = \{\underline{\underline{\sigma}} \in H_{div}(\Omega)/\ \underline{\underline{\sigma}} \cdot \underline{n} = \underline{f}\ on\ \partial_f\Omega\} \tag{3.3}$$

  - ◇ global load on $\partial_f\Omega$:

$$\mathcal{S}^F_{Ad} = \{\underline{\underline{\sigma}} \in H_{div}(\Omega)/ \int_{\partial_f\Omega} \underline{\underline{\sigma}} \cdot \underline{n}\ dS \cdot \underline{N}_0 = F_0\} \tag{3.4}$$

- the term of constitutive relation error:

$$\mathcal{J}_1(\underline{u},\underline{\underline{\sigma}},\underline{\theta}) = \frac{1}{2}\int_\Omega (\underline{\underline{\sigma}} - \mathcal{C} : \underline{\underline{\varepsilon}}(\underline{u})) : \mathcal{C}^{-1} : (\underline{\underline{\sigma}} - \mathcal{C} : \underline{\underline{\varepsilon}}(\underline{u}))d\Omega \tag{3.5}$$

- the term of distance to the displacement measurements on Ω_m:

$$\mathcal{J}_2(\underline{u}) = \frac{1}{2}\int_{\Omega_m} ||\underline{u} - \underline{\tilde{u}}||^2 d\Omega_m \tag{3.6}$$

- the term of distance to the traction distribution on $\partial_f\Omega$:

$$\mathcal{J}_3(\underline{\underline{\sigma}}) = \frac{1}{2}\int_{\partial_f\Omega} ||\underline{\underline{\sigma}}\cdot\underline{n} - \underline{f}||^2 dS \tag{3.7}$$

- the term of distance to the global load on $\partial_f\Omega$:

$$\mathcal{J}_4(\underline{\underline{\sigma}}) = \frac{1}{2}(\int_{\partial_f\Omega} \underline{\underline{\sigma}}\cdot\underline{n}\; dS\cdot\underline{N}_0 - F_0)^2 \tag{3.8}$$

Depending on the available data and its reliability, in particular concerning the traction/load, it is possible to propose various identification formulations, as sum up in Table 3.1. For example, in the case of missing load boundary conditions, the first study case with free edge is the basic formulation. If the traction distribution boundary condition is considered as reliable, we complete the admissible fields with the space associated with the constraints on traction distribution, and the functional remains unchanged, leading to the second study case. If this information is considered as less reliable, we keep the same admissible space as for the basic formulation and modify the functional adding the $\mathcal{J}_3$ term. The other cases use the same methodology with respect to the global load.

Table 3.1: Various possible formulations (α and β are positive weighting coefficients)

Study case	Constraints	Functional
$\partial_f\Omega = \emptyset$	$\mathcal{S}_{Ad} = \mathcal{S}^0_{Ad}$	$\mathcal{J}(\underline{u},\underline{\underline{\sigma}},\underline{\theta}) = \mathcal{J}_1 + \alpha\mathcal{J}_2$
Reliable traction distribution	$\mathcal{S}_{Ad} = \mathcal{S}^0_{Ad} \cap \mathcal{S}^f_{Ad}$	$\mathcal{J}(\underline{u},\underline{\underline{\sigma}},\underline{\theta}) = \mathcal{J}_1 + \alpha\mathcal{J}_2$
Less reliable traction distribution	$\mathcal{S}_{Ad} = \mathcal{S}^0_{Ad}$	$\mathcal{J}(\underline{u},\underline{\underline{\sigma}},\underline{\theta}) = \mathcal{J}_1 + \alpha\mathcal{J}_2 + \beta\mathcal{J}_3$
Reliable global load	$\mathcal{S}_{Ad} = \mathcal{S}^0_{Ad} \cap \mathcal{S}^F_{Ad}$	$\mathcal{J}(\underline{u},\underline{\underline{\sigma}},\underline{\theta}) = \mathcal{J}_1 + \alpha\mathcal{J}_2$
Less reliable global load	$\mathcal{S}_{Ad} = \mathcal{S}^0_{Ad}$	$\mathcal{J}(\underline{u},\underline{\underline{\sigma}},\underline{\theta}) = \mathcal{J}_1 + \alpha\mathcal{J}_2 + \beta\mathcal{J}_4$

3.4.2 The identification problem

We can deduce the definition of the identification problem as the following:

Find the fields $(\underline{u}, \underline{\underline{\sigma}}) \in \mathcal{U}_{Ad} \times \mathcal{S}_{Ad}$ and the parameters $\underline{\theta} \in \Theta_{Ad}$ minimizing $\mathcal{J}(\underline{u}, \underline{\underline{\sigma}}, \underline{\theta})$:

$$\min_{(\underline{u},\underline{\underline{\sigma}},\underline{\theta}) \in \mathcal{U}_{Ad} \times \mathcal{S}_{Ad} \times \Theta_{Ad}} \mathcal{J}(\underline{u}, \underline{\underline{\sigma}}, \underline{\theta}) \tag{3.9}$$

where Θ_{Ad} is the admissible space of parameters.

In practice, the minimization is split into a sequential minimization:

$$\min_{\underline{\theta} \in \Theta_{Ad}} \min_{(\underline{u},\underline{\underline{\sigma}}) \in \mathcal{U}_{Ad} \times \mathcal{S}_{Ad}} \mathcal{J}(\underline{u}, \underline{\underline{\sigma}}, \underline{\theta}) \tag{3.10}$$

defining two steps:

- For a given $\underline{\theta}$, find $(\underline{u}, \underline{\underline{\sigma}})$ minimizing $\mathcal{J}(\underline{u}, \underline{\underline{\sigma}}, \underline{\theta})$ under the above constraints:

$$\min_{(\underline{u},\underline{\underline{\sigma}}) \in \mathcal{U}_{Ad} \times \mathcal{S}_{Ad}} \mathcal{J}(\underline{u}, \underline{\underline{\sigma}}, \underline{\theta}) \tag{3.11}$$

  This defines the basic problem that yields the mechanical fields that are a trade-off of all the information for a given set of material parameters [94]. The solution of the basic problem is denoted $(\underline{u}(\underline{\theta}), \underline{\underline{\sigma}}(\underline{\theta}))$.

- Then, defining the cost function: $\mathcal{G}(\underline{\theta}) = \mathcal{J}(\underline{u}(\underline{\theta}), \underline{\underline{\sigma}}(\underline{\theta}), \underline{\theta})$, the identification of $\underline{\theta}$ is performed as the minimization of $\mathcal{G}(\underline{\theta})$:

$$\underline{\theta}^{opt} = \mathrm{Arg}\min_{\underline{\theta}} \mathcal{G}(\underline{\theta}) = \mathrm{Arg}\min_{\underline{\theta}} \mathcal{J}(\underline{u}(\underline{\theta}), \underline{\underline{\sigma}}(\underline{\theta}), \underline{\theta}) \tag{3.12}$$

Hence each evaluation of $\mathcal{G}$ in the identification process, requires the solving of the basic problem for a given set of material parameters.

3.5 The basic problem and its solution

3.5.1 Discretization of the basic problem

The basic problem is solved based on a displacement finite element formulation. Therefore, we introduce the displacement field $\underline{v}$ such that:

$$\underline{\underline{\sigma}} = \underline{\underline{\sigma}}(\underline{v}) \ with, \ \underline{\underline{\sigma}}(\underline{v}) = \mathcal{C} : \underline{\underline{\varepsilon}}(\underline{v}) \tag{3.13}$$

It is shown in [80, 88] in dynamics that such a displacement field exists for the solution of the basic problem, and in [94] for full-field data in statics. Adding boundary condition does not change this result.

Using a displacement formulation means that the stress field is statically admissible only in a finite element manner. This seems acceptable because we consider that compared to the model errors, the discretization errors should remain negligible.

It means that the basic problem is rewritten in terms of displacement and becomes:

Find, for a given $\underline{\theta}$, $(\underline{u}, \underline{v})$ such that:

$$\min_{(\underline{u},\underline{v})\in H^1(\Omega)^2, \underline{\underline{\sigma}}(\underline{v})\in\mathcal{S}_{Ad}} \mathcal{J}(\underline{u}, \underline{\underline{\sigma}}(\underline{v}), \underline{\theta}) \tag{3.14}$$

The displacement fields are given in the finite element form:

$$\begin{bmatrix} u_x(\underline{x}) \\ u_y(\underline{x}) \end{bmatrix} = [\Phi(\underline{x})]U, \qquad \begin{bmatrix} v_x(\underline{x}) \\ v_y(\underline{x}) \end{bmatrix} = [\Phi(\underline{x})]V \tag{3.15}$$

where $[\Phi(\underline{x})]$ is the matrix of shape functions, U and V are the vectors of nodal unknowns associated with the displacement fields $\underline{u}$ and $\underline{v}$.

The stress and strain fields are rewritten in a vectorial manner and $\mathcal{C}$ in a matrix one, so that:

$$\underline{\sigma} = [\mathcal{C}]\underline{\varepsilon} \tag{3.16}$$

and the corresponding finite element description:

$$\underline{\varepsilon}(\underline{u}) = [\mathcal{B}]U, \qquad \underline{\varepsilon}(\underline{v}) = [\mathcal{B}]V \tag{3.17}$$

where $[\mathcal{B}]$ is the matrix of the shape function derivatives.

Then the stiffness matrix is deduced from the weak formulation of equilibrium, taking into account Equation (3.17) in the following integral:

$$\begin{aligned} \int_\Omega \underline{\sigma}^T \underline{\varepsilon}(\underline{u}^*) d\Omega &= \int_\Omega \underline{\varepsilon}(\underline{v})^T [\mathcal{C}] \underline{\varepsilon}(\underline{u}^*) d\Omega \\ &= \int_\Omega V^T [\mathcal{B}]^T [\mathcal{C}] [\mathcal{B}] U^* d\Omega \\ &= V^T \int_\Omega [\mathcal{B}]^T [\mathcal{C}] [\mathcal{B}] d\Omega \; U^* \\ &= V^T K U^* \end{aligned} \tag{3.18}$$

where $K = \int_\Omega [\mathcal{B}]^T [\mathcal{C}][\mathcal{B}] d\Omega$ is the global stiffness matrix of the mechanical problem on Ω.

The functions introduced in a continuous manner (Section 3.4.1) are thus discretized as follows:

- the term of constitutive relation error:

$$\mathcal{J}_1(U, V, \underline{\theta}) = \frac{1}{2}(U - V)^T K (U - V) \tag{3.19}$$

- the term of distance to the displacement measurements:

$$\mathcal{J}_2(U) = \frac{1}{2}(\Pi U - \widetilde{U})^T (\Pi U - \widetilde{U}) \tag{3.20}$$

  where $\widetilde{U}$ is the displacement vector comprising the data on the grid of measurement points available on Ω_m, and Π is a discrete transfer operator. There are two functions of Π: 1. extracting the adequate dofs from U, defined on the whole domain Ω, to fit the measurements zone Ω_m; 2. projecting the extracted dofs from the finite element mesh to the data grid based on the FE shape functions [94]. In the experimental measurements, the measurement grid and the finite element mesh may be different. The transfer operator Π is then used to project the mechanical fields of the mesh to the measurement grid. We can note this is not the exact discretization of the continuous term $\mathcal{J}_2$, but it takes into account the discrete nature of the data, which is rich enough to consider continuous data in the continuous formulation.

Then, the equations associated with the admissible sets (minimization constraints) are also discretized based on the weak form of the equilibrium by choosing specific test fields.

$$\int_\Omega \underline{\underline{\sigma}} : \underline{\underline{\varepsilon}}(\underline{u}^*) d\Omega = \int_{\partial\Omega} \underline{\underline{\sigma}} \cdot \underline{n} \cdot \underline{u}^* dS, \ \forall \underline{u}^* \in H^1(\Omega) \tag{3.21}$$

The left hand side term of Equation (3.21) could be written from Equation (3.18) as:

$$\int_\Omega \underline{\underline{\sigma}} : \underline{\underline{\varepsilon}}(\underline{u}^*) d\Omega = U^{*T} K V \tag{3.22}$$

Let us note the index of internal nodes i, the index of free edge nodes d, the index of forced edge nodes f and the index of all nodes $\circ$.

- equilibrium equation on Ω, taking into account finite elements $\underline{u}^*$ which are null on $\partial\Omega$. Hence, the $U^{*T}K$ in Equation (3.22) could be expressed as the

matrix of remaining lines corresponding to the internal nodes $K_{i\circ}$:

$$K_{i\circ}V = 0 \tag{3.23}$$

- equation associated with free edge on $\partial_d\Omega$, taking into account finite elements $\underline{u}^*$ which are null at the nodes out of $\partial_d\Omega$:

$$K_{d\circ}V = 0 \tag{3.24}$$

- equation associated with traction distribution on $\partial_f\Omega$, taking into account finite elements $\underline{u}^*$ which are null at the nodes out of $\partial_f\Omega$:

$$K_{f\circ}V = \widetilde{F}_f \tag{3.25}$$

where $\widetilde{F}_f$ is the vector of the generalized load at the nodes of $\partial_f\Omega$ associated with traction measurements. In the case of less reliable traction distribution, we introduce a vector F_f for the unknown boundary condition and we set the term of constraint and the term of the functional as:

$$K_{f\circ}V = F_f \quad and \quad \mathcal{J}_3 = \frac{1}{2}(F_f - \widetilde{F}_f)^T(F_f - \widetilde{F}_f) \tag{3.26}$$

- equation associated with global load on $\partial_f\Omega$, choosing $\underline{u}^* = \underline{N}_0$ on $\partial_f\Omega$ and null elsewhere at the nodes:

$$\int_{\partial\Omega} \underline{\underline{\sigma}} \cdot \underline{n} \cdot \underline{u}^* dS = \int_{\partial_f\Omega} \underline{\underline{\sigma}} \cdot \underline{n} \cdot \underline{N}_0 dS = \widetilde{F}_0 \tag{3.27}$$

The vector of degrees of freedom associated with $\underline{u}^*$ is denoted U_0^* and hence, from Equation (3.21), (3.22) and (3.27), we can deduce:

$$U_0^{*T} K V = \widetilde{F}_0 \tag{3.28}$$

where $\widetilde{F}_0$ is the value of the load measurement on the boundary $\partial_f\Omega$. In the case of less reliable load measurement, we introduce a scalar F_0 corresponding to the global load of the basic problem and we set the term of constraint and the term of the functional as:

$$U_0^{*T} K V = F_0 \quad and \quad \mathcal{J}_4 = \frac{1}{2}(F_0 - \widetilde{F}_0)^2 \tag{3.29}$$

In order to show the basic problem unified for most case, we introduce the index g, collecting index i, d and f. Also, the projector Π_{gf} allows to transfer the vectors of generalized forces F_f to the vectors of generalized forces corresponding with the

Study case	Constraints	Functional
$\partial_f\Omega = \emptyset$	$K_{g\circ}V = 0$	$\mathcal{J}_1(U,V,\underline{\theta}) + \alpha\mathcal{J}_2(U)$
Reliable traction distribution	$K_{g\circ}V = \Pi_{gf}\widetilde{F}_f$	$\mathcal{J}_1(U,V,\underline{\theta}) + \alpha\mathcal{J}_2(U)$
Less reliable traction distribution	$K_{g\circ}V = \Pi_{gf}F_f$	$\mathcal{J}_1(U,V,\underline{\theta}) + \alpha\mathcal{J}_2(U) + \beta\mathcal{J}_3(F_f)$
Reliable global load	$K_{g\circ}V = 0$ and $U_0^{*T}KV = \widetilde{F}_0$	$\mathcal{J}_1(U,V,\underline{\theta}) + \alpha\mathcal{J}_2(U)$
Less reliable global load	$K_{g\circ}V = 0$ and $U_0^{*T}KV = F_0$	$\mathcal{J}_1(U,V,\underline{\theta}) + \alpha\mathcal{J}_2(U) + \beta\mathcal{J}_4(F_0)$

Table 3.2: Various possible formulations of the discrete basic problem

problems on the lines of index g. Table 3.2 presents the discretization of various possible formulations (given for the continuous case in Table 3.1).

3.5.2 Stationarity equations of the basic problem

This basic problem is a quadratic minimization under linear constraints, the optimality conditions of the first order are sufficient. We hence introduce the Lagrange multipliers associated with the equality constraints. In the following, we derive the stationarity equations for the various cases.

3.5.2.1 Case 1: Free edge

The basic problem is:

Find the nodal displacement vectors U,V minimizing:

$$\mathcal{J}(U,V) = \mathcal{J}_1(U,V) + \alpha\mathcal{J}_2(U) \tag{3.30}$$

under the constraint: $K_{g\circ}V = 0$

Introducing a Lagrange multiplier Λ associated with the constraint:

$$\mathcal{L}(U,V,\Lambda) = \mathcal{J}(U,V) + \Lambda^T(K_{g\circ}V) \tag{3.31}$$

The differential of the Lagrangian $d\mathcal{L}$ is expressed:

$$\left\{\begin{array}{lcl} (\frac{\partial\mathcal{L}}{\partial U},\delta U) &=& \delta U^T K(U-V) + \delta U^T\alpha\Pi^T(\Pi U - \widetilde{U}) \\ (\frac{\partial\mathcal{L}}{\partial V},\delta V) &=& \delta V^T K(V-U) + \delta V^T K_{\circ g}\Lambda \\ (\frac{\partial\mathcal{L}}{\partial\Lambda},\delta\Lambda) &=& \delta\Lambda^T K_{g\circ}V \end{array}\right. \tag{3.32}$$

The stationarity system verified by the solution of the basic problem is $d\mathcal{L} = 0$:

$$\begin{cases} K(U-V)+\alpha\Pi^T\Pi U &= \alpha\Pi^T\widetilde{U} \\ K(V-U)+K_{\circ g}\Lambda &= 0 \\ K_{g\circ}V &= 0 \end{cases} \tag{3.33}$$

We introduce $\Lambda_2 = \begin{bmatrix}\Lambda \\ 0\end{bmatrix}$,where Λ has N_g dofs (dofs of nodes with index g) and Λ_2 has N dofs (dofs of all nodes). Noting that:

$$K\Lambda_2 = \begin{bmatrix}K_{gg} & K_{gn} \\ K_{ng} & K_{nn}\end{bmatrix}\begin{bmatrix}\Lambda \\ 0\end{bmatrix} = \begin{bmatrix}K_{gg}\Lambda+0 \\ K_{ng}\Lambda+0\end{bmatrix} = K_{\circ g}\Lambda \tag{3.34}$$

where n is index of the nodes except the internal and free edge nodes.

The second equation from (3.33) can be rewritten as:

$$K(V-U)+K_{\circ g}\Lambda = 0 \Rightarrow K(V-U+\Lambda_2) = 0 \tag{3.35}$$

This equation corresponds to a finite element problem with no load (bulk and edge) nor prescribed displacement. Hence, its solution is a rigid body motion C_R:

$$V-U+\Lambda_2 = C_R \tag{3.36}$$

Choosing $C_R = 0$, we have $V = U - \Lambda_2$. This choice is validated by the fact that any choice of C_R leads to the same value of the cost function $\mathcal{G}(\underline{\theta})$. We can thus get the following equations:

$$\begin{cases} K\Lambda_2+\alpha\Pi^T\Pi U &= \alpha\Pi^T\widetilde{U} \\ K_{g\circ}U - K_{g\circ}\Lambda_2 &= 0 \end{cases} \tag{3.37}$$

And then we replace Λ_2 by Λ:

$$K_{g\circ}\Lambda_2 = \begin{bmatrix}K_{gg} & K_{gn}\end{bmatrix}\begin{bmatrix}\Lambda \\ 0\end{bmatrix} = K_{gg}\Lambda \tag{3.38}$$

$$\begin{cases} \alpha\Pi^T\Pi U+K_{\circ g}\Lambda &= \alpha\Pi^T\widetilde{U} \\ K_{g\circ}U - K_{gg}\Lambda &= 0 \end{cases} \tag{3.39}$$

Finally, we write the equations in a matrix manner which has to be solved numerically:

$$\begin{bmatrix}\alpha\Pi^T\Pi & K_{\circ g} \\ K_{g\circ} & -K_{gg}\end{bmatrix}\begin{bmatrix}U \\ \Lambda\end{bmatrix} = \begin{bmatrix}\alpha\Pi^T\widetilde{U} \\ 0\end{bmatrix} \tag{3.40}$$

The solution of the basic problem (3.33) is denoted $(U_s(\underline{\theta}), V_s(\underline{\theta}), \Lambda_s(\underline{\theta}))$.

3.5.2.2 Case 2: Reliable traction distribution

The basic problem is:

Find the nodal displacement vectors U,V minimizing:

$$\mathcal{J}(U,V) = \mathcal{J}_1(U,V) + \alpha\mathcal{J}_2(U) \tag{3.41}$$

under the constraint: $K_{g\circ}V = \Pi_{gf}\widetilde{F}_f$

Introducing a Lagrange multiplier Λ associated with the constraint:

$$\mathcal{L}(U,V,\Lambda) = \mathcal{J}(U,V) + \Lambda^T(K_{g\circ}V - \Pi_{gf}\widetilde{F}_f) \tag{3.42}$$

The differential of the Lagrangian $d\mathcal{L}$ is expressed:

$$\left\{\begin{array}{lcl} (\frac{\partial\mathcal{L}}{\partial U},\delta U) &=& \delta U^T K(U-V) + \delta U^T\alpha\Pi^T(\Pi U - \widetilde{U}) \\ (\frac{\partial\mathcal{L}}{\partial V},\delta V) &=& \delta V^T K(V-U) + \delta V^T K_{\circ g}\Lambda \\ (\frac{\partial\mathcal{L}}{\partial \Lambda},\delta \Lambda) &=& \delta\Lambda^T K_{g\circ}V - \delta\Lambda^T\Pi_{gf}\widetilde{F}_f \end{array}\right. \tag{3.43}$$

The stationarity system verified by the solution of the basic problem is $d\mathcal{L} = 0$:

$$\left\{\begin{array}{rl} K(U-V) + \alpha\Pi^T\Pi U &= \alpha\Pi^T\widetilde{U} \\ K(V-U) + K_{\circ g}\Lambda &= 0 \\ K_{g\circ}V &= \Pi_{gf}\widetilde{F}_f \end{array}\right. \tag{3.44}$$

After eliminating V by U and Λ as Equation (3.34)-(3.36) in Case 1, Equation (3.44) is denoted as:

$$\left\{\begin{array}{rl} \alpha\Pi^T\Pi U + K_{\circ g}\Lambda &= \alpha\Pi^T\widetilde{U} \\ K_{g\circ}U - K_{gg}\Lambda &= \Pi_{gf}\widetilde{F}_f \end{array}\right. \tag{3.45}$$

Finally, we write the equations in a matrix manner which has to be solved numerically:

$$\begin{bmatrix} \alpha\Pi^T\Pi & K_{\circ g} \\ K_{g\circ} & -K_{gg} \end{bmatrix}\begin{bmatrix} U \\ \Lambda \end{bmatrix} = \begin{bmatrix} \alpha\Pi^T\widetilde{U} \\ \Pi_{gf}\widetilde{F}_f \end{bmatrix} \tag{3.46}$$

The solution of the basic problem (3.44) is denoted $(U_s(\underline{\theta}), V_s(\underline{\theta}), \Lambda_s(\underline{\theta}))$.

3.5.2.3 Case 3: Less reliable traction distribution

The basic problem is:

Find the nodal displacement vectors U,V and generalized load vector F_f minimizing:

$$\mathcal{J}(U,V,F_f) = \mathcal{J}_1(U,V) + \alpha\mathcal{J}_2(U) + \beta\mathcal{J}_3(F_f) \tag{3.47}$$

under the constraint: $K_{g\circ}V = \Pi_{gf}F_f$

Introducing a Lagrange multiplier Λ associated with the constraint:

$$\mathcal{L}(U,V,F_f,\Lambda) = \mathcal{J}(U,V,F_f) + \Lambda^T(K_{g\circ}V - \Pi_{gf}F_f) \tag{3.48}$$

The differential of the Lagrangian $d\mathcal{L}$ is expressed:

$$\left\{\begin{array}{rcl} (\frac{\partial\mathcal{L}}{\partial U},\delta U) &=& \delta U^T K(U-V) + \delta U^T\alpha\Pi^T(\Pi U - \widetilde{U}) \\ (\frac{\partial\mathcal{L}}{\partial V},\delta V) &=& \delta V^T K(V-U) + \delta V^T K_{\circ g}\Lambda \\ (\frac{\partial\mathcal{L}}{\partial F_f},\delta F_f) &=& \delta F_f^T\beta(F_f - \widetilde{F}_f) - \delta F_f^T\Pi_{fg}\Lambda \\ (\frac{\partial\mathcal{L}}{\partial\Lambda},\delta\Lambda) &=& \delta\Lambda^T(K_{g\circ}V - \Pi_{gf}F_f) \end{array}\right. \tag{3.49}$$

The stationarity system verified by the solution of the basic problem is $d\mathcal{L} = 0$:

$$\left\{\begin{array}{rl} K(U-V) + \alpha\Pi^T\Pi U &= \alpha\Pi^T\widetilde{U} \\ K(V-U) + K_{\circ g}\Lambda &= 0 \\ \beta F_f - \Pi_{gf}^T\Lambda &= \beta\widetilde{F}_f \\ K_{g\circ}V - \Pi_{gf}F_f &= 0 \end{array}\right. \tag{3.50}$$

Introducing $\Lambda_2 = \begin{bmatrix}\Lambda\\0\end{bmatrix}$, where Λ has N_g dof, et Λ_2 has N dof, we can write that

$$K\Lambda_2 = \begin{bmatrix}K_{gg} & K_{gn}\\ K_{ng} & K_{nn}\end{bmatrix}\begin{bmatrix}\Lambda\\0\end{bmatrix} = K_{\circ g}\Lambda \tag{3.51}$$

where n is index of the nodes except the internal and forced edge nodes.

The second equation from (3.50) can be rewritten as:

$$K(V-U) + K_{\circ g}\Lambda = 0 \Rightarrow K(V - U + \Lambda_2) = 0 \tag{3.52}$$

This finite element problem corresponding to a free of load problem whose solution can be any rigid body C_R:

$$V - U + \Lambda_2 = C_R \tag{3.53}$$

Choosing $C_R = 0$, we have $V = U - \Lambda_2$, so from the equations (3.50) after eliminating V and F_f, we can get the following equations:

$$\begin{cases} K\Lambda_2 + \alpha\Pi^T\Pi U &= \alpha\Pi^T\widetilde{U} \\ K_{g\circ}U - K_{g\circ}\Lambda_2 &= \Lambda/\beta + \Pi_{gf}\widetilde{F}_f \end{cases} \tag{3.54}$$

And then we replace Λ_2 by Λ:

$$K_{g\circ}\Lambda_2 = \begin{bmatrix} K_{gg} & K_{gn} \end{bmatrix} \begin{bmatrix} \Lambda \\ 0 \end{bmatrix} = K_{gg}\Lambda \tag{3.55}$$

The equations (3.54) can thus be expressed as:

$$\begin{cases} \alpha\Pi^T\Pi U + K_{\circ g}\Lambda &= \alpha\Pi^T\widetilde{U} \\ K_{g\circ}U - K_{gg}\Lambda - \Lambda/\beta &= \Pi_{gf}\widetilde{F}_f \end{cases} \tag{3.56}$$

Finally, we write the equations in a matrix manner which has to be solved numerically:

$$\begin{bmatrix} \alpha\Pi^T\Pi & K_{\circ g} \\ K_{g\circ} & -(K_{gg} + I_d/\beta) \end{bmatrix} \begin{bmatrix} U \\ \Lambda \end{bmatrix} = \begin{bmatrix} \alpha\Pi^T\widetilde{U} \\ \Pi_{gf}\widetilde{F}_f \end{bmatrix} \tag{3.57}$$

The solution of the basic problem (3.50) is denoted $(U_s(\underline{\theta}), V_s(\underline{\theta}), \Lambda_s(\underline{\theta}), F_{fs}(\underline{\theta}))$.

3.5.2.4 Case 4: Reliable global load

The basic problem is:

Find the nodal displacement vectors U,V minimizing:

$$\mathcal{J}(U,V) = \mathcal{J}_1(U,V) + \alpha\mathcal{J}_2(U) \tag{3.58}$$

under the constraint: $K_{g\circ}V = 0$ and $U_0^{*T}KV = \widetilde{F}_0$

Introducing two Lagrange multipliers Λ and M associated with the constraints:

$$\mathcal{L}(U,V,\Lambda,M) = \mathcal{J}(U,V) + \Lambda^T K_{g\circ}V + M^T(U_0^{*T}KV - \widetilde{F}_0) \tag{3.59}$$

The differential of the Lagrangian $d\mathcal{L}$ is expressed:

$$\begin{cases} (\frac{\partial\mathcal{L}}{\partial U}, \delta U) &= \delta U^T K(U-V) + \delta U^T\alpha\Pi^T(\Pi U - \widetilde{U}) \\ (\frac{\partial\mathcal{L}}{\partial V}, \delta V) &= \delta V^T K(V-U) + \delta V^T K_{\circ g}\Lambda + \delta V^T K U_0^* M \\ (\frac{\partial\mathcal{L}}{\partial\Lambda}, \delta\Lambda) &= \delta\Lambda^T K_{g\circ}V \\ (\frac{\partial\mathcal{L}}{\partial M}, \delta M) &= \delta M^T U_0^{*T}KV - \delta M^T\widetilde{F}_0 \end{cases} \tag{3.60}$$

The stationarity system verified by the solution of the basic problem is $d\mathcal{L} = 0$:

$$\begin{cases} K(U-V) + \alpha\Pi^T\Pi U &= \alpha\Pi^T\widetilde{U} \\ K(V-U) + K_{\circ g}\Lambda + KU_0^*M &= 0 \\ K_{g\circ}V &= 0 \\ U_0^{*T}KV &= \widetilde{F}_0 \end{cases} \tag{3.61}$$

Introducing $\Lambda_2 = \begin{bmatrix}\Lambda \\ 0\end{bmatrix} + U_0^*M = \begin{bmatrix}\Lambda \\ U_{02}^*M \\ 0\end{bmatrix}$, where $U_0^* = \begin{bmatrix}0 \\ U_{02}^* \\ 0\end{bmatrix}$, U_0^* has N dof, U_{02}^* has N_f dof, we have:

$$K\Lambda_2 = \begin{bmatrix}K_{gg} & K_{gf} & K_{gn} \\ K_{fg} & K_{ff} & K_{fn} \\ K_{ng} & K_{nf} & K_{nn}\end{bmatrix}\begin{bmatrix}\Lambda \\ U_{02}^*M \\ 0\end{bmatrix} = \begin{bmatrix}K_{gg}\Lambda + K_{gf}U_{02}^*M \\ K_{fg}\Lambda + K_{ff}U_{02}^*M \\ K_{ng}\Lambda + K_{nf}U_{02}^*M\end{bmatrix}$$

$$= K_{\circ g}\Lambda + K_{\circ f}U_{02}^*M = K_{\circ g}\Lambda + KU_0^*M \tag{3.62}$$

The second equation from (3.61) can be rewritten as:

$$K(V-U) + K_{\circ g}\Lambda + KU_0^*M = 0 \Rightarrow K(V - U + \Lambda_2) = 0 \tag{3.63}$$

This finite element problem corresponds to a free of load problem whose solution can be any rigid body C_R:

$$V - U + \Lambda_2 = C_R \tag{3.64}$$

Choosing $C_R = 0$, we have $V = U - \Lambda_2$, so from the equations (3.61) after eliminating V, we can get the following equations:

$$\begin{cases} K\Lambda_2 + \alpha\Pi^T\Pi U &= \alpha\Pi^T\widetilde{U} \\ K_{g\circ}U - K_{g\circ}\Lambda_2 &= 0 \\ U_0^{*T}K(U-\Lambda_2) &= \widetilde{F}_0 \end{cases} \tag{3.65}$$

And then we replace Λ_2 by Λ and M:

$$K_{g\circ}\Lambda_2 = \begin{bmatrix}K_{gg} & K_{gf} & K_{gn}\end{bmatrix}\begin{bmatrix}\Lambda \\ MU_{02}^* \\ 0\end{bmatrix} = K_{gg}\Lambda + MK_{g\circ}U_0^* \tag{3.66}$$

The equations (3.65) can thus be expressed as:

$$\begin{cases} \alpha\Pi^T\Pi U + K_{\circ g}\Lambda + KU_0^*M &= \alpha\Pi^T\widetilde{U} \\ K_{g\circ}U - K_{gg}\Lambda - K_{g\circ}U_0^*M &= 0 \\ U_0^{*T}KU - U_0^{*T}K_{\circ g}\Lambda - U_0^{*T}KU_0^*M &= \widetilde{F}_0 \end{cases} \tag{3.67}$$

Finally, we write the equations in a matrix manner which has to be solved numerically:

$$\begin{bmatrix} \alpha\Pi^T\Pi & K_{\circ g} & KU_0^* \\ K_{g\circ} & -K_{gg} & -K_{g\circ}U_0^* \\ U_0^{*T}K & -U_0^{*T}K_{\circ g} & -U_0^{*T}KU_0^* \end{bmatrix} \begin{bmatrix} U \\ \Lambda \\ M \end{bmatrix} = \begin{bmatrix} \alpha\Pi^T\widetilde{U} \\ 0 \\ \widetilde{F}_0 \end{bmatrix} \tag{3.68}$$

The solution of the basic problem (3.61) is denoted $(U_s(\underline{\theta}), V_s(\underline{\theta}), \Lambda_s(\underline{\theta}), M_s(\underline{\theta}))$.

3.5.2.5 Case 5: Less reliable global load

The basic problem is:

Find the nodal displacement vectors U,V and global load F_0 minimizing:

$$\mathcal{J}(U, V, F_0) = \mathcal{J}_1(U, V) + \alpha\mathcal{J}_2(U) + \beta\mathcal{J}_4(F_0) \tag{3.69}$$

under the constraint: $K_{g\circ}V = 0$ and $U_0^{*T}KV = F_0$

Introducing two Lagrange multipliers Λ and M associated with the constraints:

$$\mathcal{L}(U, V, F_0, \Lambda, M) = \mathcal{J}(U, V, F_0) + \Lambda^T K_{g\circ}V + M^T(U_0^{*T}KV - F_0) \tag{3.70}$$

The differential of the Lagrangian $d\mathcal{L}$ is expressed as:

$$\begin{cases} (\frac{\partial\mathcal{L}}{\partial U}, \delta U) &= \delta U^T K(U - V) + \delta U^T\alpha\Pi^T(\Pi U - \widetilde{U}) \\ (\frac{\partial\mathcal{L}}{\partial V}, \delta V) &= \delta V^T K(V - U) + \delta V^T K_{\circ g}\Lambda + \delta V^T KU_0^*M \\ (\frac{\partial\mathcal{L}}{\partial F}, \delta F_0) &= \delta F^T(\beta(F_0 - \widetilde{F_0}) - M) \\ (\frac{\partial\mathcal{L}}{\partial\Lambda}, \delta\Lambda) &= \delta\Lambda^T K_{g\circ}V \\ (\frac{\partial\mathcal{L}}{\partial M}, \delta M) &= \delta M^T U_0^{*T}KV - \delta M^T F_0 \end{cases} \tag{3.71}$$

The stationarity system verified by the solution of the basic problem is $d\mathcal{L} = 0$:

$$\left\{\begin{array}{rl} K(U-V)+\alpha\Pi^T\Pi U &= \alpha\Pi^T\widetilde{U} \\ K(V-U)+K_{\circ g}\Lambda+KU_0^*M &= 0 \\ \beta(F_0-\widetilde{F_0}) &= M \\ K_{g\circ}V &= 0 \\ U_0^{*T}KV &= F_0 \end{array}\right. \tag{3.72}$$

As for the Equation from (3.62) to (3.64) in Case 4, we can deduce the following equations from Equation (3.72):

$$\left\{\begin{array}{rl} \alpha\Pi^T\Pi U+K_{\circ g}\Lambda+KU_0^*M &= \alpha\Pi^T\widetilde{U} \\ K_{g\circ}U-K_{gg}\Lambda-K_{g\circ}U_0^*M &= 0 \\ U_0^{*T}KU-U_0^{*T}K_{\circ g}\Lambda-(U_0^{*T}KU_0^*+1/\beta)M &= \widetilde{F_0} \end{array}\right. \tag{3.73}$$

Finally, we write the equations in a matrix manner which has to be solved numerically:

$$\begin{bmatrix} \alpha\Pi^T\Pi & K_{\circ g} & KU_0^* \\ K_{g\circ} & -K_{gg} & -K_{g\circ}U_0^* \\ U_0^{*T}K & -U_0^{*T}K_{\circ g} & -(U_0^{*T}KU_0^*+1/\beta) \end{bmatrix} \begin{bmatrix} U \\ \Lambda \\ M \end{bmatrix} = \begin{bmatrix} \alpha\Pi^T\widetilde{U} \\ 0 \\ \widetilde{F_0} \end{bmatrix} \tag{3.74}$$

The solution of the basic problem (3.72) is denoted $(U_s(\underline{\theta}), V_s(\underline{\theta}), \Lambda_s(\underline{\theta}), M_s(\underline{\theta}), F_{0s}(\underline{\theta}))$.

3.6 Explicit calculation of the gradient

After solving the basic problem, the next step is minimizing $\mathcal{G}(\underline{\theta})$. Here, we take the Case 2 (reliable traction distribution) as the example: $\mathcal{G}(\underline{\theta}) = \mathcal{J}(U_s(\underline{\theta}), V_s(\underline{\theta}), \underline{\theta})$. Noting that:

$$\mathcal{G}(\underline{\theta}) = \mathcal{L}(U_s(\underline{\theta}), V_s(\underline{\theta}), \Lambda_s(\underline{\theta})), \underline{\theta}) \tag{3.75}$$

We can deduce the gradient of $\mathcal{G}$ with respect to $\underline{\theta}$. Denoting θ_k the k^{th} component of $\underline{\theta}$, we have:

$$\frac{\partial\mathcal{G}(\underline{\theta})}{\partial\theta_k} = \underbrace{\frac{\partial\mathcal{L}}{\partial U_s}}_{0}\frac{\partial U_s}{\partial\theta_k} + \underbrace{\frac{\partial\mathcal{L}}{\partial V_s}}_{0}\frac{\partial V_s}{\partial\theta_k} + \underbrace{\frac{\partial\mathcal{L}}{\partial\Lambda_s}}_{0}\frac{\partial\Lambda_s}{\partial\theta_k} + \frac{\partial\mathcal{L}}{\partial\theta_k} = \frac{\partial\mathcal{L}}{\partial\theta_k} \tag{3.76}$$

In the particular case with no load data (the calculation is similar for other cases), it writes:

$$\begin{aligned}\frac{\partial \mathcal{L}(\underline{\theta})}{\partial \theta_k} =& \frac{\partial}{\partial \theta_k}[\frac{1}{2}(U_s - V_s)^T K (U_s - V_s) + \frac{\alpha}{2}(\Pi U_s - \widetilde{U})^T(\Pi U_s - \widetilde{U}) + \Lambda_s^T K_{g\circ} V_s] \\ =& \frac{1}{2}(U_s - V_s)^T \frac{\partial K}{\partial \theta_k}(U_s - V_s) + \Lambda_s^T \frac{\partial K_{g\circ}}{\partial \theta_k} V_s\end{aligned} \tag{3.77}$$

Because the global stiffness matrix K could be treated as the assembly of local stiffness matrices with different linearly elastic coefficients, it can be written as:

$$K(\underline{\theta}) = \sum_{k=1}^{n} \theta_k K_k \tag{3.78}$$

where n is the size of θ, K_k is the assembly of the local stiffness matrices corresponding to θ_k and corresponds to the global matrix for $\theta_k = 1$ and $\theta_{k'} = 0$, $k' \neq k$. Such a writing of the stiffness matrix corresponds to any case (homogeneous or heterogeneous) of elastic properties.

Hence:

$$\frac{\partial K}{\partial \theta_k} = K_k, \qquad \frac{\partial K_{g\circ}}{\partial \theta_k} = K_{k_{g\circ}} \tag{3.79}$$

Therefore, we get the derivative with respect to θ_k :

$$\frac{\partial \mathcal{G}(\underline{\theta})}{\partial \theta_k} = \frac{1}{2}(U_s - V_s)^T K_k (U_s - V_s) + \Lambda_s^T K_{k_{g\circ}} V_s \tag{3.80}$$

3.7 Algorithm of sequential minimization

As described in Section 3.4.2, the methodology is made up of two steps. From step 1, we get $\mathcal{G}(\underline{\theta}) = \mathcal{J}(\underline{u}(\underline{\theta}), \underline{\sigma}(\underline{\theta}), \underline{\theta})$ and the gradient of $\mathcal{G}(\underline{\theta})$. In step 2, we use the BFGS (Broyden - Fletcher - Goldfarb - Shanno algorithm) or MMA (Method of Moving Asymptotes) to optimize the parameters $\underline{\theta}$ from the objective function $\mathcal{G}(\underline{\theta})$ and its gradient. The algorithms are briefly described in the following.

3.7.1 BFGS algorithm

The BFGS algorithm is an iterative method for solving unconstrained nonlinear optimization problems. It is named from the four people who independently discovered it in 1970: Broyden [112], Fletcher [113], Goldfarb [114] and Shanno [115]. It is the most popular Quasi-Newton method, in which the Hessian matrix of second derivatives doesn't need to be evaluated directly. Instead of computing a complete new Hessian matrix in each iteration, we will update the Hessian matrix

using information about the curvature at the previous step. The function "fmincon" in *Matlab* can be chosen to use this method.

3.7.2 MMA algorithm

The Method of Moving Asymptotes (MMA) was first presented by Svanberg in [116] for non-linear programming in general and structural optimization in particular. MMA uses a special type of convex approximation. For each step of the iterative process, a strictly convex approximating sub-problem is generated and solved. The generation of these sub-problems is controlled by the so-called moving asymptotes, which both stabilize and speed up the convergence of the general process. Afterwards this method was further studied and developed. Its globally convergent version by using the linear searches and trust region could be found in [117] and [118]. Thanks to Prof. Krister Svanberg from KTH in Stockholm Sweden, we obtain the Matlab implementation of MMA from him (krille@math.kth.se) and adapt it to our program.

3.8 Conclusion

In this chapter, we introduced an identification strategy dedicated to full-field displacement measurements based on the Modified Constitutive Relation Error developed in our work. Its key point is to construct a trade-off between all the available information, both experimental and theoretical. A theoretical presentation in the context of static elasticity was explained in detail. The advantages of this method will be studied with the applications in the next chapter.

Application of mono-scale identification

Contents

4.1 Introduction

This chapter is dedicated to applications of the mono-scale identification based on Modified Constitutive Relation Error. In order to illustrate and study different properties of this methodology, three examples are presented. At first, an homogeneous example is studied with various positions and sizes of the measurement zone, which demonstrates the effectiveness and stability of the basic problem. Then, an heterogeneous example with a single inclusion compares the identification results with various boundary conditions: lack of boundary information, adding free edge and load information. At last, an heterogeneous example with three inclusions is analyzed with respect to the reliability and the trade-off between all the available information.

4.2 Example 1: Identification of the elastic properties of a homogeneous plate

4.2.1 Framework

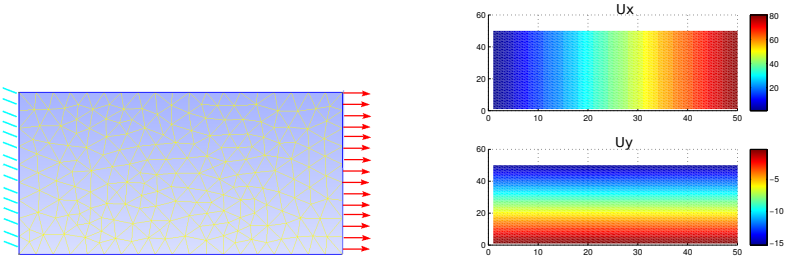

(a) Reference calculation (b) U reference displacement field

Figure 4.1: Numerical example of a homogeneous plate: reference calculation and simulated displacement exact measurement

Before identifying heterogeneous properties, we use a simple homogeneous example to illustrate the effectiveness of the M-CRE method. A first 2D calculation is performed in plane stress representing a tensile test on a plate as sketched in Figure 4.1(a), with reference values of the homogeneous and isotropic material parameters (λ_0, μ_0). The reference values of parameters are: $\lambda_0 = 1, \mu_0 = 1$. The right edge is under uniform pressure, while the left edge is fixed on the horizontal direction and one node is clamped to avoid rigid body motion, the upper and bottom edges are free. The displacements obtained from this calculation are transferred on a regular grid (50×50 data points) representing the DIC measurement grid and are illustrated on Figures 4.1(b). The projection is performed based on the same projection as the one introduced in Equation (3.21). Some noise can be added to these exact fields in order to represent the measurement perturbations. The magnitude of the additive noise is given in percent of the mean value of the displacements. In this example, we assume that only the upper and bottom edges boundary conditions are known, so we use the formulation for the free edge case. Both algorithms of sequential minimization (BFGS and MMA) are effective for the mono-scale identification. Therefore, all the examples in this chapter are calculated with BFGS.

4.2.2 Position and size of the measurement zone

It is a common situation that the measurement area does not cover the entire surface of the tested specimen. There are many reasons, for example, the algorithm

of DIC does not converge in some areas of the photographed area, particularly along the edges; or we want to choose to focus on a specific specimen part to get a higher resolution for the displacement. The proposed formulation of M-CRE allows to perform the identification on a zone where the displacements are measured through DIC on a sub-part of the considered zone. Yet, when no boundary condition is available, the basic problem can be ill-posed as the ratio of measurement zone to calculation zone decreases. This point has to be studied. To illustrate this, the same example is treated, but the position or size of the displacement measurement zone is changed (Figure 4.2). Since the bottom boundary is free-edge, the bottom position means that partial boundary condition information is close to the displacement information, hence their confrontation is emphasized. On the contrary, the center position will lose part of the experimental data confrontation. The size of the measurement zone is characterized by its width l_m and compared to the width of the plate l_p through $\frac{l_m}{l_p}$ ratio. In this case, l_p remains the same and l_m reduces, so that $\frac{l_m}{l_p}$ changes from 1 to 0.7, which means the size of the measurement zone reduces from 50×50 data points to 35×35 data points.

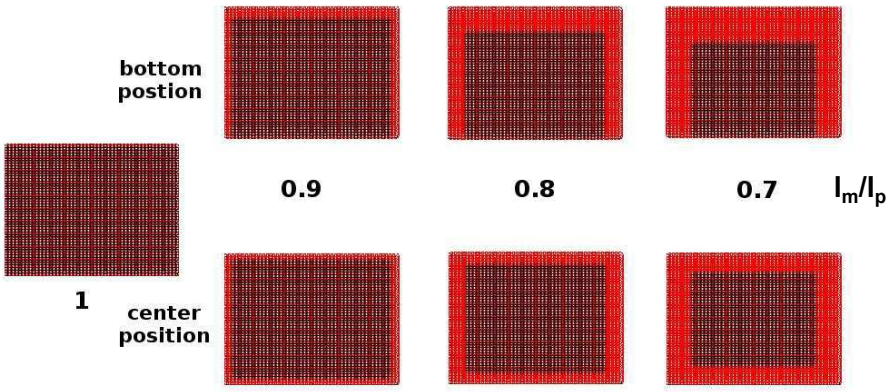

Figure 4.2: Various positions and sizes of measurement zone

In the comparison, we fix $\lambda = 1$, and then identify μ with a 3% displacement noise. Figure 4.3 presents the identification objective functions as a function of μ. Figure 4.3(a) corresponding to a bottom position of the measurement zone various sizes, whereas Figure 4.3(b) corresponding to a center position. We can find that all the objective functions are convex and that their minimum is close to the exact value of μ. It means the calculation and the identification can be performed on the whole domain, even if the measurement zone is smaller. Table 4.1 presents the change of the rank and condition number of the matrix for the basic problem with different $\frac{l_m}{l_p}$ when $\mu = \mu_{ref}$. We can find that although the rank deficiency and condition number are large when the measurement zone is small, we can still use

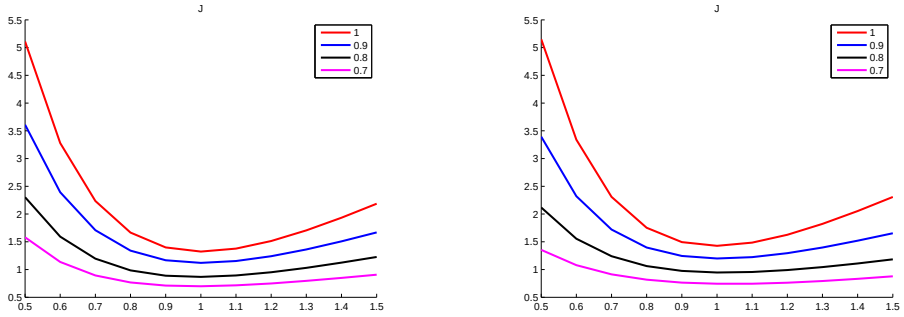

(a) Objective functions for various sizes of measurement zone in bottom position

(b) Objective functions for various sizes of measurement zone in center position

Figure 4.3: Comparison of objective function for various positions and sizes of the measurement zone with a 3% noise

the QR algorithm to solve the basic problem. However, the gradient of the objective function becomes smaller around its minimum when the ratio of size reduces. It is normal to lose sensitivity because of the information lost (the number of data points reduces).

	$\frac{l_m}{l_p}$	1	0.9	0.8	0.7
Bottom position	Matrix rank deficiency	0	0	2	5
	Condition number	1.5e+04	3.5e+07	1.9e+17	3.2e+16
Center position	Matrix rank deficiency	0	0	2	4
	Condition number	1.5e+04	3.5e+07	2.5e+17	4.9e+16

Table 4.1: The rank deficiency and condition number of the matrix for the basic problem (Case 1 with free edge) when $\mu = \mu_{ref}$

4.3 Example 2: Identification of the elastic properties of a plate with a single inclusion

4.3.1 Framework

In this section, we propose the illustration of the method on a numerical example based on the identification of the elastic properties of a plate with a single inclusion. The plate is assumed to be isotropic and heterogeneous for this illustrating example. The behavior is thus described by the Lame coefficients: matrix (λ_1, μ_1) and inclusion (λ_2, μ_2). The purpose of this example is to compare the identification results of heterogeneous material properties according to the information on the

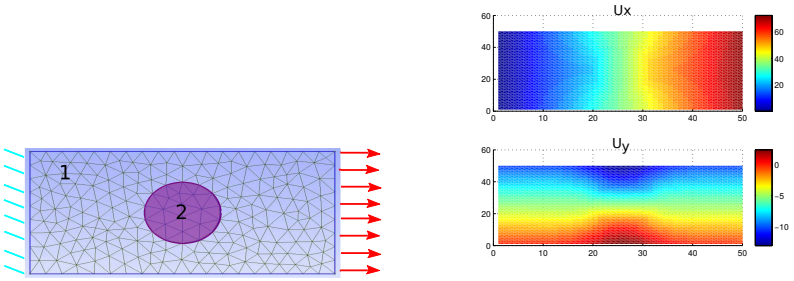

(a) Reference calculation (b) Reference displacement field

Figure 4.4: Numerical example of a plate with a single inclusion: reference calculation and simulated displacement exact measurement

boundary conditions.

In order to create the measurements, a first calculation is performed representing a tensile test on a plate as sketched in Figure 4.4(a), with reference values of the heterogeneous and isotropic material parameters ($\lambda_1 = \mu_1 = 1, \lambda_2 = \mu_2 = 0.5$). The displacements obtained from this calculation are transferred on a regular grid (50×50 data points) representing the DIC measurement grid and are illustrated on Figures 4.4(b). The projection is performed based on the same projection as the one introduced in Equation (3.21). Some noise can be added to these exact fields in order to represent the measurement perturbations. The magnitude of the additive noise is given in percent of the mean value of the displacements or the mean value of the load measurement.

4.3.2 Taking into account free edge information

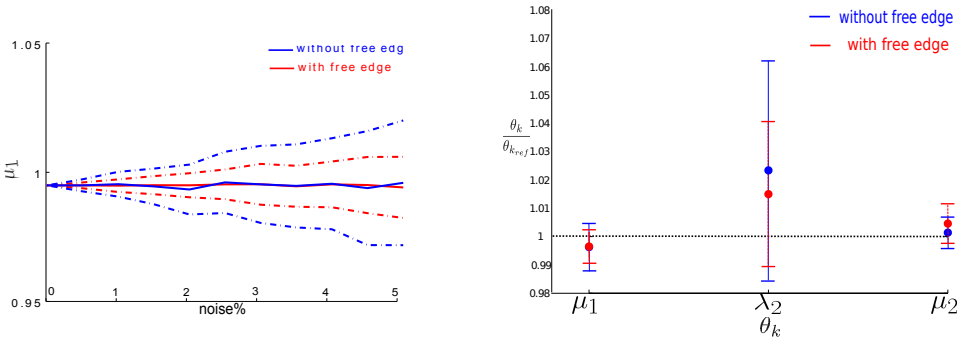

(a) Identified μ_1 on 200 samples (mean value and standard deviation) as a function of the relative noise level

(b) Identified $\frac{\theta_k}{\theta_{k_{ref}}}$ on 200 samples (mean value and standard deviation) with 5% noise

Figure 4.5: Comparison of without information of boundary conditions and with free edge

The proposed formulation allows to perform the identification on a zone where the boundary conditions can be completely or partially unknown. At first, we compare the case without any information on the boundary condition (completely unknown) and the case of adding information of free edge on the upper and bottom boundaries (partially unknown). We take two independent analysis: (1) fix λ_1, λ_2 and μ_2, identify μ_1 with various levels of noise. Figure 4.5(a) presents the identification results on 200 samples of measurement noise, in terms of mean value and standard deviation of the identified μ_1 property as a function of the relative noise level. It can be noted that the level of error is quite linear with respect to the noise level. Hence, in the following, we will consider a single noise level; (2) fix λ_1 and the noise level, identify μ_1, λ_2 and μ_2. Figure 4.5(b) presents the identification results on 200 samples of 5% measurement noise, in terms of mean value and standard deviation of the ratio of identified parameters and the reference parameters. From Figure 4.5 we can find that both formulations (with free edge or not) can obtain a reasonable identification result even though the noise level reaches 5%, but considering the free edge improves significantly the identification results. However, even with the free edge information, we cannot identify the four material parameters at the same time due to the lack of information on the load level. In order to identify all heterogeneous properties, we need more available boundary information.

4.3.3 Adding load information

	free edge		traction distribution		global load	
	λ_1 unknown	λ_1 known	reliable	less reliable	reliable	less reliable
λ_1	1.2479	1	1	1	1	1
μ_1	1.2479	1	1	1	1	1
λ_2	0.6239	0.5	0.5	0.5	0.5	0.5
μ_2	0.6239	0.5	0.5	0.5	0.5	0.5

Table 4.2: The identification results for various boundary conditions ($\lambda_{1ref} = \mu_{1ref} = 1, \lambda_{2ref} = \mu_{2ref} = 0.5$)

Beside the information of free edge on the boundary condition, we can also add the information on load. Therefore the second comparison is carried out between the case only with free edge and the ones with prescribed load edge. From the identification results of the Table 4.2, we can find that the information of load is very important. Without the information of load, one of the parameter is to be known (fixed), in order to identify the others. Otherwise, if we try to identify all four

parameters, only the ratio of the parameters could be identified ($\frac{1.2479}{0.6239} = \frac{1}{0.5} = 2$); but with the information on load, all the parameters could be identified, no matter the way the load is taken into account.

4.3.4 Optimizing the weighting coefficient α

In order to analyze the effect of the weighting coefficient α associated with the distance to the displacement measurement, firstly, we determine $\alpha_0 = \frac{U_{ref} K U_{ref}}{(\Pi U)^T \Pi U}$, and define α as: $\alpha = 10^{\gamma}\alpha_0$. Then we change γ from 0 to 6 and solve the identification problem independently for each value of γ in two cases: without measurement noise, and with a 5% measurement noise on the displacement. Taking the case of reliable traction distribution as an example, we compare the objective function $\mathcal{J}_1$ and $\mathcal{J}_2$ with the increasing γ and get the L-curve as presented Figure 4.6. The L-curve criterion [119] suggests to choose the point of the $\mathcal{J}_1 - \mathcal{J}_2$ curve, which is the closest to (0,0), where both terms are sensitive. Hence, this would lead to a choice of $\gamma = 1$ in the case without measurement noise (Figure 4.6(a)). However, in the case with a 5% measurement noise, choice becomes $\gamma = 3$ (Figure 4.6(b)). The other cases of boundary condition yield similar curves and value.

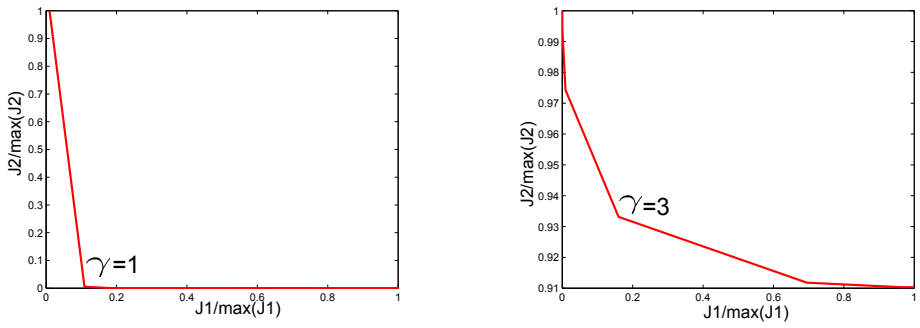

(a) Without measurement noise (b) With 5% measurement noise

Figure 4.6: L-curve of $\mathcal{J}_1$ and $\mathcal{J}_2$ with the increasing γ

Without noise on the measurement, we can identify the exact parameters with γ from 0 to 6 while the calculation time reduces (Figure 4.7(a)). The reason could be concluded that the more sensitive the objective functions are, the faster the convergence reaches. Yet, if we compare the identification results with a 5% measurement noise, although the calculation time is reduced when $\gamma = 3$ (Figure 4.7(b)), but the relative errors of identification result are large when γ increase (Figure 4.8). We know that increasing γ leads to increasing objective function, which will lose the accuracy of the identification result. The choice of $\gamma = 3$ is

unreasonable and a pragmatic choice of $\gamma = 0$ is used in the following.

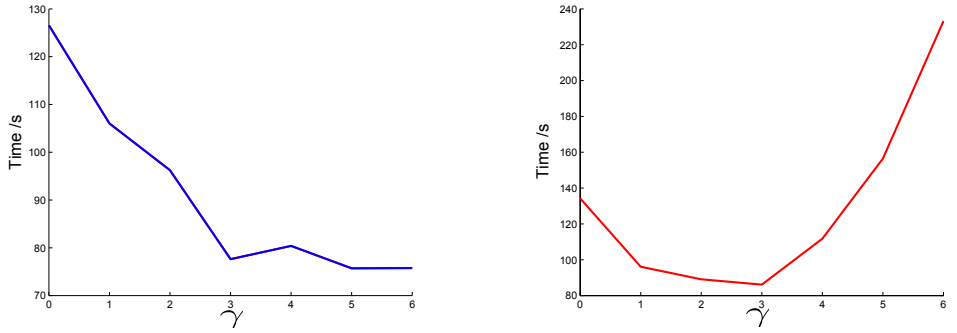

(a) Without measurement noise (b) With a 5% measurement noise

Figure 4.7: The calculation time with various α

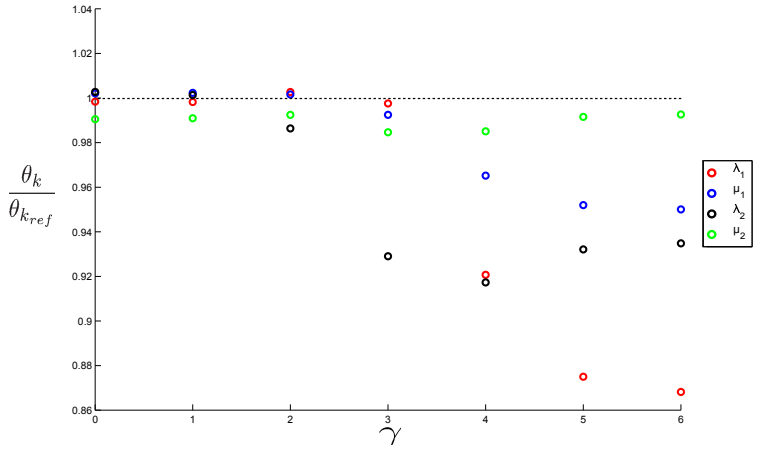

Figure 4.8: Identified $\frac{\theta_k}{\theta_{k_{ref}}}$ with various α in the case of 5% measurement noise

4.4 Example 3: Identification of the elastic properties of a plate with three inclusions

4.4.1 Framework

In this section, we propose the illustration of the method on a numerical example based on the study of the elastic properties of a plate with three inclusion. The plate is assumed to be isotropic and heterogeneous for this illustrating example. The behavior is thus described by the Lame coefficients: matrix (λ_1, μ_1) and inclusions

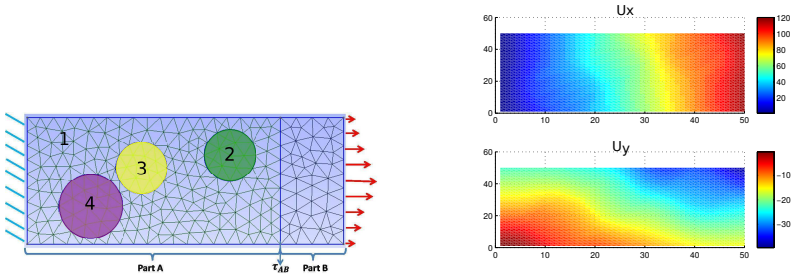

(a) Reference calculation (b) Reference displacement field

Figure 4.9: Numerical example of a plate with three inclusions: reference calculation and simulated displacement exact measurement

$(\lambda_2, \mu_2), (\lambda_3, \mu_3), (\lambda_4, \mu_4)$. The purpose of this example is to compare different ways to take into account the load data. In particular, the stress distribution is hardly measured experimentally. Therefore, the formulation with traction distribution needs a hypothesis of the distribution, which may introduce a model error.

In order to create the measurements, a calculation is performed representing a tensile test on a whole plate as sketched in Figure 4.9(a), with reference values of the heterogeneous and isotropic material parameters. The displacements obtained from this calculation are transferred on a regular grid (50×50 data points) representing the DIC measurement grid and are illustrated on Figures 4.9(b). The global load can be measured, but no local information on its distribution is known.

4.4.2 Taking into account the load as reliable information

In order to compare the boundary condition of traction distribution and global load, we perform the identification on part A whose boundary is close to inclusion 2 so that the load distribution on boundary Γ_{AB} is affected by the inclusion. Yet, only the global load on Γ_{AB} is supposed to be known. In the first study, we take into account the load as reliable information. It means the equation related to the load is considered within the constraints: $\mathcal{S}_{Ad} = \mathcal{S}^0_{Ad} \cap \mathcal{S}^f_{Ad}$ or $\mathcal{S}_{Ad} = \mathcal{S}^0_{Ad} \cap \mathcal{S}^F_{Ad}$.

In the case of reliable global load, we just need the sum of the global load. However, a hypothesis of distribution is needed in the case of reliable traction distribution. Since this information is assumed to be unknown as it is usually the case in experimental set ups, we assume that the traction distribution on Γ_{AB} is constant, as the blue curve in Figure 4.10(a), where the exact stress distribution corresponds to the green curve.

Figure 4.10(b) presents the identification results of parameters for the two boundary condition formulations. The results are significantly better by presuming

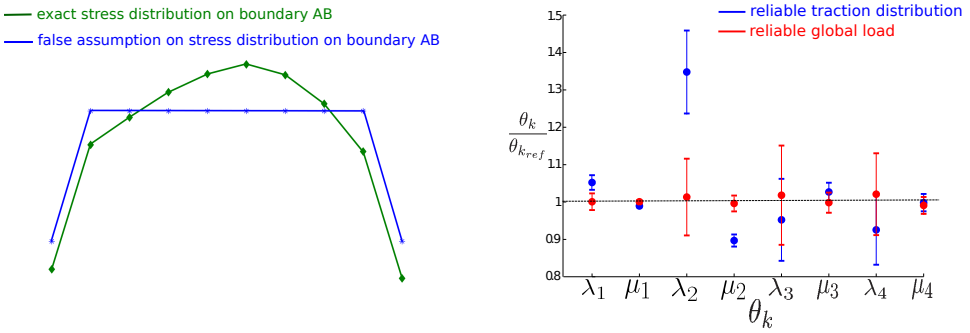

(a) *Assumption on stress distribution*

(b) *Identified* $\frac{\theta_k}{\theta_{k_{ref}}}$ *on 100 samples (mean value and standard deviation) with a 5% noise on measured displacement*

Figure 4.10: Comparison of reliable traction distribution and reliable global load

the load condition as a global load (the red groups: the mean value of the ratio of identified parameter and reference is almost equal to 1). Moreover, we can find that, in the case of traction distribution (the blue groups), identification relative error on the part near the false boundary assumption is the largest (error on λ_2: 34.8% and on μ_2: 10.3%). It means that the model error on the traction distribution would lead to wrong identification results.

4.4.3 Taking into account the load as less reliable information

In the second study, we take into account the load as less reliable information. It means the equation related to the load is included as a distance in the functional: $\mathcal{J}(\underline{u}, \underline{\sigma}, \underline{\theta}) = \mathcal{J}_1 + \alpha\mathcal{J}_2 + \beta\mathcal{J}_3$. First, the formulation with a less reliable traction distribution is studied. In particular, the choice of the weighting coefficient β is discussed by comparing the results with the previous ones. Then, the global load approach is addressed and the identification results are discussed.

4.4.3.1 Traction distribution: optimizing the weighting coefficient

Firstly, we define $\beta_0 = \frac{U_{ref}^T K U_{ref}}{\widetilde{F}^T \widetilde{F}}$ and $\beta = \beta_0 10^\gamma$. Then we change γ from -9 to 8 and solve the identification problem independently. Figure 4.11 shows the influence of the weighting coefficient β on the identification results of λ and μ for the four parameters. We can divide the results into three groups:

- $-9 \leq \gamma < -6$: $\underline{\theta}_{id} \neq \underline{\theta}_{ref}$, but $\frac{\theta_{id}^k}{\theta_{ref}^k} = 0.8657(constant\ \forall k)$: the identification values are not the good ones but the rigidity ratios are correct, as if no load data was available (due to a very small weighting factor).
- $-6 \leq \gamma < -2$: $\underline{\theta}_{id} \approx \underline{\theta}_{ref}$: the identification result are reasonable.

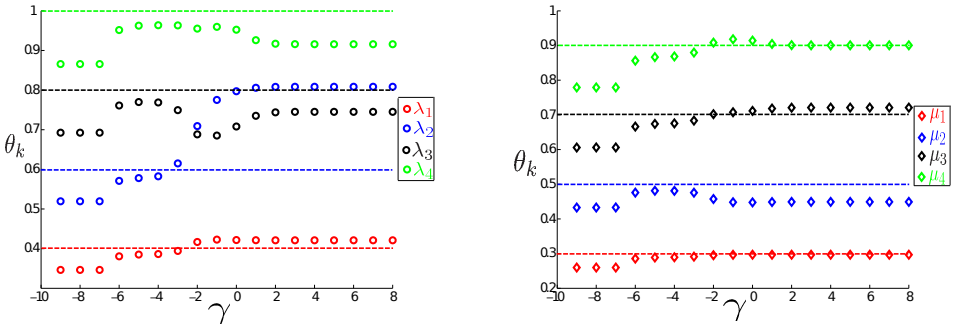

(a) *Identification result of* λ (b) *Identification result of* μ

Figure 4.11: Comparison of influence of weighting coefficient β on the identification result

- $\gamma \geq -2$: $\underline{\theta}_{id} \neq \underline{\theta}_{ref}$, $\frac{\underline{\theta}^k_{id}}{\underline{\theta}^k_{ref}} \neq constant$: the identification results get erroneous, in particular near Γ_{AB}, and are close to the case with a false traction distribution (see Figure 4.10).

In order to find out the reason, on one hand, we calculate and compare the normal stress on the boundary Γ_{AB} from the result. From Figure 4.12(a) we find that:

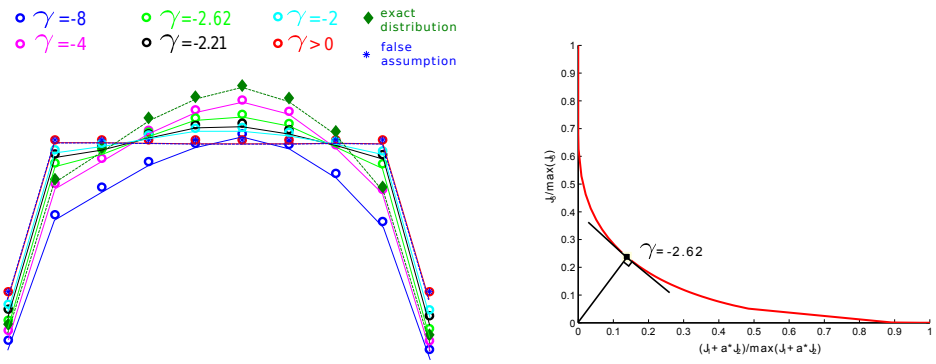

(a) *Calculated traction distribution from the identification result of different* β (b) *L-curve of* $J_1 + \alpha J_2$ *and* J_3

Figure 4.12: Comparison of influence of weighting coefficient β on stress distribution and objective function

- when $\gamma = -8$, the normal stress distribution (the blue line) has the same shape as the exact distribution, but with a constant ratio. We can conclude that too small β means weak influence of load information, so the identification result is similar to the case with only information of free edge, which has good ratio between parameters, but loses the global stiffness;
- when $\gamma = -4$, the normal stress distribution (the magenta line) is the closest curve to the exact stress distribution and still has the same shape;

- when $\gamma = -2.62, -2.21, -2$, the influence of load information continue to increase, so the normal stress distribution gets closer to the false assumption distribution;
- If $\gamma > 0$, the normal stress distribution will approximate the false assumption distribution, leading to identification results similar to the case with reliable traction distribution.

Hence, we can conclude there is an optimal choice of the weighting factor leading to both good identification results and stress distribution, despite the false assumption.

In order to determine this optimal weighting factor, the L-curve [119] was used to compare different terms of the objective function. Figure 4.12(b) shows that $\gamma = -2.62$ is the compromise point where both values of $\mathcal{J}_1 + \alpha\mathcal{J}_2$ and $\mathcal{J}_3$ are reasonable.

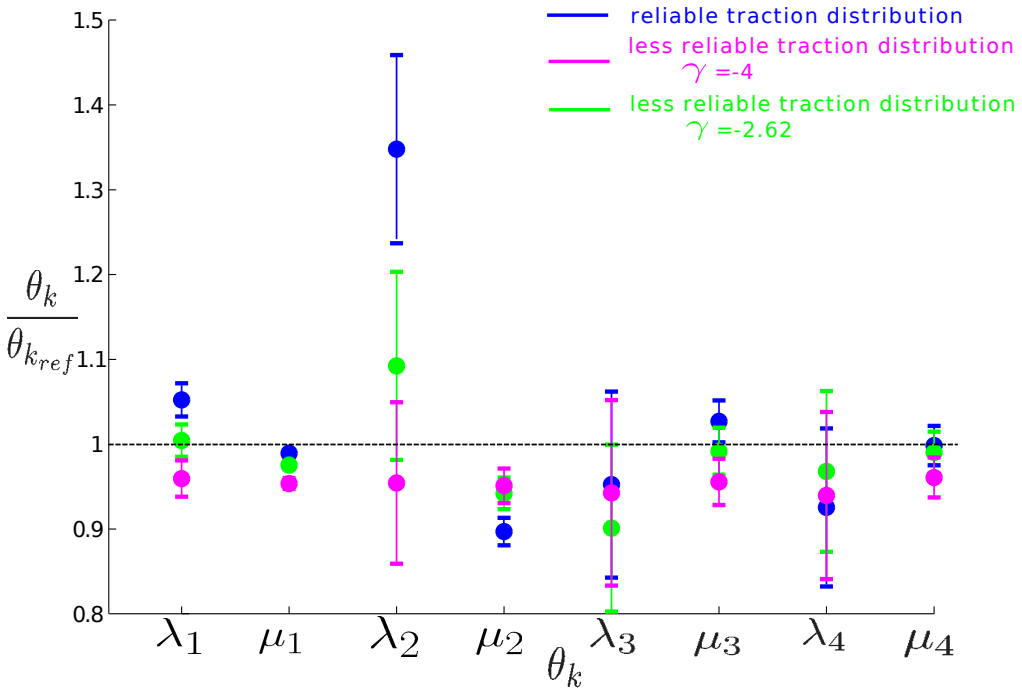

Figure 4.13: Comparison of reliable traction distribution and less reliable traction distribution: Identified $\frac{\theta_k}{\theta_{k_{ref}}}$ on 100 samples (mean value and standard deviation) with a 5% noise on measured displacement

Figure 4.13 presents the identification results with both prescribed traction distribution and traction distribution distance with reasonable weighting coefficient (two groups of less reliable traction distribution). The latter improve significantly the identification results. Since defining $\gamma = -4$ can correct the model error of the traction distribution, the parameters of inclusion 2 (near Γ_{AB}) are the best in the

magenta group. However, it reduces the global rigidity: all the ratio of parameters are below 1. In contrast, based on the L-curve, when $\gamma = -2.62$ (the green group), the parameters of global matrix and inclusion 4 (far from Γ_{AB}) are the best. We can conclude that the model error of traction distribution could be reduced by optimizing the weighting coefficient and restore the balance between strain and displacement. Yet, the choice of the weighting factor may remain tricky and time consuming due to the L-curve strategy.

4.4.3.2 Global load: effect of measurement perturbation

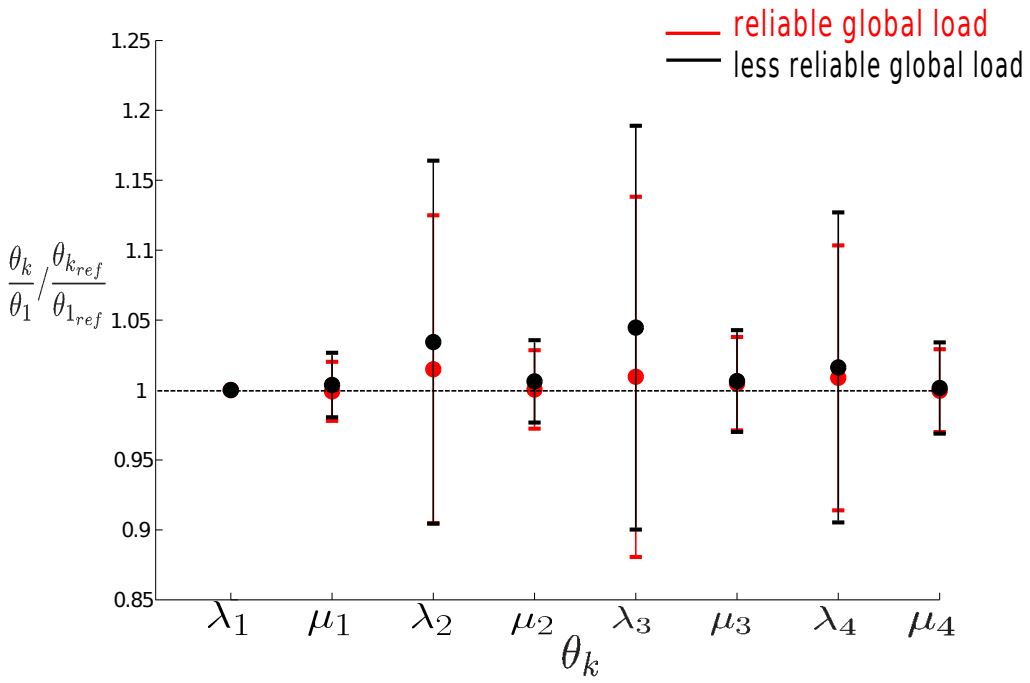

Figure 4.14: Comparison of reliable global load and less reliable global load: Identified $\frac{\theta_k}{\theta_1}/\frac{\theta_{k_{ref}}}{\theta_{1_{ref}}}$ on 100 samples (mean value and standard deviation) with a 5% noise on measured displacement and a 5% noise on measured force

In order to compare the influence of measurement noise, we use the same example of a plate with three inclusions (Figure 4.9), and consider two cases: the global load on the boundary is reliable or not. We add 5% noise on both displacement measurement and force measurement.

The result are compared in terms of $\frac{\theta_k}{\theta_1}/\frac{\theta_{kref}}{\theta_{1ref}}$ to compensate the fact that perturbation on the load leads to an erroneous global rigidity. Figure 4.14 shows that both formulations (reliable or less reliable global load) can obtain a reasonable identification result, but the influence of noise is slightly greater in the case assuming less reliable global load. The results are quite independent to the choice of the weighting factor. The results are slightly better than for the traction distribution

(with false assumption) approach and the question of the choice of the weighting factor is not to be addressed. Hence, when the traction distribution is not known, it is preferred to choose a global load approach.

4.5 Conclusion

The first illustrating example presented that the calculation could be performed without some or all boundary conditions, but it was still solved on the whole domain. On the second illustrating example, it was shown that the method allowed the calculation with different kinds of boundary conditions and the taking into account of load-edge improved significantly the identification results. The last illustrating example showed how to balance between the various possible experimental information so that the inverse problem was well-posed. In the further application, we propose a two-scale approach where heterogeneous properties are sought at the measurement level and homogeneous ones at the specimen/structure level.

Multi-scale identification

Contents

5.1 Introduction

In the usual experiment cases, the measurement zone is only a sub-part of the specimen. If we use the mono-scale approach, we can only identify the local heterogeneous properties of the measurement zone. It means that the lack of displacement information outside the measurement zone prevents from identifying heterogeneous properties in this area. Yet, some experimental information such as boundary conditions could be available outside the measurement zone. It was shown in the previous chapter that the taking into account of all available information leads to more accurate identification results. Hence, we would expect a methodology allowing such a taking into account. A multi-scale approach is therefore proposed to account for any specimen where micro heterogeneous properties are sought at the measurement level and macros homogeneous ones at the specimen level.

The M-CRE is a suitable framework to achieve such a multi-scale identification. In order to adapt it to a multi-scale approach, we need to address the following three questions:

1. How to trade off the information from different scales?
2. How to combine the information between two scales?

3. How to develop a multi-scale algorithm for the basic problem?

In this chapter, it is proposed to define the identification problem taking into account the measurement sub-part. Stress and displacement are defined at both macro and micro scales, and the equations are split according to the reliability of information. A coupling scheme is then to be defined between the scales, leading to a basic problem defined at the two scales with the corresponding coupling equation.

5.2 Framework: direct problem and measurements

The identification framework is the one of a mechanical test on a specimen Ω_M where the load is measured on $\partial_f\Omega$ as well as the displacement field on a sub-part of the specimen surface Ω_m (Figure 5.1). We can also assume a part of the edge of the specimen $\partial_d\Omega$ to be free of load and we have no idea on the boundary condition on $\partial_\emptyset\Omega$. The elastic properties of the specimen at the macro level, collected in the vector $\underline{\theta}^M$, are sought as homogeneous and isotropic, and the ones of the measurement part at the micro level collected in the vector $\underline{\theta}^m$ are sought as heterogeneous and isotropic. The boundary conditions are only known at the macro level and displacement is only measured at the micro level. This can lead to the following model and equations describing the available information, both experimental and theoretical. The equations verified by the macro stress $\underline{\underline{\sigma}}^M$, the macro displacement $\underline{u}^M$, the macro parameters $\underline{\theta}^M$, the micro stress $\underline{\underline{\sigma}}^m$, the micro displacement $\underline{u}^m$ and the micro parameters $\underline{\theta}^m$ are as follow:

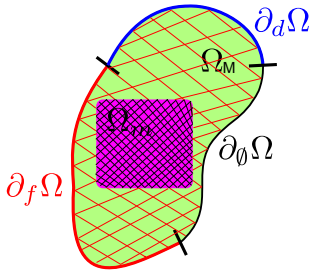

Figure 5.1: Direct problem for multi-scale

- On Ω_M,
  - ◇ Equilibrium: $\underline{div}\ \underline{\underline{\sigma}}^M = \underline{0}$
  - ◇ Macro constitutive relation: $\underline{\underline{\sigma}}^M = \mathcal{C}(\underline{\theta}^M) : \underline{\underline{\varepsilon}}^M$
  - ◇ Kinematic compatibility: $\underline{\underline{\varepsilon}}^M = \underline{\underline{\nabla}}^s \underline{u}^M$
- On Ω_m,
  - ◇ Equilibrium: $\underline{div}\ \underline{\underline{\sigma}}^m = \underline{0}$
  - ◇ Micro constitutive relation: $\underline{\underline{\sigma}}^m = \mathcal{C}(\underline{\theta}^m) : \underline{\underline{\varepsilon}}^m$

  - ◇ Kinematic compatibility: $\underline{\underline{\varepsilon}}^m = \underline{\underline{\nabla}}^s \underline{u}^m$
  - ◇ Displacement measurement: $\underline{u}^m = \underline{\tilde{u}}$
- On $\partial_d\Omega$,
  - ◇ Free edge boundary condition: $\underline{\underline{\sigma}}^M \cdot \underline{n} = \underline{0}$
- On $\partial_f\Omega$,
  - ◇ Measured traction boundary condition: $\underline{\underline{\sigma}}^M \cdot \underline{n} = \underline{f}$, on $\partial_f\Omega$

  or
  - ◇ Measured global load F_0 along a given direction $\underline{N}_0$: $\int_{\partial_f\Omega} \underline{\underline{\sigma}}^M \cdot \underline{n} dS \cdot \underline{N}_0 = F_0$
- On $\partial_\emptyset\Omega = \partial\Omega \backslash (\partial_d\Omega \cup \partial_f\Omega)$, unknown boundary condition

5.3 Splitting of the equations and coupling macro fields and micro fields

5.3.1 Splitting of the equations

As for the mono-scale approach, the various equations of the identification problem are split into two groups as presented in Table 5.1. At each scale, the splitting is similar to the one proposed for the mono-scale approach (Section 3.3). Considering the load data, it is chosen to deal with it as a reliable information in this first approach. Nonetheless considering such information as less reliable is a straightforward adaptation of the purposed methodology.

Table 5.1: Different groups of multi-scale equations

	Macro fields Ω_M	Micro fields Ω_m
Reliable	$\underline{div}\ \underline{\underline{\sigma}}^M = \underline{0}$ $\underline{\underline{\varepsilon}}^M = \nabla^s \underline{u}^M$ $\underline{\underline{\sigma}}^M \cdot \underline{n} = \underline{0}$ $\underline{\underline{\sigma}}^M \cdot \underline{n} = \underline{f}$, or $\int_{\partial\Omega_f} \underline{\underline{\sigma}}^M \cdot \underline{n} dS \cdot \underline{N}_0 = F_0$	$\underline{div}\ \underline{\underline{\sigma}}^m = \underline{0}$ $\underline{\underline{\varepsilon}}^m = \nabla^s \underline{u}^m$
Less reliable	$\underline{\underline{\sigma}}^M = \mathcal{C}(\underline{\theta}^M) : \underline{\underline{\varepsilon}}^M$	$\underline{u}^m = \underline{\tilde{u}}$ $\underline{\underline{\sigma}}^m = \mathcal{C}(\underline{\theta}^m) : \underline{\underline{\varepsilon}}^m$

5.3.2 Coupling the scales

The coupling is used to transfer the information from one scale to the other: transfer the information of kinematic field measurement to the macro fields, and the load and boundary condition information to the micro fields.

The key point is to know how to achieve the coupling. We hence need to define the method to get the equality of the fields in a given manner. There is no doubt that

it would be interesting to base the method on the ideas of homogenization where the strain energies at the two scales are equal, but there are actually very few practical applications if we would like to keep the coupling operator linear. Therefore, we try a few coupling operators which permit the equality between micro fields and macro fields through the following ways:

- For the kinematic admissible fields: some possibilities have been proposed (see Section 5.5.1) to make sure that the equality of the displacement and strain fields is on average upon zones of adjustable size. Considering the continuous fields, the coupling operator can be noted:

$$\mathcal{L}_u(\underline{u}^M, \underline{u}^m) = 0 \tag{5.1}$$

- For the static admissible fields: in the case where the stress is described by the displacement field $\underline{v}$ as introduced in Section 3.5.1, the same coupling operator could be used as for $\underline{u}$. Otherwise we can impose equality for the stress , either as an average on volume or on lines where the global loads are forced to be equal (see Section 5.5.2). In all cases, we can note the coupling operator as:

$$\mathcal{L}_\sigma(\underline{\underline{\sigma}}^M, \underline{\underline{\sigma}}^m) = 0 \tag{5.2}$$

5.4 Identification strategy

5.4.1 Admissible sets and functional

In order to identify the properties of the material, $(\underline{u}^M, \underline{\underline{\sigma}}^M, \underline{u}^m, \underline{\underline{\sigma}}^m, \underline{\theta}^M, \underline{\theta}^m)$ are sought as the solution of a minimization problem where the reliable equations are considered as constraints and the less reliable equations define a functional that is to be minimized. Here we take the case of reliable traction distribution as an example to explain in detail. We introduce:

- the space associated with the constraints on macro displacement:

$$\mathcal{U}_{Ad}^M = \{\underline{u}^M \in H^1(\Omega_M)\} \tag{5.3}$$

- the space associated with the constraints on micro displacement:

$$\mathcal{U}_{Ad}^m = \{\underline{u}^m \in H^1(\Omega_m)\} \tag{5.4}$$

- the space associated with the constraints on macro stress:

◇ equilibrium and free edge:

$$\mathcal{S}_{Ad}^{0M} = \{\underline{\underline{\sigma}}^M \in H_{div}(\Omega_M)/\underline{div}\ \underline{\underline{\sigma}}^M = \underline{0}\ on\ \Omega_M, \underline{\underline{\sigma}}^M \cdot \underline{n} = \underline{0}\ on\ \partial_d\Omega\} \quad (5.5)$$

◇ traction distribution on $\partial_f\Omega$:

$$\mathcal{S}_{Ad}^{fM} = \{\underline{\underline{\sigma}}^M \in H_{div}(\Omega_M)/\ \underline{\underline{\sigma}}^M \cdot \underline{n} = \underline{f} on\ \partial_f\Omega\} \quad (5.6)$$

- the space associated with the constraints on micro stress:

$$\mathcal{S}_{Ad}^{0m} = \{\underline{\underline{\sigma}}^m \in H_{div}(\Omega_m)/\underline{div}\ \underline{\underline{\sigma}}^m = \underline{0}\ on\ \Omega_m\} \quad (5.7)$$

- the term of macro constitutive relation error:

$$\mathcal{J}_1(\underline{\underline{\sigma}}^M, \underline{u}^M, \underline{\theta}^M) = \frac{1}{2}\int_{\Omega_M} (\underline{\underline{\sigma}}^M - \mathcal{C}^M\ \underline{\underline{\varepsilon}}(\underline{u}^M)) : \mathcal{C}^{M^{-1}} : (\underline{\underline{\sigma}}^M - \mathcal{C}^M\ \underline{\underline{\varepsilon}}(\underline{u}^M))d\Omega_M \quad (5.8)$$

- the term of micro constitutive relation error:

$$\mathcal{J}_2(\underline{\underline{\sigma}}^m, \underline{u}^m, \underline{\theta}^m) = \frac{1}{2}\int_{\Omega_m} (\underline{\underline{\sigma}}^m - \mathcal{C}^m\ \underline{\underline{\varepsilon}}(\underline{u}^m)) : \mathcal{C}^{m-1} : (\underline{\underline{\sigma}}^m - \mathcal{C}^m\ \underline{\underline{\varepsilon}}(\underline{u}^m))d\Omega_m \quad (5.9)$$

- the term of distance to the displacement measurements on Ω_m:

$$\mathcal{J}_3(\underline{u}^m) = \frac{1}{2}\int_{\Omega_m} ||\underline{u}^m - \underline{\tilde{u}}||^2 d\Omega_m \quad (5.10)$$

Because it is the first time the coupling equations for the multi-scale problem are introduced, we need to explore the reliability of these equations.

- If they are treated as reliable:
  ◇ the space associated with the coupling on displacement:

$$\mathcal{C}_u = \{\underline{u}^M \in H^1(\Omega_m), \underline{u}^m \in H^1(\Omega_m)/\ \mathcal{L}_u(\underline{u}^M, \underline{u}^m) = 0\} \quad (5.11)$$

  ◇ the space associated with the coupling on stress:

$$\mathcal{C}_\sigma = \{\underline{\underline{\sigma}}^M \in H_{div}(\Omega_m), \underline{\underline{\sigma}}^m \in H_{div}(\Omega_m)/\ \mathcal{L}_\sigma(\underline{\underline{\sigma}}^M, \underline{\underline{\sigma}}^m) = 0\} \quad (5.12)$$

- If they are treated as less reliable:
  ◇ the term of distance to the displacement coupling on Ω_m:

$$\mathcal{J}_4(\underline{u}^M, \underline{u}^m) = \frac{1}{2}(\mathcal{L}_u(\underline{u}^M, \underline{u}^m))^2 \quad (5.13)$$

◇ the term of distance to the stress coupling on Ω_m:

$$\mathcal{J}_5(\underline{\underline{\sigma}}^M, \underline{\underline{\sigma}}^m) = \frac{1}{2}(\mathcal{L}_\sigma(\underline{\underline{\sigma}}^M, \underline{\underline{\sigma}}^m))^2 \tag{5.14}$$

Depending on the choice concerning the reliability of the equations of coupling, we can define different study cases which are shown in Table 5.2. And then, various possible formulations for these study cases are derived in Table 5.3.

Table 5.2: Different reliability of the equations of coupling

Study case	1	2	3	4
Coupling on displacement	Reliable	Reliable	Less reliable	Less reliable
Coupling on stress	Reliable	Less reliable	Less reliable	Reliable

Table 5.3: Various possible formulations for multi-scale problem (α, γ and ξ are positive weighting coefficients)

Study case	Kinematic and static constraints	Coupling constraints	Functional
1	$\mathcal{U}_{Ad} = \mathcal{U}_{Ad}^M \times \mathcal{U}_{Ad}^m$	$\mathcal{C}_{Ad} = \mathcal{C}_u \cap \mathcal{C}_\sigma$	$\mathcal{J} = \mathcal{J}_1 + \mathcal{J}_2 + \alpha\mathcal{J}_3$
2		$\mathcal{C}_{Ad} = \mathcal{C}_u$	$\mathcal{J} = \mathcal{J}_1 + \mathcal{J}_2 + \alpha\mathcal{J}_3 + \xi\mathcal{J}_5$
3	$\mathcal{S}_{Ad} = (\mathcal{S}_{Ad}^{0M} \cap \mathcal{S}_{Ad}^{fM}) \times \mathcal{S}_{Ad}^{0m}$	$\mathcal{C}_{Ad} = \emptyset$	$\mathcal{J} = \mathcal{J}_1 + \mathcal{J}_2 + \alpha\mathcal{J}_3 + \gamma\mathcal{J}_4 + \xi\mathcal{J}_5$
4		$\mathcal{C}_{Ad} = \mathcal{C}_\sigma$	$\mathcal{J} = \mathcal{J}_1 + \mathcal{J}_2 + \alpha\mathcal{J}_3 + \gamma\mathcal{J}_4$

From the identification results 6.2.2, we found that the cost functions are very large in Case 1 and Case 2. It means that the constraints of coupling on displacement are too strong, so we need to relax the constraints. However, if we relax all the coupling constraints and put them in the cost function, as in Case 3, the condition number of the system will be too large and the basic problem less accurately solved. As a consequence, Case 4 appears to be the best choice in the treated cases for the proposed couplings. We thus define the coupling on stress as constraint, and the coupling on displacement within the functional in order to present the implementation and the identification in the following sections (even though all the four study cases have been implemented).

5.4.2 The identification problem

From the splitting of the equations and the proposed bridging of the scales, we can conclude the definition of the identification problem as the following:

Find the fields $(\underline{u}^M, \underline{u}^m, \underline{\underline{\sigma}}^M, \underline{\underline{\sigma}}^m) \in (\mathcal{U}_{Ad} \times \mathcal{S}_{Ad}) \cap \mathcal{C}_{Ad}$ and the set of parameters $(\underline{\theta}^M, \underline{\theta}^m) \in \Theta_{Ad}$ minimizing :

$$\mathcal{J}(\underline{u}^M, \underline{u}^m, \underline{\underline{\sigma}}^M, \underline{\underline{\sigma}}^m, \underline{\theta}^M, \underline{\theta}^m) = \mathcal{J}_1 + \mathcal{J}_2 + \alpha \mathcal{J}_3 + \gamma \mathcal{J}_4 \tag{5.15}$$

where $\mathcal{U}_{Ad} = \mathcal{U}_{Ad}^M \times \mathcal{U}_{Ad}^m$, $\mathcal{S}_{Ad} = (\mathcal{S}_{Ad}^{0M} \cap \mathcal{S}_{Ad}^{fM}) \times \mathcal{S}_{Ad}^{0m}$, $\mathcal{C}_{Ad} = \mathcal{C}_\sigma$, and Θ_{Ad} is the admissible space of parameters.

In practice, as for the mono-scale approach, the minimization is split into a sequential minimization:

$$\min_{(\underline{\theta}^M, \underline{\theta}^m) \in \Theta_{Ad}} \min_{(\underline{u}^M, \underline{u}^m, \underline{\underline{\sigma}}^M, \underline{\underline{\sigma}}^m) \in (\mathcal{U}_{Ad} \times \mathcal{S}_{Ad}) \cap \mathcal{C}_{Ad}} \mathcal{J}(\underline{u}^M, \underline{u}^m, \underline{\underline{\sigma}}^M, \underline{\underline{\sigma}}^m, \underline{\theta}^M, \underline{\theta}^m) \tag{5.16}$$

- For a given $(\underline{\theta}^M, \underline{\theta}^m)$, find $(\underline{u}^M, \underline{u}^m, \underline{\underline{\sigma}}^M, \underline{\underline{\sigma}}^m)$ minimizing $\mathcal{J}(\underline{u}^M, \underline{u}^m, \underline{\underline{\sigma}}^M, \underline{\underline{\sigma}}^m, \underline{\theta}^M, \underline{\theta}^m)$ under the above constraints. This is the basic problem:

$$\min_{(\underline{u}^M, \underline{u}^m, \underline{\underline{\sigma}}^M, \underline{\underline{\sigma}}^m) \in (\mathcal{U}_{Ad} \times \mathcal{S}_{Ad}) \cap \mathcal{C}_{Ad}} \mathcal{J}(\underline{u}^M, \underline{u}^m, \underline{\underline{\sigma}}^M, \underline{\underline{\sigma}}^m, \underline{\theta}^M, \underline{\theta}^m) \tag{5.17}$$

  The solution of the basic problem is denoted:

$$(\underline{u}^M(\underline{\theta}^M, \underline{\theta}^m), \underline{u}^m(\underline{\theta}^M, \underline{\theta}^m), \underline{\underline{\sigma}}^M(\underline{\theta}^M, \underline{\theta}^m), \underline{\underline{\sigma}}^m(\underline{\theta}^M, \underline{\theta}^m)) \tag{5.18}$$

- Then, defining: $\mathcal{G}(\underline{\theta}^M, \underline{\theta}^m) = \mathcal{J}(\underline{u}^M(\underline{\theta}^M, \underline{\theta}^m), \underline{u}^m(\underline{\theta}^M, \underline{\theta}^m), \underline{\underline{\sigma}}^M(\underline{\theta}^M, \underline{\theta}^m), \underline{\underline{\sigma}}^m(\underline{\theta}^M, \underline{\theta}^m), \underline{\theta}^M, \underline{\theta}^m)$, the identification of $(\underline{\theta}^M, \underline{\theta}^m)$ is performed as the minimization of $\mathcal{G}(\underline{\theta}^M, \underline{\theta}^m)$:

$$(\underline{\theta}^{M^{opt}}, \underline{\theta}^{m^{opt}}) = \mathrm{Arg} \min_{(\underline{\theta}^M, \underline{\theta}^m) \in \Theta_{Ad}} \mathcal{G}(\underline{\theta}^M, \underline{\theta}^m) \tag{5.19}$$

5.5 Coupling operators between the scales

5.5.1 Coupling the displacement fields

The displacement fields are sought in the finite element form. Hence, the coupling operator aims at coupling the macro dofs and the micro dofs and will be presented in the discrete form here.

Several approaches have been tested:

- equality in the weak form with macro finite element test fields
- coupling the displacement by diffuse approximation method
- coupling the strain by diffuse approximation method

5.5.1.1 Coupling in the weak form

The first attempt is to purpose a coupling based on the weak form of the equality between macro and micro fields. We started from the easiest case of 1D problem with hierarchical macro and micro meshes (Figure 5.2). The micro and macro displacements are defined as:

$$u_m(x) = \sum_i^n \varphi_i^m(x) u_i^m = [\phi^m(x)]U^m \tag{5.20}$$

$$u_M(x) = \sum_i^N \varphi_i^M(x) u_i^M = [\phi^M(x)]U^M \tag{5.21}$$

we denote N the number of macro dofs, and n the number of micro dofs.

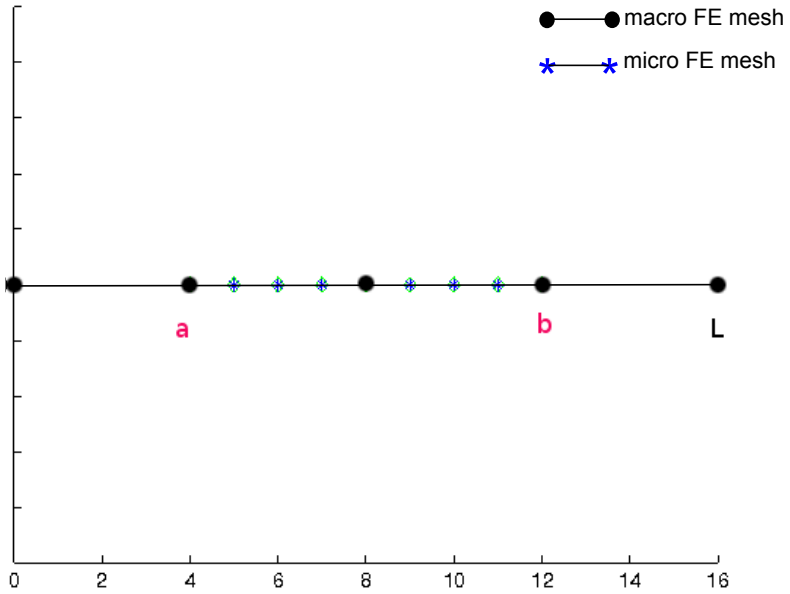

Figure 5.2: 1D problem with hierarchical macro and micro meshes

The equality between the micro and the macro fields can be written in a weak form as:

$$\int_0^L \lambda^T(x)(u_M(x) - u_m(x))dx = 0, \forall \lambda \in L^2([0, L]) \tag{5.22}$$

$\lambda(x)$ can be chosen in the macro finite element space or in the micro one. We compare these two methods in the following:

- $\lambda(x)$ in the macro finite element space:$\lambda^M(x) = [\phi^M(x)]\Lambda$

$$\int_0^L \lambda^{M^T}(x)(u^M(x) - u^m(x))dx = 0 \tag{5.23}$$

$$\int_0^L \Lambda^T [\phi^M]^T ([\phi^M] U^M - [\phi^m] U^m) dx = 0 \tag{5.24}$$

$$\Lambda^T [\underbrace{(\int_0^L [\phi^M]^T [\phi^M] dx)}_{A} U^M - \underbrace{(\int_0^L [\phi^M]^T [\phi^m] dx)}_{B} U^m] = 0 \tag{5.25}$$

$$\Rightarrow AU^M - BU^m = 0 \tag{5.26}$$

Because A is a square matrix, corresponding to finite element mass matrix, hence A is reversible. If U^m is known, we can calculate U^M from Equation (5.26). More generally, Equation (5.26) leaves $n - N$ degrees of freedom for the displacement fields.

- $\lambda(x)$ in the micro finite element space: $\lambda^m(x) = [\phi^m(x)]\Lambda$

$$\int_0^L \lambda^{m^T}(x)(u^M(x) - u^m(x)) dx = 0 \tag{5.27}$$

$$\int_0^L \Lambda^T [\phi^m]^T ([\phi^M] U^M - [\phi^m] U^m) dx = 0 \tag{5.28}$$

$$\Lambda^T [\underbrace{(\int_0^L [\phi^m]^T [\phi^M] dx)}_{A} U^M - \underbrace{(\int_0^L [\phi^m]^T [\phi^m] dx)}_{B} U^m] = 0 \tag{5.29}$$

$$\Rightarrow AU^M - BU^m = 0 \tag{5.30}$$

Because A is a $n \times N$ matrix, Equation (5.30) has n equations for $N + n$ dofs. Since n in practical case should be much larger than N, Equation (5.30) should lead to an over-constrained problem.

Consequently, $\lambda(x)$ in the macro finite element space is the reasonable choice.

We succeed to identify the 1D problem with such kind of coupling in various boundary conditions. However, the calculation becomes more complex when the macro and micro meshes are not hierarchical. Moreover, this kind of coupling depends on the size of macro mesh, not on the size of Representative Volume Element (RVE), which is more important in the coupling multi-scale problem. Hence, we turn to try the diffuse approximation method for the coupling.

5.5.1.2 Displacement coupling through diffuse approximation

The Diffuse Approximation has been initially developed to generate smooth approximation functions from a given set of data points [120] in the early 1990s. The basic idea of the diffuse approximation is to replace the "finite element

approximation" interpolation, which is valid on an element, by a local weighted least squares fitting, which is valid on a small neighborhood of a point. Later, it has been widely used in different fields, such as optimization through response surfaces [121], field transfer in non linear inelastic analysis [122] and reconstructing the gradients of noisy full-field data [123].

In our case, the macro mesh and the micro mesh will be hierarchical, so that every macro node position corresponds to a micro node position as well.

The coupling will then consist in equaling the macro displacement at any macro node k at position $\underline{x}_k$ with an approximated field estimated at $\underline{x}_k$, $u_k^M(\underline{x})$, constructed from the micro field based on diffuse approximation on a bounded neighborhood V_k of the macro node k.

Figure 5.3 illustrate a model of a coupling scheme in measured domain Ω_m. We choose the span of reconstruction R (Figure 5.3(a)) for the macro node k (red cross) to define its neighborhood V_k.

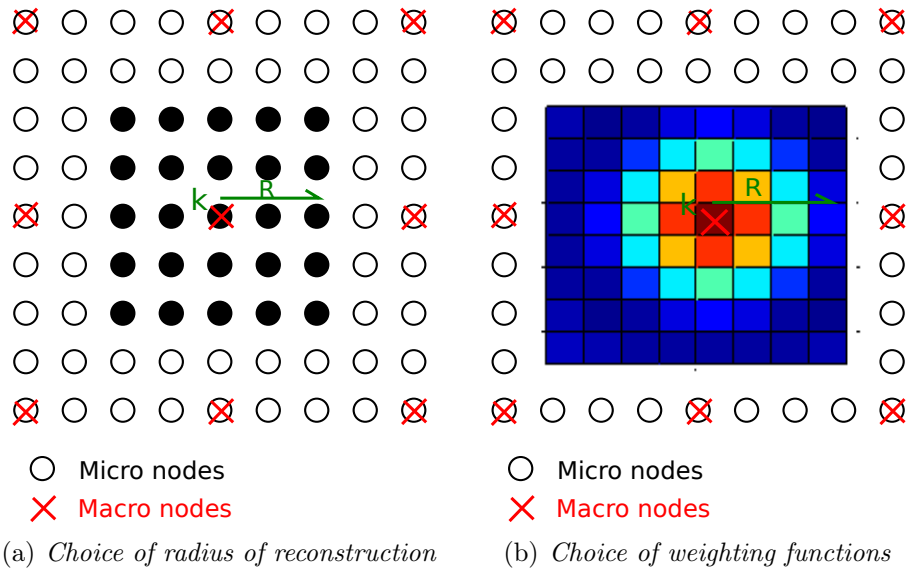

(a) *Choice of radius of reconstruction* (b) *Choice of weighting functions*

Figure 5.3: Coupling with diffuse approximation

For each component of the displacement u, the approximated field $u_k^M(\underline{x})$ is then sought as a linear combination of monomials:

$$u_k^M(\underline{x}) = \langle p(\underline{x}_k - \underline{x}) \rangle \{a^M\} = \sum_{j=1}^{m} p_j(\underline{x}_k - \underline{x}) a_j^M \tag{5.31}$$

where p is a vector of m independent functions, chosen here as polynomial terms, and $\{a^M\}$ is a vector of m parameters to be determined.

The approximated displacements at every micro nodes i in the neighborhood V_k

can be collected in a vector $\{U_k^M\}$ and expressed as a function of $\{a^M\}$:

$$\{U_k^M\} = \begin{bmatrix} \dots \\ \langle p_j(\underline{x}_k - \underline{x}_i)\rangle \\ \dots \end{bmatrix} \{a^M\} = [P_k]\{a^M\} \tag{5.32}$$

where n is the total number of micro nodes in V_k, and the matrix $[P_k]$ has n rows and m columns.

The micro displacement at the micro nodes u_i^m in V_k are collected in a vector $\{u^m\}$. The coefficients a_j^M, corresponding to the macro node k, are obtained by minimizing the following expression:

$$\mathcal{J}(a^M) = \sum_{i=1}^{n} w(\underline{x}_k - \underline{x}_i)(u_i^m - \{U_k^M\}_i)^2 \tag{5.33}$$

where $w(\underline{x}_k - \underline{x}_i)$ is a positive weighting function, which equals 0 outside V_k. It is classically chosen as a cubic spline. Relation (5.33) with (5.32) becomes:

$$\mathcal{J}(a^M) = \sum_{i=1}^{n} w(\underline{x}_k - \underline{x}_i)(u_i^m - \langle p(\underline{x}_k - \underline{x}_i)\rangle\{a^M\})^2 = (\{u^m\} - [P_k]\{a^M\})^T[W](\{u^m\} - [P_k]\{a^M\}) \tag{5.34}$$

where $[W]$ is the diagonal matrix with $W_{ii} = w(\underline{x}_k - \underline{x}_i)$.

In practice, the weighting function vanished outside V_k, thus the only nodes involved in the summation in (5.34) are located in V_k, preserving the local character of the approximation. $w(\underline{x}_k - \underline{x}_i)$ can be any positive function defined over a bounded domain. Because of the square grid of micro nodes in our case, the weighting function is defined as follows:

$$w(\underline{x}_k - \underline{x}_i) = w_{ref}(\frac{x - x_k}{R_x}) w_{ref}(\frac{y - y_k}{R_y}) \tag{5.35}$$

where w_{ref} is a dimensionless window function whose derivative zeros at 0 and 1 [123], and here $R_x = R_y = R$.

The stationarity of $\mathcal{J}(a^M)$ (5.34) with respect to $\{a^M\}$ leads to the following linear relation between $\{a^M\}$ and $\{u^m\}$:

$$\{a^M\} = ([P_k]^T[W][P_k])^{-1}[P_k]^T[W]\{u^m\} \tag{5.36}$$

Then, if the functions for the approximated field (5.31) are monomial from degree 0 to at least 1, it comes that:

- a_1 corresponds to the approximated displacement component at point $\underline{x}_k$
- a_2 corresponds to the approximated derivative with respect to x at point $\underline{x}_k$
- a_3 corresponds to the approximated derivative with respect to y at point $\underline{x}_k$

Such a reconstruction operator can be build at all the macro nodes belonging to Ω_m as the first line of the matrix system involved in Equation (5.36) for both components of the displacement. We therefore can define the coupling between the macro and micro finite element displacement as:

$$AU_c^M = BU^m \tag{5.37}$$

where U_c^M corresponds to the displacement of the macro nodes coupled with the micro ones, A is the identity matrix and B collects the corresponding first lines of Equation (5.36).

5.5.1.3 Strain coupling based on diffuse approximation

An alternative coupling consists in coupling the macro strain field to the micro strain field at the location of the macro coupled node.

In this case, the strains are reconstructed by diffuse approximation with two scales:

- apply on the macro node displacements at the macro scale
- apply on the micro node displacements at the micro scale

The neighborhood on micro and macro used in the reconstruction of diffuse approximations should have the same physical size (so the number of points for the micro diffuse approximation is more important). This size, a priori, corresponding to the order of magnitude of RVE size, ought to be studied.

As the above introduced diffuse approximation method, we only need to replace the approximated displacement field u_k^M and u_i^m by the approximated strain field ε_k^M and ε_i^m at the corresponding micro (i) and macro (k) nodes of the hierarchical meshes. Here, ε is defined as the symmetric gradient of u, which means:

$$\varepsilon = \frac{1}{2}(\nabla u + \nabla^T u) \tag{5.38}$$

$$\varepsilon = \begin{bmatrix} \varepsilon_{xx} \\ \varepsilon_{yy} \\ 2\varepsilon_{xy} \end{bmatrix} = \begin{bmatrix} \frac{\partial u_x}{\partial x} \\ \frac{\partial u_y}{\partial y} \\ \frac{\partial u_x}{\partial y} + \frac{\partial u_y}{\partial x} \end{bmatrix} \tag{5.39}$$

In order to simplify, we use the following discretization expressions as:

$$\varepsilon_k^M = \mathcal{C}_k^M U^M, \varepsilon_i^m = \mathcal{C}_i^m U^m \tag{5.40}$$

where C_k^M and C_i^m are based on (5.39) and the second and third lines of (5.36) for both displacement components.

Considering (5.40) at all the macro coupled nodes, we therefore can define the coupling between the macro and micro finite element displacement as:

$$AU_c^M = BU^m \tag{5.41}$$

where U_c^M corresponds to the displacement of the macro nodes coupled with the micro ones.

5.5.2 Coupling the stress fields

We considered two ways for coupling the stress fields: by averaging either on volumes (surface in 2D), or on lines.

5.5.2.1 Coupling on the associated displacement field

In the case where stress field is represented by a displacement field v at both scales, it is possible to use the coupling operators developed for U to couple the micro and macro V.

In order to distinguish from the coupling of the displacement fields, we express the stress field coupling relation as:

$$CV_c^M = DV^m \tag{5.42}$$

where V_c^M corresponds to the displacement of the macro nodes coupled with the micro ones, $C = A$ and $D = B$ as the coupling operators developed for U.

However, when we use these coupling operators, we find that the coupling error on stress is always large. It means that we cannot obtain reasonable V. The reason is due to unlike the displacement information, the stress information is transfered from macro field to micro field. Since macro field has fewer data points than micro field, the coupling system becomes indeterminate. Moreover, coupling on volume introduces a lot of data points, which enlarges the system and increases the calculating time.

5.5.2.2 Coupling with global load

Since coupling the stress fields on volume leads to many difficulties, the method of coupling with global load on some lines of the mesh is proposed. Advantage of this method is evident. It can avoid the indeterminate problem and guarantee the existence of V, because the number of lines for macro mesh is equal to the one for micro mesh. It is also easy and quick to calculate the global load. However, this kind of coupling will lose some homogenization sprite.

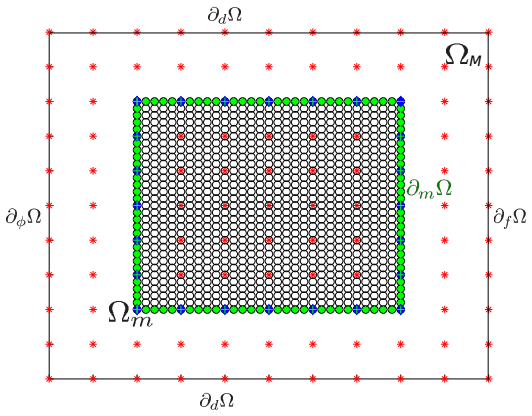

Figure 5.4: Coupling with force

The basic idea of this coupling method is simple: the force of every measurement boundary calculated by macro stress field (the green nodes in Figure 5.4) should be theoretically equal to that calculated by micro stress field (the blue nodes in Figure 5.4).

Here the boundary of the micro domain is split into four parts:

$$\partial_m\Omega = \cup_{k=1}^{4}\partial_m^k\Omega \tag{5.43}$$

Then the coupling relationship could be expressed by:

$$\int_{\partial_m^k\Omega} \underline{\underline{\sigma}}^M \cdot \underline{n} dS = \int_{\partial_m^k\Omega} \underline{\underline{\sigma}}^m \cdot \underline{n} dS,\ \forall k \in \{1,4\} \tag{5.44}$$

In order to get the corresponding equation on V (dofs of the displacement representing the stress field), we can choose particular test fields in the weak form of equilibrium (3.22) as proposed in Section 3.5.1 for the mono-scale approach.

At both scales, we choose a finite element test fields such that $\underline{u}^* = \underline{N}_k$ on $\partial_m^k\Omega$ and $\underline{0}$ elsewhere at the nodes, where $\underline{N}_k$ is the normal vector to the boundary $\partial_m^k\Omega$. Hence:

$$\int_{\Omega_m} \underline{\underline{\sigma}}^M : \underline{\underline{\varepsilon}}(\underline{u}^*_{Mk}) d\Omega = \int_{\partial^k_m \Omega} \underline{\underline{\sigma}}^M \cdot \underline{n} \cdot \underline{u}^*_{Mk} dS \tag{5.45}$$

$$\int_{\Omega_m} \underline{\underline{\sigma}}^m : \underline{\underline{\varepsilon}}(\underline{u}^*_{mk}) d\Omega = \int_{\partial^k_m \Omega} \underline{\underline{\sigma}}^m \cdot \underline{n} \cdot \underline{u}^*_{mk} dS \tag{5.46}$$

By denoting U^*_{Mk} the dofs associated to $\underline{u}^*_{Mk}$ and U^*_{mk} the dofs associated to $\underline{u}^*_{mk}$, we can deduce the discrete form of Equation (5.44), based on (5.45)-(5.46):

$$U^{*T}_{Mk} K^M V^M = U^{*T}_{mk} K^m V^m, \ \forall k \in \{1, 4\} \tag{5.47}$$

By collecting Equation (5.47) in the same matrix system, we can express the coupling equation as:

$$CV^M = DV^m \tag{5.48}$$

where the k^{th} line of C and D are: $C_k = U^{*T}_{Mk} K^M$ and $D_k = U^{*T}_{mk} K^m$.

C and D are also denoted:

$$C = U^{*T}_{dM} K^M, \ D = U^{*T}_{dm} K^m \tag{5.49}$$

where U^*_{dM} collects the lines U^*_{Mk} and U^*_{dm} collects the lines U^*_{mk}, $\forall k \in \{1, 4\}$.

5.6 Solving the basic problem

5.6.1 Choice of a displacement formulation

As for the mono-scale approach, we would like to use a displacement finite element formulation, hence representing $\underline{\underline{\sigma}}$ by a displacement field $\underline{v}$ such that:

$$\underline{\underline{\sigma}} = \underline{\underline{\sigma}}(\underline{v}) = \mathcal{C} : \underline{\underline{\varepsilon}}(\underline{v}) \tag{5.50}$$

While the existence of $\underline{v}$ in the mono-scale case can be shown easily from the equation of the basic problem, it is not straightforward for the multi-scale approach. Its existence indeed depends on the choice of the coupling operators between the scales (Section 5.5.2). The existence of $\underline{v}$ is usually based on the stationarity equation with respect to the stress $\underline{\underline{\sigma}}$. Hence the coupling on the stress will modify this equation and it needs to be further investigated in order to determine if we can construct a $\underline{v}$ field.

It is rather certain that such a field will not exist in the case of a bulk coupling operator for the micro-macro stress fields. This is one of the reasons why we first

implemented a coupling operator on the boundaries of the micro domain.

An alternative would be to use a stress-displacement formulation as in [86]. Yet, another way to circumvent this difficulty is to choose to formulate the basic problem in terms of displacement from the beginning.

As consequence, we propose here a displacement based definition of the basic problem:

Find, for a given $(\underline{\theta}^M, \underline{\theta}^m)$, $(\underline{u}^M, \underline{u}^m, \underline{v}^M, \underline{v}^m)$ such that:

$$\min_{(\underline{v}^M,\underline{v}^m)\in\mathcal{U}_{Ad},(\underline{u}^M,\underline{u}^m,\underline{\underline{\sigma}}^M(\underline{v}^M),\underline{\underline{\sigma}}^m(\underline{v}^m))\in(\mathcal{U}_{Ad}\times\mathcal{S}_{Ad})\cap\mathcal{C}_{Ad}} \mathcal{J}(\underline{u}^M, \underline{u}^m, \underline{\underline{\sigma}}^M(\underline{v}^M), \underline{\underline{\sigma}}^m(\underline{v}^m), \underline{\theta}^M, \underline{\theta}^m) \tag{5.51}$$

5.6.2 Discretization of the basic problem

Compared to the model errors, the discretization errors are considered here as negligible in the weak formulation of finite element. The macro displacement fields and the associated macro strain fields are given in the finite element form:

$$\begin{bmatrix} u_x^M(\underline{x}) \\ u_y^M(\underline{x}) \end{bmatrix} = [\Phi^M(\underline{x})]U^M, \qquad \begin{bmatrix} v_x^M(\underline{x}) \\ v_y^M(\underline{x}) \end{bmatrix} = [\Phi^M(\underline{x})]V^M \tag{5.52}$$

$$\underline{\underline{\varepsilon}}^M(\underline{u}^M) = [\mathcal{B}^M]U^M, \qquad \underline{\underline{\varepsilon}}^M(\underline{v}^M) = [\mathcal{B}^M]V^M \tag{5.53}$$

where $[\phi^M(\underline{x})]$ is the matrix of shape function for the macro mesh, U^M and V^M are the nodal unknown vectors associated with the macro displacement fields $\underline{u}^M$ and $\underline{v}^M$.

As for the macro fields, the micro displacement fields and strain fields are in the following form:

$$\begin{bmatrix} u_x^m(\underline{x}) \\ u_y^m(\underline{x}) \end{bmatrix} = [\Phi^m(\underline{x})]U^m, \qquad \begin{bmatrix} v_x^m(\underline{x}) \\ v_y^m(\underline{x}) \end{bmatrix} = [\Phi^m(\underline{x})]V^m \tag{5.54}$$

$$\underline{\underline{\varepsilon}}^m(\underline{u}^m) = [\mathcal{B}^m]U^m, \qquad \underline{\underline{\varepsilon}}^m(\underline{v}^m) = [\mathcal{B}^m]V^m \tag{5.55}$$

where $[\phi^m(\underline{x})]$ is the matrix of shape function for the micro mesh, U^m and V^m are the nodal unknown vectors associated with the micro displacement fields $\underline{u}^m$ and $\underline{v}^m$.

The functions can be written in the discrete form as follows:

- the term of macro model error:

$$\mathcal{J}_1(U^M, V^M, \underline{\theta}^M) = \frac{1}{2}(U^M - V^M)^T K^M (U^M - V^M) \tag{5.56}$$

  where K^M is the global stiffness matrix of the mechanical macro problem on Ω_M;
- the term of micro model error:

$$\mathcal{J}_2(U^m, V^m, \underline{\theta}^m) = \frac{1}{2}(U^m - V^m)^T K^m (U^m - V^m) \tag{5.57}$$

  where K^m is the global stiffness matrix of the mechanical micro problem on Ω_m;
- the term of distance to the displacement measurements:

$$\mathcal{J}_3(U^m) = \frac{1}{2}(\Pi U^m - \widetilde{U})^T (\Pi U^m - \widetilde{U}) \tag{5.58}$$

- the term of micro-macro displacement coupling error:

$$\mathcal{J}_4(U^M, U^m) = \frac{1}{2}(AU^M - BU^m)^T (AU^M - BU^m) \tag{5.59}$$

  where A and B are the displacement coupling operators defined in Section 5.5.1.

The constraint equations are deduced from the weak form of equilibrium at each scale by choosing specific virtual fields as explained in Section 3.5.1 for the mono-scale approach. At both scales, we denote the index i for internal nodes, the index g for collection of internal nodes i, free edge d and load edge f, and the index $\circ$ for all nodes. The projector Π_{gf} allows to transfer the vectors of generalized forces F_f to the vectors of generalized forces corresponding with the problems on the lines of index g.

- macro field equilibrium constraint:

$$K^M_{g\circ} V^M = \Pi_{gf} \widetilde{F}_f \tag{5.60}$$

- micro field equilibrium constraint:

$$K^m_{i\circ} V^m = 0 \tag{5.61}$$

Finally, the coupling between the micro and macro stresses is taken into account as a constraint as explained in Section 5.4.1, based on the coupling operators C and D introduced in Section 5.5.2:

$$CV^M - DV^m = 0 \tag{5.62}$$

5.6.3 Monolithic micro-macro basic problem

Firstly, we try to solve the macro and micro problems at the same time. Based on the above discretization, the basic problem writes:

Find the displacement U^M, V^M, U^m, V^m with fixed $\underline{\theta}^M$ and $\underline{\theta}^m$ minimizing:

$$\mathcal{J}(U^M, V^M, U^m, V^m, \underline{\theta}^M, \underline{\theta}^m) = \mathcal{J}_1 + \mathcal{J}_2 + \alpha\mathcal{J}_3 + \gamma\mathcal{J}_4 \tag{5.63}$$

with the constraints $K^M_{g\circ}V^M = \Pi_{gf}\widetilde{F}_f$, $K^m_{i\circ}V^m = 0$, $CV^M - DV^m = 0$.

The solution of the basic problem is denoted $(U^M(\underline{\theta}^M), V^M(\underline{\theta}^M), U^m(\underline{\theta}^m), V^m(\underline{\theta}^m))$.

This basic problem is a quadratic minimization with linear constraints, the optimality conditions of the first order are sufficient. We can use the method of Lagrange multipliers to find the local minimal of the function subject to equality constraints.

Introducing the Lagrange multipliers $\Lambda_1, \Lambda_2, \Lambda_3$:

$$\begin{aligned}\mathcal{L}(U^M, V^M, U^m, V^m, \Lambda_1, \Lambda_2, \Lambda_3) =& \mathcal{J}(U^M, V^M, U^m, V^m) + \Lambda_1^T(K^M_{g\circ}V^M - \Pi_{gf}\widetilde{F}_f) \\ &+ \Lambda_2^T(K^m_{i\circ}V^m) + \Lambda_3^T(CV^M - DV^m)\end{aligned} \tag{5.64}$$

where C and D are chosen as defined by Equation (5.49).

The differential of the Lagrangian $d\mathcal{L}$ is expressed:

$$\left\{\begin{array}{rcl}
(\frac{\partial\mathcal{L}}{\partial U^M}, \delta U^M) &=& \delta {U^M}^T K^M(U^M - V^M) + \delta {U^M}^T\gamma A^T(AU^M - BU^m) \\
(\frac{\partial\mathcal{L}}{\partial V^M}, \delta V^M) &=& \delta {V^M}^T K^M(V^M - U^M) + \delta {V^M}^T K^M_{\circ g}\Lambda_1 + \delta {V^M}^T K^M U^*_{dM}\Lambda_3 \\
(\frac{\partial\mathcal{L}}{\partial U^m}, \delta U^m) &=& \delta {U^m}^T K^m(U^m - V^m) + \delta {U^m}^T\alpha\Pi^T(\Pi U^m - \widetilde{U}) + \delta {U^m}^T\gamma B^T(BU^m - AU^M) \\
(\frac{\partial\mathcal{L}}{\partial V^m}, \delta V^m) &=& \delta {V^m}^T K^m(V^m - U^m) + \delta {V^m}^T K^m_{\circ i}\Lambda_2 - \delta {V^m}^T K^m U^*_{dm}\Lambda_3 \\
(\frac{\partial\mathcal{L}}{\partial\Lambda_1}, \delta\Lambda_1) &=& \delta\Lambda_1^T(K^M_{g\circ}V^M - \Pi_{gf}\widetilde{F}_f) \\
(\frac{\partial\mathcal{L}}{\partial\Lambda_2}, \delta\Lambda_2) &=& \delta\Lambda_2^T(K^m_{i\circ}V^m) \\
(\frac{\partial\mathcal{L}}{\partial\Lambda_3}, \delta\Lambda_3) &=& \delta\Lambda_3^T(U^{*T}_{dM}K^M V^M - U^{*T}_{dm}K^m V^m)
\end{array}\right. \tag{5.65}$$

The stationarity system is $d\mathcal{L} = 0$, and finally we write the equations in a matrix manner, in terms of U^M, U^m and the Lagrange multipliers:

$$\begin{bmatrix} \gamma A^T A & -\gamma A^T B & K^M_{\circ g} & 0 & K^M U^*_{dM} \\ -\gamma B^T A & \alpha \Pi^T \Pi + \gamma B^T B & 0 & K^m_{\circ i} & -K^m U^*_{dm} \\ K^M_{g\circ} & 0 & -K^M_{gg} & 0 & -K^M_{g\circ} U^*_{dM} \\ 0 & K^m_{i\circ} & 0 & -K^m_{ii} & K^m_{i\circ} U^*_{dm} \\ U^{*T}_{dM} K^M & -U^{*T}_{dm} K^m & -U^{*T}_{dM} K^M_{\circ g} & U^{*T}_{dm} K^m_{\circ i} & -U^{*T}_{dM} K^M U^*_{dM} - U^{*T}_{dm} K^m U^*_{dm} \end{bmatrix} \begin{bmatrix} U^M \\ U^m \\ \Lambda_1 \\ \Lambda_2 \\ \Lambda_3 \end{bmatrix} = \begin{bmatrix} 0 \\ \alpha \Pi^T \widetilde{U} \\ \Pi_{gf} \widetilde{F}_f \\ 0 \\ 0 \end{bmatrix} \tag{5.66}$$

V^M and V^m can be deduced as:

$$V^M = U^M - \Lambda_1 - U^*_{dM} \Lambda_3 \tag{5.67}$$

$$V^m = U^m - \Lambda_2 + U^*_{dm} \Lambda_3 \tag{5.68}$$

The system (5.66) can be solved numerically. Yet, it can be noted that it may be rank deficient or badly scaled leading to the use of a truncated QR algorithm [38]. Furthermore, the numbers of dofs is about three times the number of macro dofs plus two times the number of micro ones, leading to a possibly quite large system.

Then, the identification step is based on the cost function defined as:

$$\mathcal{G}(\underline{\theta}^M, \underline{\theta}^m) = \mathcal{J}(U^M(\underline{\theta}^M), V^M(\underline{\theta}^M), U^m(\underline{\theta}^m), V^m(\underline{\theta}^m), \underline{\theta}^M, \underline{\theta}^m) \tag{5.69}$$

The identification of $\underline{\theta}^M$ and $\underline{\theta}^m$ is performed as the minimization of $\mathcal{G}(\underline{\theta}^M, \underline{\theta}^m)$:

$$(\underline{\theta}^M_{opt}, \underline{\theta}^m_{opt}) = \text{Arg} \min_{\underline{\theta}^M, \underline{\theta}^m} \mathcal{G}(\underline{\theta}^M, \underline{\theta}^m) \tag{5.70}$$

5.6.4 Micro-macro iterative solution

Due to the drawbacks associated with the monolithic approach, it is proposed here to split the basic problem into a coupled problem: one at the micro scale and the other one at the macro scale that are to be solved iteratively.

5.6.4.1 The coupled micro and macro basic problems

Considering given macro material parameters $\underline{\theta}^M$ and macro mechanical fields U^M, V^M, the macro basic problem is defined as follows:

Find the macro displacement U^M, V^M with fixed macro parameters $\underline{\theta}^M$ and known micro U^m and V^m minimizing:

$$\mathcal{J}^M(U^M, V^M) = \mathcal{J}_1 + \gamma \mathcal{J}_4 \tag{5.71}$$

with the macro constraints $K^M_{g\circ} V^M = \Pi_{gf} \widetilde{F}_f$.

The solution of (5.71) is denoted: $U^M(\underline{\theta}^M, U^m, V^m), V^M(\underline{\theta}^M, U^m, V^m)$.

The equations associated with (5.71) are obtained from the stationarity of the following Lagrangian:

$$\mathcal{L}(U^M, V^M, \Lambda_1) = \mathcal{J}(U^M, V^M) + \Lambda_1^T (K^M_{g\circ} V^M - \Pi_{gf} \widetilde{F}_f) \tag{5.72}$$

The differential of the Lagrangian $d\mathcal{L}$ is expressed as:

$$\left\{ \begin{array}{rcl} (\frac{\partial \mathcal{L}}{\partial U^M}, \delta U^M) & = & \delta {U^M}^T K^M (U^M - V^M) + \delta {U^M}^T \gamma A^T (A U^M - B U^m) \\ (\frac{\partial \mathcal{L}}{\partial V^M}, \delta V^M) & = & \delta {V^M}^T K^M (V^M - U^M) + \delta {V^M}^T K^M_{\circ g} \Lambda_1 \\ (\frac{\partial \mathcal{L}}{\partial \Lambda_1}, \delta \Lambda_1) & = & \delta \Lambda_1^T (K^M_{g\circ} V^M - \Pi_{gf} \widetilde{F}_f) \end{array} \right. \tag{5.73}$$

The stationarity system is $d\mathcal{L} = 0$, and finally it leads to the following equations in terms of U^M and Λ_1 corresponding to the macro basic problem:

$$\begin{bmatrix} \gamma A^T A & K^M_{\circ g} \\ K^M_{g\circ} & -K^M_{gg} \end{bmatrix} \begin{bmatrix} U^M \\ \Lambda_1 \end{bmatrix} = \begin{bmatrix} \gamma A^T B U^m \\ \Pi_{gf} \widetilde{F}_f \end{bmatrix} \tag{5.74}$$

Then, for given micro material parameters $\underline{\theta}^m$ and macro displacements U^M, V^M, the micro basic problem is defined as follows:

Find the micro displacement U^m, V^m with fixed micro parameters $\underline{\theta}^m$ and known macro U^M, V^M minimizing:

$$\mathcal{J}^m(U^m, V^m) = \mathcal{J}_2 + \alpha \mathcal{J}_3 \tag{5.75}$$

with the micro constraints $K^m_{i\circ} V^m = 0$, $D V^m = C V^M$

The solution of (5.75) is denoted: $U^m(\underline{\theta}^m, U^M, V^M), V^m(\underline{\theta}^m, U^M, V^M)$.

The equations associated with (5.75) are obtained from the stationarity of the following Lagrangian:

$$\mathcal{L}(U^m, V^m, \Lambda_2, \Lambda_3) = \mathcal{J}(U^m, V^m) + \Lambda_2^T (K^m_{i\circ} V^m) + \Lambda_3^T (D V^m - C V^M) \tag{5.76}$$

The differential of the Lagrangian $d\mathcal{L}$ is expressed as:

$$\left\{\begin{array}{rcl} (\frac{\partial \mathcal{L}}{\partial U^m}, \delta U^m) & = & \delta U^{mT} K^m (U^m - V^m) + \delta U^{mT} \alpha \Pi^T (\Pi U^m - \widetilde{U}) \\ (\frac{\partial \mathcal{L}}{\partial V^m}, \delta V^m) & = & \delta V^{mT} K^m (V^m - U^m) + \delta V^{mT} K^m_{\circ i} \Lambda_2 + \delta V^{mT} K^m U^*_{dm} \Lambda_3 \\ (\frac{\partial \mathcal{L}}{\partial \Lambda_2}, \delta \Lambda_2) & = & \delta \Lambda_2^T (K^m_{i\circ} V^m) \\ (\frac{\partial \mathcal{L}}{\partial \Lambda_3}, \delta \Lambda_3) & = & \delta \Lambda_3^T (U^{*T}_{dm} K^m V^m - U^{*T}_{dM} K^M V^M) \end{array}\right. \tag{5.77}$$

The stationarity system is $d\mathcal{L} = 0$, and finally we write the equations in terms of U^m, Λ_2 and Λ_3 corresponding to the micro basic problem:

$$\begin{bmatrix} \alpha \Pi^T \Pi & K^m_{\circ i} & K^m U^*_{dm} \\ K^m_{i\circ} & -K^m_{ii} & -K^m_{i\circ} U^*_{dm} \\ U^{*T}_{dm} K^m & -U^{*T}_{dm} K^m_{\circ i} & -U^{*T}_{dm} K^m U^*_{dm} \end{bmatrix} \begin{bmatrix} U^m \\ \Lambda_2 \\ \Lambda_3 \end{bmatrix} = \begin{bmatrix} \alpha \Pi^T \widetilde{U} \\ 0 \\ U^{*T}_{dM} K^M V^M \end{bmatrix} \tag{5.78}$$

Consequently we solve the basic problem with smaller matrix which could be calculated faster and more stable. The problems (5.74) and (5.78) are then solved iteratively, through a fixed point scheme. In order to initiate the algorithm, we define the micro displacement by projecting in a least square manner the measurements on the finite element mesh: $U^m = (\Pi^T \Pi)^{-1} \Pi^T \widetilde{U}$.

5.6.4.2 Identification step

From the solution of the macro basic problem, we define the macro cost function:

$$\mathcal{G}^M(\underline{\theta}^M) = \mathcal{J}^M(U^M(\underline{\theta}^M), V^M(\underline{\theta}^M), \underline{\theta}^M) \tag{5.79}$$

The identification of $\underline{\theta}^M$ is performed as the minimization of $\mathcal{G}^M(\underline{\theta}^M)$:

$$\underline{\theta}^M_{opt} = \mathrm{Arg} \min_{\underline{\theta}^M} \mathcal{G}^M(\underline{\theta}^M) \tag{5.80}$$

Then, from the solution of the micro basic problem, we can define the micro cost function:

$$\mathcal{G}^m(\underline{\theta}^m) = \mathcal{J}^m(U^m(\underline{\theta}^m), V^m(\underline{\theta}^m), \underline{\theta}^m) \tag{5.81}$$

The identification of $\underline{\theta}^m$ is performed as the minimization of $\mathcal{G}^m(\underline{\theta}^m)$:

$$\underline{\theta}^m_{opt} = \mathrm{Arg} \min_{\underline{\theta}^m} \mathcal{G}^m(\underline{\theta}^m) \tag{5.82}$$

There are two possibilities to deal with the identification step:

- We can solve (5.74) and (5.78) for a given $\underline{\theta}$, until convergence is reached, based

on the proposed criterion, and perform the identification of $\underline{\theta}^M$ and $\underline{\theta}^m$ by the minimization of $(\mathcal{J}^M + \mathcal{J}^m)$. This corresponds to a sequential minimization of $\mathcal{J}$ with respect to $\underline{\theta}$ and the mechanical fields on the whole two-scale problem;

- We can also perform the identification step at each scale within the fixed point algorithm. In this case, (5.71) and (5.80) are solved sequentially at the macro step before moving to the micro step. Then (5.75) and (5.82) are solved sequentially at the micro scale before keeping on the iteration of the fixed point algorithm.

Here, we chose the second identification strategy, because the values of the two scales cost function $\mathcal{J}$ are of different orders of magnitude, and the sensibilities of $\mathcal{J}$ on $\underline{\theta}^M$ and $\underline{\theta}^m$ are also different. It is difficult to reach convergence when we use the first identification step. In order to avoid this difficulty, we also need to define different convergence criterion for the macro and micro parameters in the second identification step.

5.7 Conclusion

This chapter introduced a multi-scale identification strategy based on the modified constitutive relation error. It allows to identify the global homogeneous properties of the whole specimen and also the local heterogeneous properties of the sub-part measurement zone. We proposed two coupling scheme, one based on diffuse approximation and the other one based on load, which can combine the stress and displacement fields at both the micro and the macro scales. As for the mono-scale approach, the equations are split according to the reliability of information and here we consider the coupling on displacement as less reliable while the coupling on stress as reliable. Two multi-scale algorithms are proposed for the basic problem depending on the size of problem system. The applications of this multi-scale approach will be presented in the next chapter.

Application of multi-scale identification

Contents

6.1 Introduction

This chapter aims at showing the applications of the multi-scale identification based on Modified Constitutive Relation Error. First of all, we need to study the reliability of the coupling equations and choose a suitable multi-scale basic problem formulation. Then in order to illustrate this methodology, two steps of validation are presented. On the first step, only the macro properties are identified for both homogeneous and heterogeneous examples. The frames of local errors are studied with the identification results. In order to validate the accuracy of macro properties for heterogeneous example, we compare with the result of numerical homogenization. Then on the second step, all the macro and micro properties are identified for both tension and bending tests. The effects of measurement zone size and noise are analyzed for the effectiveness of such method. The multi-scale identification results are also compared with those using mono-scale method for the macro problem. At last, an heterogeneous example with real material properties is studied.

6.2 Study of the reliability of the coupling equations

The first study is focused on the choice of a suitable basic problem formulation. Section 5.4.1 shows that the coupling equations could be considered as constraints or functionals depending on their reliability. Here, we explain our choice in details based on numerical examples.

6.2.1 Framework

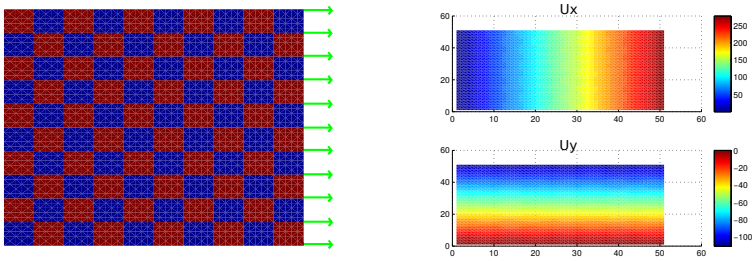

(a) Reference calculation (b) U reference displacement field

Figure 6.1: Numerical example of tension test: reference calculation and simulated displacement exact measurement

The calculation is performed representing a tensile test on a plate as sketched in Figure 6.1(a), with reference values of local isotropic elastic Lamé parameters (blue composition: λ_1, μ_1 and red composition: λ_2, μ_2) under assumption of plane stress. The right edge is under uniform pressure, while the left edge is fixed on the horizontal direction and one node is clamped to avoid rigid body motion, the upper and bottom edges are free. The displacements obtained from this calculation are transferred on a regular grid (51×51 data points) representing the DIC measurement grid and are illustrated on Figure 6.1(b). Since the effect of the various boundaries formulation (traction distribution or global load, reliable or less reliable) have been studied for the mono-scale approach, in the following examples, we only consider the case of reliable traction distribution (with no false assumption) to be studied in detail.

6.2.2 Comparison of multi-scale basic problem

Various possible basic problem formulations for various study cases (Table 5.2) are derived in Table 5.3. We fix the parameters of heterogeneous reference properties ($\lambda_1 = 0.9$, $\lambda_2 = 0.8$, $\mu_1 = 0.7$, $\mu_2 = 0.5$) and calculate the basic problem directly.

Table 6.1 presents the rank deficiency and the condition number of the matrix associated to the basic problem and the cost function for the multi-scale basic problem for the various study cases.

Table 6.1: Comparison of multi-scale basic problem

	Study case	1	2	3	4
Macro	matrix rank deficiency	80	80	0	0
	condition number	Inf	Inf	5.6357e+07	5.6357e+07
	$\mathcal{J}^M$	3.3438	3.3438	0.0317	0.0317
	$\mathcal{J}_1$	3.3438	3.3438	7.4078e-04	7.4078e-04
	$\mathcal{J}_4$	/	/	0.7939	0.7939
Micro	matrix rank deficiency	0	0	0	0
	condition number	1.0581e+06	1.9164e+16	1.4566e+16	9.9296e+05
	$\mathcal{J}^m$	1.0493e-04	1.0474e-04	1.1018e-04	1.1027e-04
	$\mathcal{J}_2$	1.8586e-07	1.8515e-07	1.9455e-07	1.9534e-07
	$\mathcal{J}_3$	0.0539	0.0538	0.0566	0.0567
	$\mathcal{J}_5$	/	3.2431e-07	3.4098e-07	/

From the comparison, we found that the cost functions are very large in Case 1 and Case 2 due to the deficient rank. It means that the constraints of coupling on displacement are too strong, so we need to relax the constraints. However, if we relax all the coupling constraints and put them in the cost function, as in Case 3, although the cost function seems small, the condition number of the system is too large and the basic problem may be badly solved. As a consequence, Case 4 appears to be the best choice in the treated cases for the proposed couplings. We thus define the coupling on stress as constraint, and the coupling on displacement within the functional in order to present the implantation and the identification in the following examples.

6.3 Identification of macro properties

In order to validate the multi-scale identification approach, the first step is to identify only the macro properties of the sample assuming the micro properties are known. The framework is the same as in Section 6.2.1.

6.3.1 Example 4: a homogeneous plate

The first test is performed with homogeneous reference properties ($\lambda_1 = \lambda_2 = 1$, $\mu_1 = \mu_2 = 0.5$). We fix the micro parameters and identify the macro ones.

λ_M	μ_M	$\mathcal{J}$	$\mathcal{J}_1$	$\mathcal{J}_2$	$\mathcal{J}_3$	$\mathcal{J}_4$
1	0.5	$4.5239e^{-11}$	$6.9068e^{-12}$	$1.6913e^{-19}$	$6.4229e^{-14}$	$1.3528e^{-9}$

Table 6.2: The identification results of macro properties of a homogeneous plate

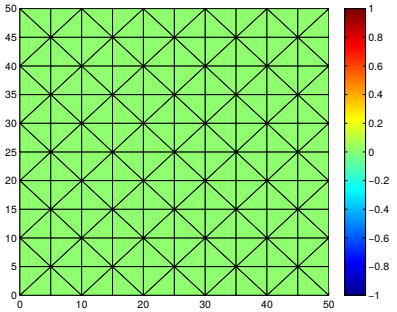

(a) Local macro constitutive relation error

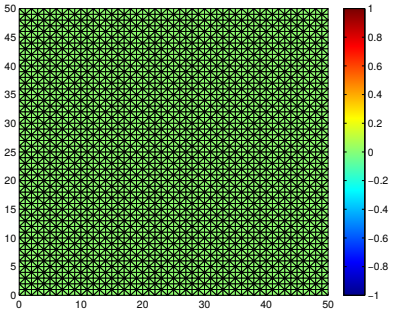

(b) Local micro constitutive relation error

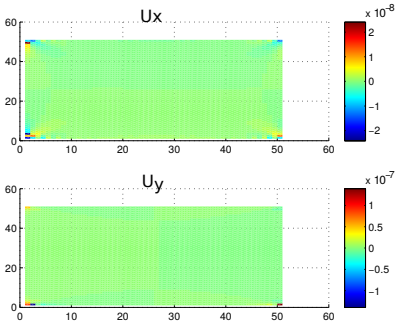

(c) Local displacement measurement error

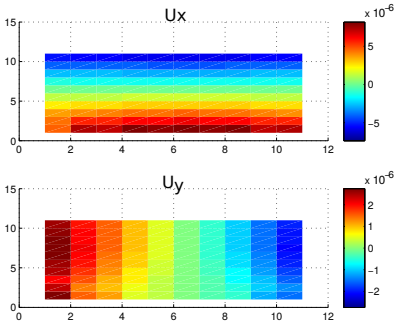

(d) Local coupling error with displacement

Figure 6.2: Local contributions to the terms of $\mathcal{J}$ - case of a homogeneous plate

Table 6.2 shows the identification results of macro properties and the various terms of the objective function ($\mathcal{J} = \mathcal{J}_1 + \mathcal{J}_2 + \alpha\mathcal{J}_3 + \gamma\mathcal{J}_4$). We can find that the value of identified macro parameters are equal to the reference value of micro parameters. The values of the objective function terms are also very small, which could be examined by the frame of local error (Figure 6.2). Because we obtain the exact values of parameters, the local macro and micro constitutive relation errors are uniform and almost equal to 0 (Figure 6.2(a)-6.2(b)). Although the local displacement measurement error is also small, there is some error concentration at the corner of the plate (Figure 6.2(c)) due to the error of compulsive assumption of boundary condition. On the contrary, the local coupling error with displacement appears to be symmetric (Figure 6.2(d)), which means the coupling operator with diffuse approximation plays a role in the average when the material is homogeneous.

6.3.2 Example 5: a heterogeneous plate

The second test is changed to the case of heterogeneous reference properties ($\lambda_1 = 0.9$, $\lambda_2 = 0.8$, $\mu_1 = 0.7$, $\mu_2 = 0.5$). We fix the micro parameters to the exact ones and identify the macro ones.

λ_M	μ_M	$\mathcal{J}$	$\mathcal{J}_1$	$\mathcal{J}_2$	$\mathcal{J}_3$	$\mathcal{J}_4$
0.8483	0.6472	0.0921	0.0057	$3.1498e^{-8}$	0.0103	2.3444

Table 6.3: The identification results of macro properties of a heterogeneous plate

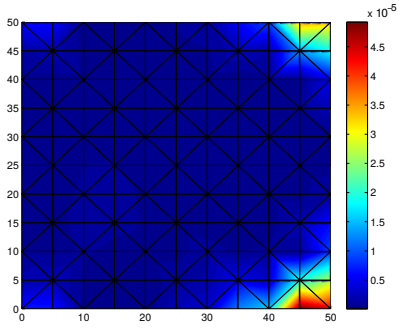

(a) Local macro constitutive relation error

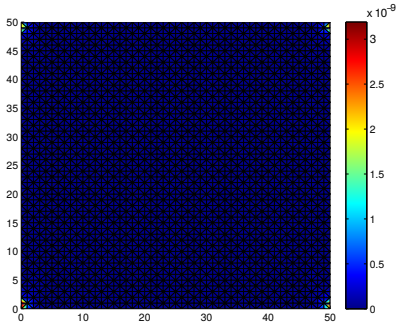

(b) Local micro constitutive relation error

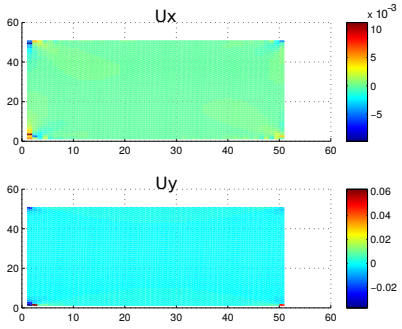

(c) Local displacement measurement error

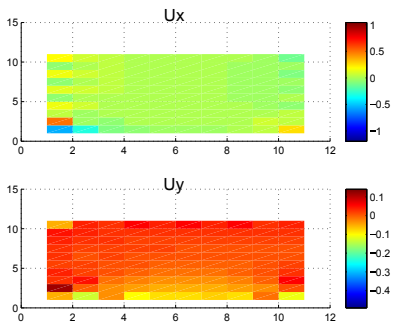

(d) Local coupling error with displacement

Figure 6.3: Local contributions to the terms of $\mathcal{J}$ - case of a heterogeneous plate

Table 6.3 presents the identification results of macro properties and the various terms of the objective function ($\mathcal{J} = \mathcal{J}_1 + \mathcal{J}_2 + \alpha\mathcal{J}_3 + \gamma\mathcal{J}_4$). In the heterogeneous case, the identified macro parameters are between the two values of micro parameters ($\lambda_1 > \lambda_M > \lambda_2$, $\mu_1 > \mu_M > \mu_2$). The value of the objective function remains small, but it is larger than in the homogeneous case, especially concerning the term of coupling with displacement $\mathcal{J}_4$. Figure 6.3 shows the local contributions to the

terms of $\mathcal{J}$. The local macro and constitutive relation error is concentrated at the corner of the plate (Figure 6.3(a)), as is the local displacement measurement error (Figure 6.3(c)). However, we can find that the local coupling error with displacement distributes on the whole plate, but it is more important on the load boundary and the fixed edge (Figure 6.3(d)). It means that the coupling operator with diffuse approximation functions better on the center part than on the edges.

In order to validate the identification results of the heterogeneous plate, we compare them with the results of a numerical homogenization [124]. After calculation, we find that the identified properties are very close to those obtained by numerical homogenization: $\lambda_M^H = 0.8483$, $\mu_M^H = 0.6476$. It is clearly shown that the first validation of the multi-scale approach succeeded.

6.4 Identification of macro and micro properties

6.4.1 Example 6: tension test

The second step to validate the multi-scale identification approach is to identify both the macro and micro properties. We carry out the calculation on the same case as Example 5 (Section 6.3.2) (Figure 6.1(a)), hence with heterogeneous properties. We use BFGS to carry out the minimization, but BFGS appears to be too slow to perform convergence for the micro problem, which is due to a very elongated valley of the objective function. In order to speed up the convergence, we try to add a relaxation on the parameters after every iteration step:

$$\underline{\theta}_{n+1} = p\underline{\theta}^0_{n+1} + (1-p)\underline{\theta}_n \tag{6.1}$$

where $\underline{\theta}_n$ are the previous iteration parameters, $\underline{\theta}^0_{n+1}$ are the original new parameters obtained from the previous step based on a classic method, $\underline{\theta}_{n+1}$ are the final new enter parameters and $0 < p < 1$ is the weighting coefficient, here we chose $p = 0.8$.

However, it is difficult to add this relaxation on every new iteration when we use BFGS, because for BFGS, we used the function "fmincon" in *Matlab* as a "black box". That is why we choose MMA with such an added relaxation step. A quick convergence is achieved by this method.

λ_M	μ_M	λ_1	λ_2	μ_1	μ_2	$\mathcal{J}$	$\mathcal{J}_1$	$\mathcal{J}_2$	$\mathcal{J}_3$	$\mathcal{J}_4$
0.8483	0.6472	0.9001	0.8001	0.7	0.6	0.0921	0.0057	$3.1353e^{-8}$	0.0102	2.3444

Table 6.4: The identification results of macro and micro properties of a heterogeneous plate on the tension test

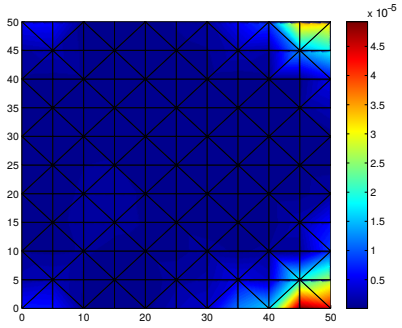

(a) Local macro constitutive relation error

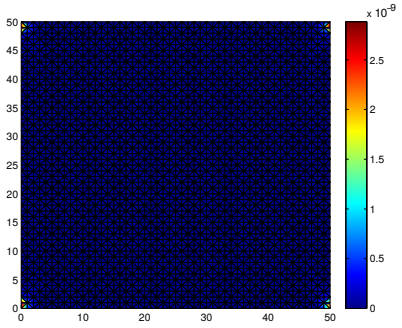

(b) Local micro constitutive relation error

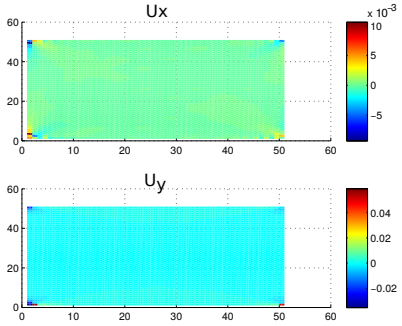

(c) Local displacement measurement error

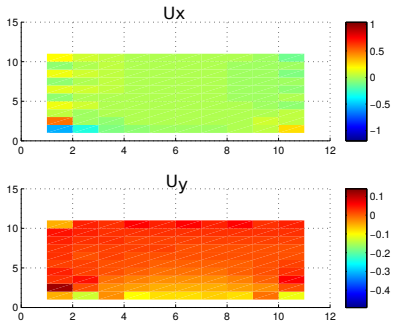

(d) Local coupling error with displacement

Figure 6.4: Local contributions to the terms of $\mathcal{J}$ - case of a heterogeneous plate for identifying both macro and micro properties on the tension test

From Table 6.4, in the part of macro identification, we find $\lambda_M = 0.8483$ and $\mu_M = 0.6472$, which are validated based on numerical homogenization. In the part of micro identification, the identified micro values are almost equal to the reference values. Figure 6.4 shows the local error of the functional for the identified properties. Similarly to the heterogeneous case with only macro parameters identification, the most important error is the coupling error in terms of displacement. From this point of view, we succeed to validate the multi-scale approach for identifying both the macro and micro parameters together. In order to further illustrate the robustness of this multi-scale approach, in the following analysis, we will study the effect of the size of the measurement zone and the effect of noise on the identification results.

6.4.1.1 Effect of the size of the measurement zone

The proposed multi-scale formulation allows to perform the identification on a zone where the displacements are measured through DIC on a sub-part of the identification zone. To illustrate this, the same measurement zone size is treated in various sizes of specimen as shown Figure 6.5. The ratio of the size of the

measurement zone to the global size is characterized by the ratio of its surface S_m to the global identification surface S_i: $\frac{S_m}{S_i}$.

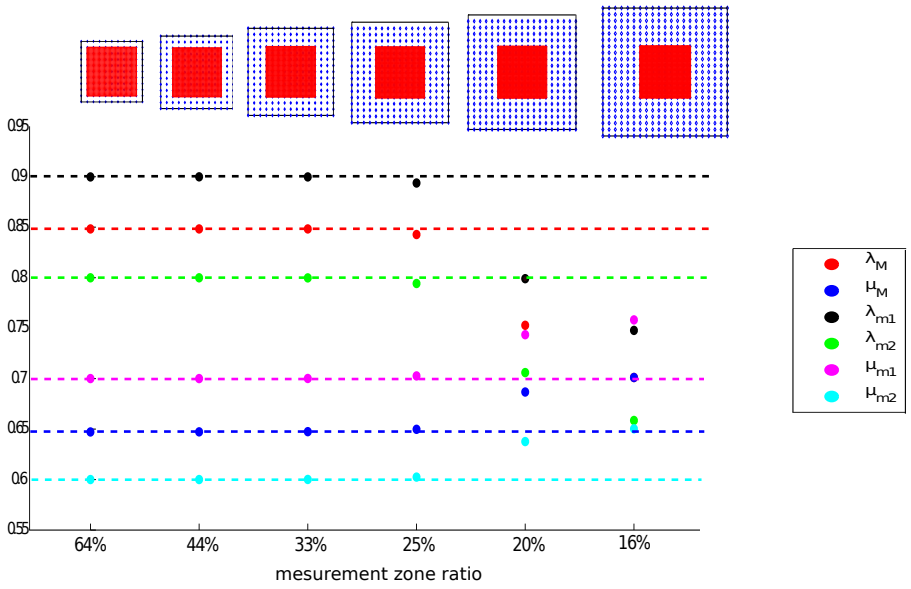

Figure 6.5: Comparison of identified θ_k for various measurement zone sizes on the tension test

	reference value	64%	44%	33%	25%	20%	16%
λ_M	0.8483	0.8483	0.8483	0.8483	0.8427	0.7528	0.7011
μ_M	0.6472	0.6472	0.6473	0.6474	0.6498	0.6867	0.7011
$\lambda_m 1$	0.9	0.8998	0.8999	0.8998	0.8938	0.7990	0.7478
$\lambda_m 2$	0.8	0.7999	0.7999	0.7998	0.7942	0.7060	0.6585
$\mu_m 1$	0.7	0.7000	0.7000	0.7001	0.7027	0.7435	0.7582
$\mu_m 2$	0.6	0.6000	0.6000	0.6001	0.6024	0.6376	0.6503

Table 6.5: The identification results of macro and micro properties for various measurement zone sizes on the tension test

Figure 6.5 and Table 6.5 present the identification results for various measurement zone size. Obviously, until the ratio reduces to 25%, the method of multi-scale is very effective and the identification results are accurate. However, when the ratio is smaller than 25%, the identification results lose accuracy. The reason is that measurement zone is far away from the boundary, and it loses too many information. The problem becomes ill-conditioned with a high condition number in the field of numerical analysis. The solving of the basic problem should have to be further investigated in this framework.

6.4.1.2 Effect of noise

We choose two different ratios of measurement size (64% and 25%) to analyze the effect of noise. Figure 6.6 shows the identification results on 100 samples with a 1% measurement noise for each ratio, in terms of mean value and standard deviation of the identified $\frac{\theta_k}{\theta_{ref}}$ properties. The first point to be noticed is that the multi-scale method can lead to a reasonable identification result from disturbed measurement. Then, as could be expected, the identification results are more sensitive to the noise when the ratio of measurement zone size reduces.

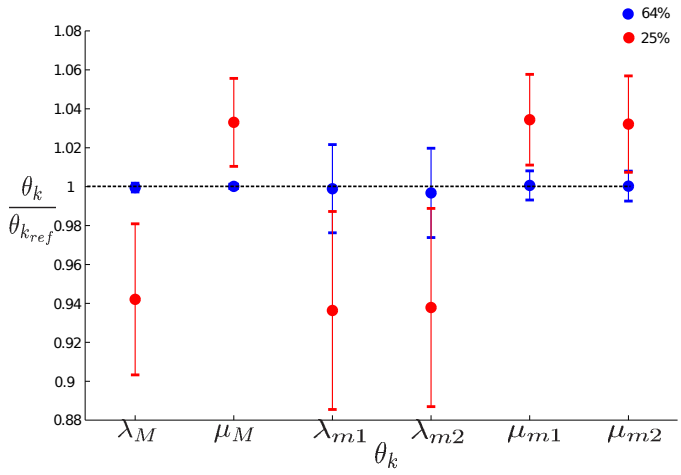

Figure 6.6: Comparison of identified $\frac{\theta_k}{\theta_{k_{ref}}}$ on 100 samples of 64% and 25% measurement zone sizes (mean value and standard deviation) with a 1% noise on the tension test

6.4.1.3 Mono-scale method for the macro problem

In all the above examples, displacements at the two scales are coupled through diffuse approximation. Yet, we address here the question of identifying the macro properties from the measurements through a mono-scale approach (despite the fact the measurement are rather at the micro-scale). It is therefore proposed to transfer the displacement measurement to the macro scale using the operator Π_M. The function of Π_M is the same as the one of Π in the mono-scale approach: transfer the finite element field to the data grid based on the FE shape functions. The difference is the mesh size for the finite element field. Here, Π_M transfers the macro finite element field to the data grid. Meanwhile, the micro basic problem keeps the same as the one in the multi-scale approach. To compare the results with Figure 6.5 and Table 6.5, Figure 6.7 and Table 6.6 show the identified θ_k for various measurement zone sizes on the tension test with mono-scale method for the macro problem. The

ratio of the size of the measurement zone to the global size is characterized by the ratio of its surface S_m to the global identification surface S_i: $\frac{S_m}{S_i}$.

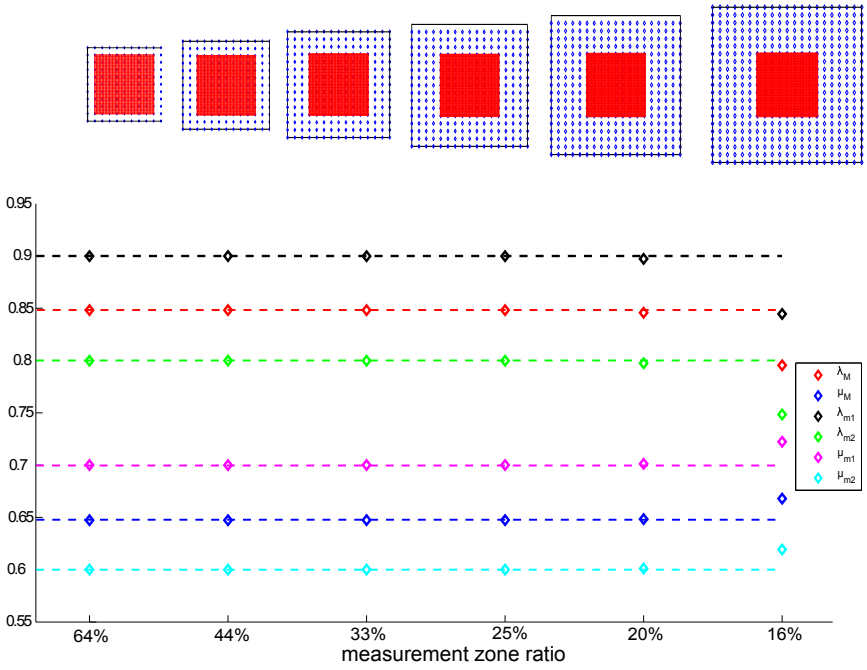

Figure 6.7: Comparison of identified θ_k for various measurement zone sizes on the tension test with mono-scale method for the macro problem

	reference value	64%	44%	33%	25%	20%	16%
λ_M	0.8483	0.8482	0.8482	0.8482	0.8482	0.8457	0.7954
μ_M	0.6472	0.6473	0.6473	0.6474	0.6474	0.6484	0.6679
$\lambda_m 1$	0.9	0.8998	0.8999	0.8998	0.8998	0.8972	0.8445
$\lambda_m 2$	0.8	0.7998	0.7999	0.7998	0.7998	0.7974	0.7484
$\mu_m 1$	0.7	0.7001	0.7000	0.7001	0.7001	0.7012	0.7223
$\mu_m 2$	0.6	0.6001	0.6000	0.6001	0.6001	0.6011	0.6193

Table 6.6: The identification results of macro and micro properties for various measurement zone sizes on the tension test with mono-scale method for the macro problem

Obviously, until the ratio reduces to 20%, this method is very effective and the identification results are accurate. It is a little better than that using diffuse approximation coupling, especially for the ratio under 20%. However, when the ratio is too small, the identification results also lose accuracy. The reason is the same as above: measurement zone is far away from the boundary, and it loses too many information. The problem becomes ill-conditioned with a high condition number in the field of numerical analysis. Moreover, this mono-scale method for the macro problem is not always effective, such as in the case of bending test. We will show the details in Section 6.4.2.4.

6.4.2 Example 7: bending test

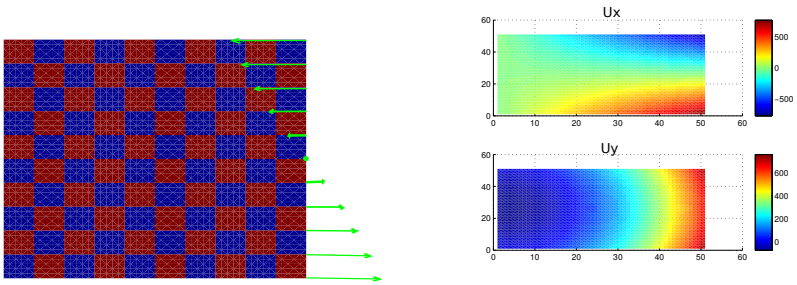

(a) Reference calculation (b) U reference displacement field

Figure 6.8: Numerical example of bending test: reference calculation and simulated displacement exact measurement

In order to extend the approach of multi-scale identification to other mechanical experiments, a bending test is taken into account. The calculation is performed representing a bending test on the half part of a symmetric plate as sketched in Figure 6.8(a), with reference values of local composition elastic Lamé parameters (blue composition: λ_1, μ_1 and red composition: λ_2, μ_2) under assumption of plane stress. The left edge is fixed on the horizontal direction and one node is clamped to avoid rigid body motion, the upper and bottom edges are free. The displacements obtained from this calculation are transferred on a regular grid (51×51 data points) representing the DIC measurement grid size and are illustrated on Figures 6.8(b). Some noise can be added to these exact fields in order to represent the measurement perturbations. The magnitude of the additive noise is given in percent of the mean value of the displacements or the mean value of the load measurement. For the bending examples, we consider the case of reliable global load M-CRE formulation to be studied in detail.

λ_M	μ_M	λ_1	λ_2	μ_1	μ_2	$\mathcal{J}$	$\mathcal{J}_1$	$\mathcal{J}_2$	$\mathcal{J}_3$	$\mathcal{J}_4$
0.8402	0.6466	0.9008	0.7995	0.7002	0.6003	3.86	0.02	$3.42e^{-6}$	4.01	258.91

Table 6.7: The identification results of macro and micro properties of a heterogeneous plate on the bending test

From Table 6.7, in the part of macro identification, we find $\lambda_M = 0.8402$ and $\mu_M = 0.6466$, which are close to the values obtained from numerical homogenization. In the part of micro identification, the identified micro values are almost equal to the reference values. However, all the identification results for the bending test have a little more error compared to those for the tension test. The reason can be

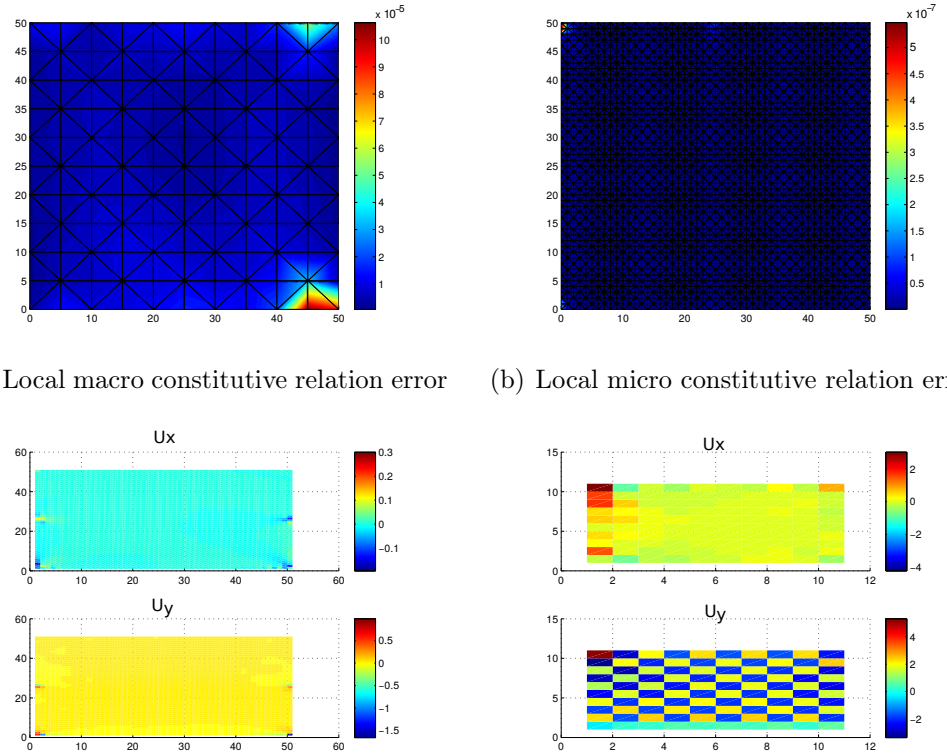

(a) Local macro constitutive relation error (b) Local micro constitutive relation error

(c) Local displacement measurement error (d) Local coupling error with displacement

Figure 6.9: Local contributions to the terms of $\mathcal{J}$ - case of a heterogeneous plate for identifying both macro and micro properties on the bending test

found from Figure 6.9, which shows the local error for the identified properties. The displacement measurement errors 6.9(c) and the coupling errors with different scale of displacement 6.9(d) are greater than those on tension test. In order to further illustrate the robustness of this multi-scale approach on the bending test, in the following analysis, we will study the effect of the size of the measurement zone and the effect of the position of the measurement zone, before studying the effect of noise and comparing to a macro mono-scale approach.

6.4.2.1 Effect of the size of the measurement zone

As for the above tension test example, firstly, it needs to illustrate that the proposed multi-scale formulation allows to perform the identification on a zone where the displacements are measured through DIC on a sub-part of the identification zone. Figure 6.10 shows various ratios of the size of the measurement zone to the global size, which is characterized by the ratio of its surface S_m to the global identification surface S_i: $\frac{S_m}{S_i}$.

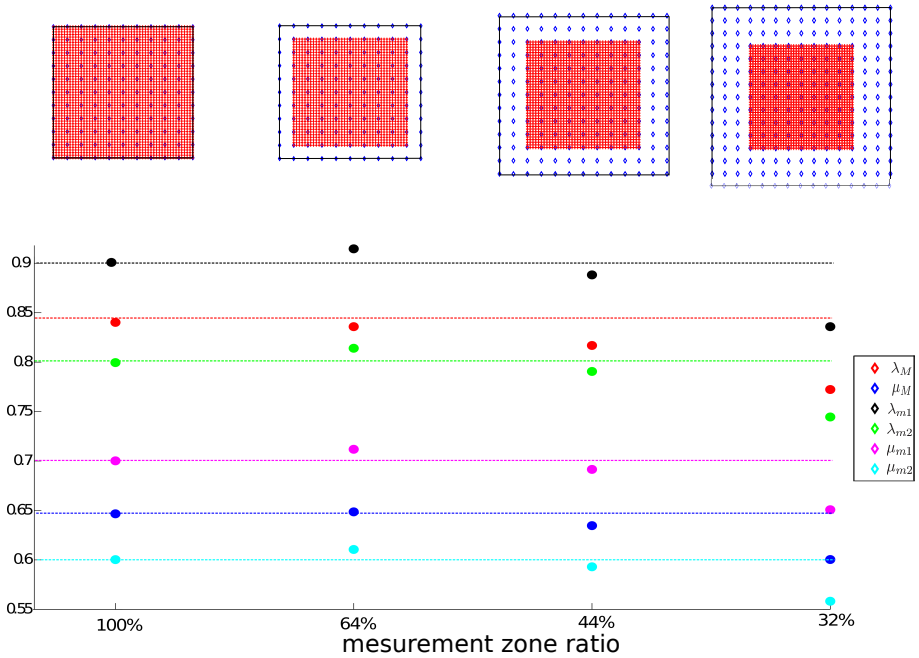

Figure 6.10: Comparison of identified θ_k for various measurement zone sizes on the bending test

	reference value	100%	64%	44%	33%
λ_M	0.8483	0.8402	0.8359	0.8168	0.7723
μ_M	0.6472	0.6466	0.6486	0.6347	0.6004
$\lambda_m 1$	0.9	0.9008	0.9146	0.8882	0.8359
$\lambda_m 2$	0.8	0.7995	0.814	0.7906	0.7445
$\mu_m 1$	0.7	0.7002	0.7119	0.6915	0.6508
$\mu_m 2$	0.6	0.6003	0.6106	0.5931	0.5582

Table 6.8: The identification results of macro and micro properties for various measurement zone sizes on the bending test

Figure 6.10 and Table 6.8 present the identification results for various measurement zone sizes. Obviously, until the ratio reduces to 44%, the multi-scale method is effective and the identification results are accurate. However, when ratio is smaller than 44%, the identification results lose accuracy. The reason is that measurement zone is far away from the boundary, and it loses too many information. The problem becomes ill-conditioned with a high condition number in the field of numerical analysis.

6.4.2.2 Effect of the position of the measurement zone

From the above analysis, we find that the size of the measurement zone will affect the identification results because of the quantity of available information. The next analysis is about the influence of the quality of available information. The examples

shown in Figure 6.11 are divided into two groups: 64% and 44% of measurement size, and every group has two different positions of the measurement zone: center and right.

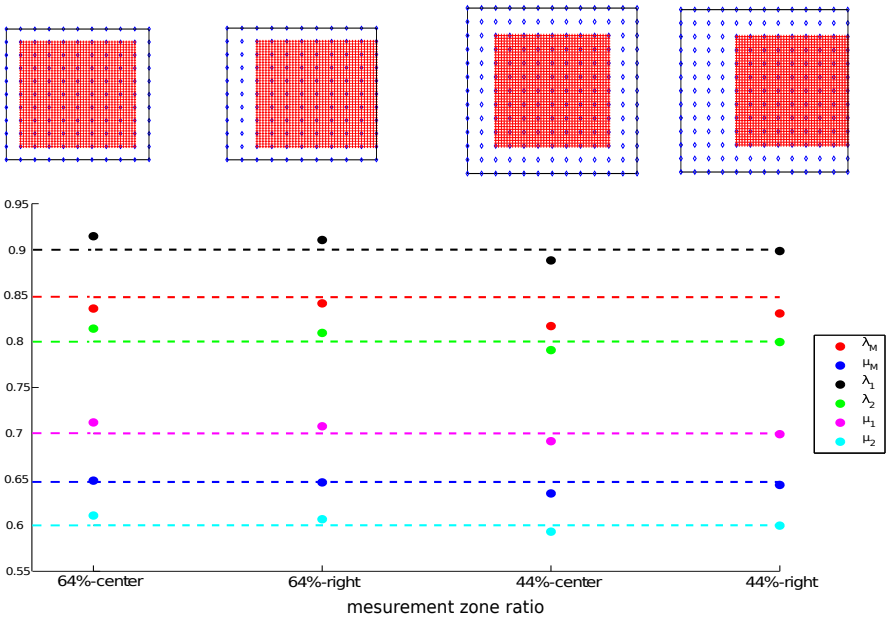

Figure 6.11: Comparison of identified θ_k for various measurement zone positions on the bending test

	reference value	64%-center	64%-right	44%-center	44%-right
λ_M	0.8483	0.8359	0.8415	0.8168	0.8305
μ_M	0.6472	0.6486	0.6467	0.6347	0.6439
$\lambda_m 1$	0.9	0.9146	0.9105	0.8882	0.8984
$\lambda_m 2$	0.8	0.814	0.8093	0.7906	0.7994
$\mu_m 1$	0.7	0.7119	0.7007	0.6915	0.6992
$\mu_m 2$	0.6	0.6106	0.6066	0.5931	0.5997

Table 6.9: The identification results of macro and micro properties for various measurement zone positions on the bending test

Figure 6.11 and Table 6.9 present the identification results for the two measurement zone positions. Obviously, the results are improved when the position is on the right side. From Figure 6.8(a) we can find that the load boundary is on the right side of the specimen, therefore, if the measurement zone cover the load boundary, it means that partial boundary condition information is close to the displacement information, hence their confrontation is emphasized. On the contrary, the center position will lose part of the experimental data confrontation. From the mono-scale identification examples, we know that load information is very important to identify

the heterogeneous properties. Consequently, improving the quality of information can help to improve the identification results.

6.4.2.3 Effect of noise

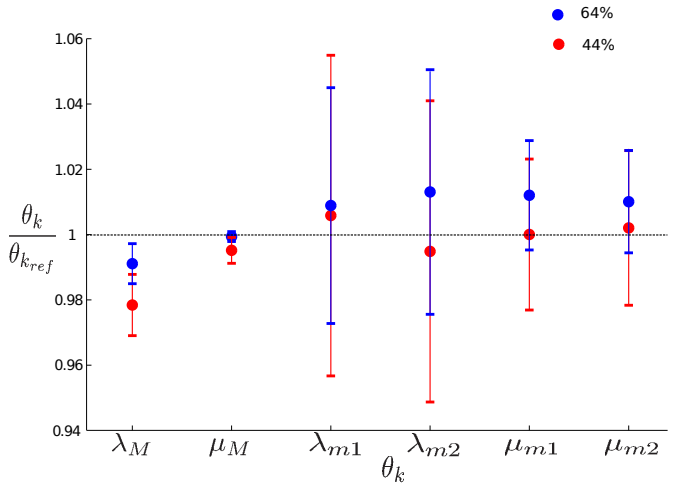

Figure 6.12: Comparison of identified $\frac{\theta_k}{\theta_{k_{ref}}}$ on 100 samples of 64% and 44% measurement zone sizes (mean value and standard deviation) with a 1% noise on the bending test

We choose two different ratios of the measurement size (64% and 44%) to analyze the effect of noise. Figure 6.12 shows the identification results on 100 samples with a 1% measurement noise for each ratio, in terms of mean value and standard deviation of the identified $\frac{\theta_k}{\theta_{ref}}$ properties. The first point to be noticed is that the multi-scale method can obtain reasonable identification results from perturbed measurement. Then, as could be expected, the identification results are more sensitive to the noise when the ratio of the measurement zone size to the global size reduces.

6.4.2.4 Mono-scale method for the macro problem

As for the tension test, we also compared the multi-scale approach to a macro mono-scale one using the operator Π_M to transfer the macro finite element field to the data grid for the macro basic problem. However, we keep the micro basic problem the same as the one in the multi-scale approach. Table 6.10 shows identified θ_k for various measurement zone sizes on the bending test with mono-scale method for the macro problem. The ratio of the size of the measurement zone to the global size is characterized by the ratio of its surface S_m to the global identification surface S_i: $\frac{S_m}{S_i}$.

	reference value	100%	64%	44%	33%
λ_M	0.8483	0.8441	0.8417	0.764	1.2
μ_M	0.6472	0.6476	0.6496	0.2972	0.9244
$\lambda_m 1$	0.9	0.902	0.841	1.2	1.2
$\lambda_m 2$	0.8	0.801	0.7287	1.2	1.2
$\mu_m 1$	0.7	0.7013	0.643	1.2	1.2
$\mu_m 2$	0.6	0.6011	0.5545	1.2	1.2

Table 6.10: The identification results of macro and micro properties for various measurement zone sizes on the bending test with mono-scale method for the macro problem

Contrary to the tension test, this method becomes ineffective for the bending test for ratios of size under 44%. It cannot identify the exact macro parameters, so that all the identified micro parameters equal to the setting Θ_{Ad} upper limit. It means that the transfer operator Π_M fails to transfer the displacement information when the stress conditions are more complex. It also means that the identification of homogeneous properties from data with micro information can lead to erroneous results if the multi-scale property is not taken into account properly. On the other hand, it shows that the multi-scale approach with displacement coupling is suitable for various loading experiments.

6.4.3 Example 8: with real material properties

In order to further verify the multi-scale identification approach, a calculation is performed representing a tensile test on a plate as sketched in Figure 6.1(a), but with real material properties values (not dimensionless ones as in previous examples). We choose a kind of carbon-epoxy composite with parameters shown in Table 6.11, noting that subscript f refers to the carbon fibres, and subscript m refers to the epoxy matrix.

E_f(GPa)	E_m(GPa)	ν_f	ν_m
350	3.5	0.2	0.35
λ_f(GPa)	λ_m(GPa)	μ_f(GPa)	μ_m(GPa)
73	1.4	145	1.3

Table 6.11: Real material properties of carbon-epoxy composite

Table 6.12 shows the identification results with real material properties. We find that the identified macro properties are close to those obtained by numerical homogenization: $\lambda_M^H = 26.2$GPa, $\mu_M^H = 16.5$GPa, and the identified micro properties

λ_M(GPa)	μ_M(GPa)	λ_f(GPa)	λ_m(GPa)	μ_f(GPa)	μ_m(GPa)
24.4416	14.56	73.7328	1.4014	144.706	1.2999

Table 6.12: Identification results for real material properties of carbon-epoxy composite on the tension test

are also close to the reference values. It further illustrates that the multi-scale approach can apply to real experiments.

6.5 Conclusion

In this chapter, we used two steps to validate the multi-scale approach. The first step was the identification of the macro properties alone, and the second step was the identification of both the macro and micro properties at the same time. We obtained the exact values of macro parameters which were validated by numerical homogenization, and accurate values of the micro parameters. Furthermore, the study of the measurement zone size effect and noise effect on the tension test illustrated the robustness of this multi-scale approach. Moreover, the extension to the heterogeneous elasticity was conducted to numerical examples of a bending test. Through the measurement zone size effect and position effect studies, we illustrated the importance of the quantity and quality of available information. And it was shown the multi-scale approach could yields more accurate results than a mono-scale one. Finally, the example with real material parameters shows that the multi-scale approach is applicable in real experiments.

Conclusions and Prospects

Contents

7.1 Conclusions

The work in this dissertation aims at identifying the heterogeneous elastic material parameters of composites from inhomogeneous static test and kinematics field measurements based on Digital Image Correlation. There are two central issues: one is the management of uncertainties of both experimental data and theoretical model; the other is the management of different scales between measurement and identification.

At first, a mono-scale approach based on the Modified Constitutive Relation Error has been proposed with different boundary conditions. There are two reasons to make this choice among all inverse approaches. Firstly, most of other approaches require all the boundary conditions of the studied domain. However, the information of boundary is not always reliable. It means that some will include noisy measurements as boundary condition, and others will introduce additional model errors with model assumptions. Secondly, the solutions of the other identification methods are often only on the measurement area, smaller than the actual size of the sample, which does not allow to take advantage of reliable information on the boundary. M-CRE can overcome these limitations by constructing a trade-off between all the available information, in a strong physical manner. M-CRE is also very flexible to deal with different kinds of boundary conditions depending on the case, which is applicable in the real industry analysis.

The first homogeneous numerical example showed that the calculation with M-CRE could be performed without some or all boundary condition, but it was still solved on the whole domain. However, by adding free edge information, the

identification results were significantly improved. And then on the illustrating heterogeneous example, it was shown that the method allowed the calculation with different kinds of boundary conditions and the taking into account of load-edge could yield the identification of heterogeneous parameters. Another comparison, taking into account the load condition as reliable information, showed that the identification results were better by presuming the load condition as a global load rather than a traction distribution. The reason was that the model error on the traction distribution would lead to wrong identification results. In order to decrease this model error and restore the balance, we could take into account the traction distribution as less reliable information and optimize the weighting coefficient of the distance to traction distribution.

For the second issue, a multi-scale identification strategy based on the M-CRE has been introduced, which permits to identify the global homogeneous properties of the whole specimen and also the local heterogeneous properties of the sub-part measurement zone. As for the mono-scale approach, the equations are split according to the reliability of information. The particularity is that the displacement measurement is only on the micro scale formulation, while the load boundary condition is only on the macro scale. In order to combine the stress and displacement fields at both the micro and macro scales, two coupling schemes have been proposed, one based on diffuse approximation and the other based on load. Two multi-scale algorithm are also proposed for the basic problem depending on the size of problem system.

Some numerical examples were used to validate this new multi-scale approach. There were two steps for validations, the first step was the identification of only the macro properties of the sample, and the second step was the identification of both the macro and micro properties at the same time. We obtained values of macro parameters in very good agreement with numerical homogenization, and the accurate values of micro parameters. Furthermore, the study of measurement zone size effect and noise effect illustrated the robustness of this multi-scale approach. Finally, the extension to the heterogeneous elasticity was conducted to numerical examples of a bending test.

7.2 Prospects

The methodology developed in this dissertation is very promising. In the future work, for short-term outlook, we should continue to adapt M-CRE to multi-scale identification in the case of composite plate: firstly, the coupling operators need to improve, especially for the zones near boundaries; secondly, the algorithm of

resolution needs to adapt with smaller measurement area, which means the solving of the basic problem should be further investigated in this framework; thirdly, the algorithm of minimization needs to improve in order to speed up the identification step; finally, the real experiment should be introduced to validate the methodology.

For long-term outlook, we should extend the application of M-CRE: studying the identification of anisotropic properties of composites with different orientation fibers; exploiting the images in the life cycle until rupture to identify the damage properties; attempting to model and locate the properties of complex materials and structures; extending to the identification on volume with the technique of tomography and 3D-DIC.

Reference

[1] D. Hull (1981) An introduction to composite materials. *Cambridge University Press*.

[2] W.P. De Wilde and H. Sol (1987) Anisotropic material identification using measured resonant frequencies of rectangular composite plates. *Composite Structures 4*, 317-324.

[3] R.M. Jones (1975) Mechanics of composite materials. *McGraw-Hill*, New York.

[4] J.E. Ashton, J.C. Halpin and P.H. Petit (1969) Primer on composite materials: Analysis. *Technomic*, Westport, Connecticut.

[5] M. Grédiac (2004) The use of full-field measurement methods in composite material characterization: interest and limitations. *Composites Part A: applied science and manufacturing*, vol.35(7-8), 751-761.

[6] J.C. Dainty (1984) Laser speckle and related phenomenon. *Berlin: Springer*.

[7] J.S. Sirkis (1990) System response to automated grid method. *Optical Engineering*, vol.29(12), 1485-1493.

[8] M.A. Sutton, W.J. Wolters, W.H. Peters, W.F. Ranson and S.R. Mcneill (1983) Determination of displacements using an improved digital correlation method. *Image and Vision Computing*, vol.1(3), 133-139.

[9] J.A. Leendertz (1970) Interferometric displacement measurement on scattering surface utilizing speckle effect. *Journal of Physics E: Scientific Instruments*, vol.3(3), 214-218.

[10] D. Post, B. Han and P. Ifju (1994) High sensitivity moiré: experimental analysis for mechanics and materials. *Berlin: Springer*.

[11] C. Joenathan (1997) Speckle photography, shearography and ESPI. *Optical measurement techniques and applications*, vol.6, 151-182.

[12] V. Parks (1990) Strain measurement using grids. *Optical Engineering*, vol.21(4), 663-669.

[13] B. Zhao and A. Asundi (2001) Microsopic grid methods-resolution and sensitivity. *Optics and Lasers in Engineering*, vol.36, 437-450.

[14] R. Jones and C. Wykes (1989) Holographic and Speckle Interferometry. *Cambridge University Press.*

[15] J. Molimard and Y. Surrel (2013) Grid Method, Moiré and Deflectometry. *Full-Field Measurements and Identification in Solid Mechanics*, chapter 3, 62-91.

[16] A. Asundi, M.T. Cheung and C.S. Lee (1989) Moiré interferometry for simultaneous measurement of u,v,w. *Experimental Mechanics*, vol.29, 258-260.

[17] T.C. Chu, W.F. Ranson, M.A. Sutton and W.H. Petters (1985) Application of digital image correlation techniques to experimental mechanics. *Experimental Mechanics*, vol.3, 232-244.

[18] B.D. Lucas and T. Kanade (1981) An iterative image registration technique with an application to stereo vision. *Proceedings of the 7th International Joint Conference on Artificial Intelligence, IJCAI'81*, vol.2, San Francisco, CA, USA, 674-679.

[19] P.J. Burt, C. Yen and X. Xu (1982) Local correlation measures for motion analysis: a comparative study. *Proceedings of the IEEE Conference on Pattern Recognition and Image Processing*, Las Vegas, NV, USA, 269-274.

[20] W.H. Peter and W.F. Ranson (1982) Digital imaging techniques in experimental stress analysis. *Optical Engineering*, vol.21, 427-432.

[21] H.A. Bruck, S.R. McNeill and W.H. Peters (1989) Digital image correlation using Newton-Raphson method of partial differential correction. *Experimental Mechanics*, vol.29(3), 261-267.

[22] D.J. Chen, F.P. Chiang, Y.S. Tan and H.S. Don (1993) Digital speckle-displacement measurement using a complex spectrum method. *Applied Optics*, vol.32(11), 1839-1849.

[23] F. Hild (2002) CORRELI^{LMT}: A software for displacement field measurements by digital image correlation. *Technical Report 254*, Laboratoire de Mécanique et Technologie, Cachan.

[24] P.F. Luo, Y.J. Chao, M.A. Sutton and W.H. Peters (1993) Accurate measurement of three-dimensional deformations in deformable and rigid bodies using computer vision. *Experimental Mechanics*, vol.33(2), 123-132.

[25] J.D. Helm, S.R. McNeill and M.A. Sutton (1996) Improved 3-D Image Correlation for Surface Displacement Measurement. *Optical Engineering*, vol.35(7), 1911-1920.

[26] B.K. Bay, T.S. Smith, D.P. Fyhrie and M. Saad (1999) Digital volume correlation: Three-dimensional strain mapping using X-ray tomography. *Optical Engineering*, vol.39(3), 217-226.

[27] P. Doumalin and M. Bornert (2000) Micromechanical applications of digital image correlation techniques. *Interferometry in Speckle Light: Theory and Applications*, 67-74.

[28] I. Chasiotis and W.G. Knauss (2002) A new microtensile tester for the study of MEMS materials with the aid of atomic force microscopy. *Experimental Mechanics*, vol.42, 51-57.

[29] J.D. Helm, M.A. Sutton and M.L. Boone (2001) Characterizing Crack Growth in Thin Aluminum Panels Under Tension-Torsion Loading with Three-Dimensional Digital Image Correlation. *Nontraditional Methods of Sensing Stress, Strain and Damage in Materials and Structures, ASTM STP*, 1323, 3-14.

[30] B.K. Bay (2008) Methods and applications of digital volume correlation. *Journal of Strain Analysis for Engineering Design*, vol.43(8), 745-760.

[31] M.A. Sutton (2014) Image-based Measurements in Solid Mechanics: A Brief History, Static and Dynamic Application Examples and Recent Developments. *BSSM 50th Anniversary.*

[32] M. Bonnet, F. Hild, J.J. Orteu and S. Roux (2013) Digital Image Correlation. *Full-field Measurements and Identification in Solid Mechanics*, chapter 6, 158-190.

[33] M.A. Sutton, F. Hild (2015) Recent Advances and Perspectives in Digital Image Correlation. *Experimental Mechanics*, vol.55, 1-8.

[34] G.M. Hassan (2014) A Comparative Study of Techniques of Distant Reconstruction of Displacement Fields by using DISTRESS Simulator. *arXiv:1411.3423 [cs.CV]*.

[35] J. Réthoré, F. Hild, S. Roux (2008) Extended digital image correlation with crack shape optimization. *International Journal for Numerical Methods in Engineering*, vol.73, 248-274.

[36] M. Bonnet (2013) Introduction to identification methods. *Full-field Measurements and Identification in Solid Mechanics*, chapter 8, 223-246.

[37] J. Hadamard (1902) Sur les problèmes aux dŕivées partielles et leur signification physique. *Princeton University Bulletin*, 49-52.

[38] M. Ben Azzouna (2013) Identification à partir de mesures de champs application de l'erreur en relation de comportement modifiée. *Thèse de doctorat.*

[39] H.W. Engl, M. Hanke and A. Neubauer (1996) Regularization of Inverse Problems. *Netherlands: Springer.*

[40] A. Tarantola (2005) Inverse problem theory and model parameter estimation. *Society for Industrial and Applied Mathematics.*

[41] A.N. Tikhonov (1963) Solution of incorrectly formulated problems and the regularization method. *Dokl. Akad. Nauk. SSSR* vol.151(3), 501-504.

[42] S. Avril, M. Bonnet, A.S. Bretelle and others (2008) Overview of identification methods of mechanical parameters based on full-field measurements. *Experimental Mechanics*, vol.48(4), 381-402.

[43] M. Grédiac (1989) Principe des travaux virtuels et identification/ Principle of virtual work and identification. *Comptes Rendus de l'Académie des Sciences*, vol.309, 1-5, In French with abridged English version.

[44] H.D. Bui (1993) Introduction aux problèmes inverse en mécanique des matériaux. *Ed. Eyrolles.*

[45] J. Collins, G. Hart and B. Kennedy (1974) Statistical identification of structures. *AIAA Journal*, vol.12(2), 185-190.

[46] D. Claire, F. Hild and S. Roux (2002) Identification of damage fields using kinematic measurements. *Comptes Rendus Mécanique*, vol.330(11), 729-734.

[47] P. Ladevèze and D. Leguillon (1983) Error estimate procedure in the finite element method and applications. *SIAM Journal on Numerical Analysis*, vol.20, 485-509.

[48] M. Grédiac, F. Pierron and A. Vautrin (1994) The Iosipescu in-plane shear test applied to composites: A new approach based on displacement field processing. *Composites Science and Technology*, vol.51, 409-417.

[49] M. Grédiac, F. Pierron and Y. Surrel (1999) Novel procedure for complete in-plane composite characterization using a T-shaped specimen. *Experimental Mechanics* , vol.39(2), 142-149.

[50] F. Pierron, S. Zhavaronok and M. Grédiac (2000) Identification of the through-thickness properties of thick laminates using the virtual fields method. *International Journal of Solids and Structures*, vol.37(32), 4437-4453.

[51] H. Chalal, S. Avril, F. Pierron and F. Meraghni (2006) Experimental identification of a nonlinear model for composites using the grid technique coupled to the virtual fields method. *Composites Part A: Applied Science and Manufacturing*, vol.37(2), 315-325.

[52] J.H. Kim, F. Pierron, M. Wisnom and K. Syed-Muhamad (2007) Identification of the local stiffness reduction of a damaged composites plate using the virtual fields method. *Composites Part A: Applied Science and Manufacturing*, vol.38(9), 2065-2075.

[53] S. Avril and F. Pierron (2007) General framework for the identification of constitutive parameters from full-field measurements in linear elasticity. *International Journal of Solids and Structures*, vol.44, 4978-5002.

[54] S. Andrieux, H.D. BUI and A. Constantinescu (2013) Reciprocity Gap Method. *Full-field Measurements and Identification in Solid Mechanics*, chapter 13, 363-378.

[55] S. Andrieux and A. Ben Abda (1996) Identification of planar cracks by complete overdetermined data: inversion formulae. *Inverse Problems*, vol.12, 553-563.

[56] T. Bannour, A. Ben Abda and M. Jaoua (1999) Identification of 2D cracks by elastic boundary measurements. *Inverse Problems*, vol.15(1), 67-77.

[57] H.D. Bui, A. Constantinescu and H. Maigre (2004) Numerical identification of planar cracks in elastodynamics using the instantaneous reciprocity gap. *Inverse Problems*, vol.20, 993-1001.

[58] S. Andrieux and H.D. Bui (2006) Écart à la réciprocité et identification de fissures en thermo-élasticité isotrope transitoire. *Comptes Rendus de l'Académie des Sciences (Série I)*, vol.334(4), 225-229.

[59] H.D. Bui, S. Chaillat, A. Constantinescu and E. Grasso (2010) Identification of a planar crack in Zener type viscoelasticity. *Annals of Solid and Structural Mechanics*, vol.1, 3-8.

[60] K. Bathe (1996) Finite element procedures. *Prentice Hall.*

[61] K.T. Kavanagh and R.W. Clough (1971) Finite element applications in the characterization of elastic solids. *International Journal of Solids and Structures*, vol.7, 11-23.

[62] E. Pagnacco, A.S. Caro-Bretelle and P. Ienny (2013) Parameter identification from mechanical field measurements using finite element model updating strategies. *Full-field Measurements and Identification in Solid Mechanics*, chapter 9, 247-274.

[63] B. Rahmani, F. Mortazavi, I. Villemure and M. Levesque (2013) A new approach to inverse identification of mechanical properties of composite materials: Regularized model updating. *Composite Structures*, vol.105, 116-125.

[64] K. Genovese, L. Lamberti and C. Pappalettere (2005) Improved global-local simulated annealing formulation for solving non-smooth engineering optimization problems. *International Journal of Solids and Structures*, vol.42(1), 203-237.

[65] D. Lecompte, A. Smits, H. Sol, J. Vantomme and D. Van Hemelrijck (2007) Mixed numerical-experimental technique for orthotropic parameter identification using biaxial tensile tests on cruciform specimens. *International Journal of Solids and Structures*, vol.44(5), 1643-1656.

[66] Y.L. Kang, X.H. Lin and Q.H. Qin (2004) Inverse/genetic method and its application in identification of mechanical parameters of interface in composite. *Composite Structures*, vol.66(1-4), 449-458.

[67] J. Wang, Q.H. Qin Y.L. Kang, X.Q Li and Q.Q Rong (2010) Viscoelastic adhesive interfacial model and experimental characterization for interfacial parameters. *Mechanics of Materials*, vol.42(5), 537-4547.

[68] M. Anghileri, E. Chirwa, L. Lanzi and F. Mentuccia (2005) An inverse approach to identify the constitutive model parameters for crashworthiness modelling of composite structures. *Composite Structures*, vol.68(1), 65-74.

[69] P. Sztefek and R. Olsson (2008) Tensile stiffness distribution in impacted composite laminates determined by an inverse method. *Composites Part A: applied science and manufacturing*, vol.39(8), 1282-1293.

[70] P. Sztefek and R. Olsson (2009) Nonlinear compressive stiffness in impacted composite laminates determined by an inverse method. *Composites Part A: applied science and manufacturing*, vol.40(3), 260-272.

[71] H. Leclerc, J.N. Périé, S. Roux and F. Hild (2009) Integrated Digital Image Correlation for the Identification of Mechanical Properties. *Computer Vision/Computer Graphics Collaboration Techniques Volume 5496 of the series Lecture Notes in Computer Science*, 161-171.

[72] M. Ben Azzouna, J.N. Périé, J.M. Guimard, F. Hild and S. Roux (2011) On the identification and validation of an anisotropic damage model using full-field measurement. *International Journal for Damage Mechanics*,vol.20(8), 1130-1150.

[73] D. Claire, F. Hild and S. Roux (2004) A finite element formulation to identify damage fields: the equilibrium gap method. *International Journal for Numerical Methods in Engineering*, vol.61(2), 189-208.

[74] D. Claire, F. Hild and S. Roux (2007) Identification of a Damage Law by Using Full-Field Displacement Measurements. *International Journal for Damage Mechanics*, vol.16(2), 179-197.

[75] S. Roux and F. Hild (2008) digital image mechanical identification (DIMI). *Experimental Mechanics*,vol.48(4), 495-508.

[76] L. Crouzeix, J.N. Périé, F. Collombet and B. Douchin (2009) An orthotropic variant of the equilibrium gap method applied to the analysis of a biaxial test on a composite material. *Composites Part A: applied science and manufacturing*, vol.40(11), 1732-1740.

[77] J.N. Périé, H. Leclerc, S. Roux and F. Hild (2009) Digital image correlation and biaxial test on composite material for anisotropic damage law identification. *International Journal of Solids and Structures*, vol.46, 2388-2396.

[78] R. Kohn and M. Vogelius (1984) Determining conductivity by boundary measurements. *Communications on Pure and Applied Mathematics*, vol.37, 289-298.

[79] M. Reynier (1990) Sur le contrôle de modélisations éléments finis: recalage à partir d'essais dynamiques. *PhD Thesis*, UPMC, Paris.

[80] P. Ladevèze, M. Reynier and N.Maya (1994) Error on the constitutive relation in dynamics. *Inverse problems in Engineering*, 251-256.

[81] A. Chouaki, P. Ladevèze and L. Proslier (1998) Updating structural dynamic model with emphasis on the damping properties. *AIAA journal*, vol.36(6), 1094-1099.

[82] A. Deraemaeker, P. Ladevèze and Ph. Leconte (2002) Reduced bases for model updating in structural dynamics based on constitutive relation error. *Computer Methods in Applied Mechanics and Engineering*, vol.191(21-22), 2427-2444.

[83] G. Geymonat, F. Hild and S. Pagano (2002) Identification of elastic parameters by displacement field measurement. *Comptes Rendus Mécanique*, vol.330, 403-408.

[84] S. Calloch, D. Dureisseix and F. Hild (2002) Identification de modèles de comportement de matériaux solides: utilisation d'essais et de calculs. *Technologies et Formations*, vol.100, 36-41.

[85] F. Latourte (2007) Identification des paramètres d'une loi élastoplastique de Prager et calcul de champs de contraintes dans des matériaux hétérogénes. *Thèse de doctorat*, Université de Montpellier.

[86] E. Florentin and G. Lubineau (2010) Identification of the parameters of an elastic material model using the constitutive equation gap method. *Computer Methods in Applied Mechanics and Engineering*, vol.196, 1968-1983.

[87] S. Pagano and M. Bonnet (2013) Constitutive Equation Gap. *Full-field Measurements and Identification in Solid Mechanics*, chapter 10, 275-300.

[88] P. Feissel and O. Allix (2007) Modified constitutive relation error identification strategy for transient dynamics with corrupted data: The elastic case. *Computer Methods in Applied Mechanics and Engineering*, vol.196, 1968-1983.

[89] P. Ladevèze, G. Puel, A. Deraemaeker and T. Romeuf (2006) Validation of structural dynamics models containing uncertainties, *Computer Methods in Applied Mechanics and Engineering*, vol.195, 373-393.

[90] O. Allix, P. Feissel and P. Thévenet (2003) A delay damage mesomodel of laminates under dynamic loading: basic aspects and identification issues. *Computers and Structures*, vol.81, 1177-1191.

[91] H.M. Nguyen, O. Allix and P. Feissel (2008) A robust identification strategy for rate-dependent models in dynamics. *Inverse Problems*, vol.24, 065006.

[92] B. Banerjee, T.F. Walsh, W. Aquino and M. Bonnet (2012) Large scale parameter estimation problems in frequency-domain elastodynamics using an error in constitutive equation functional. *Computer Methods in Applied Mechanics and Engineering*, vol.253, 60-72.

[93] G. Geymonat, F. Hild and S. Pagano (2002) Identification of elastic parameters by displacement field measurement. *Comptes-Rendus Mécanique*, vol.330(6), 403-408.

[94] M. Ben Azzouna, P. Feissel and P. Villon (2015) Robust identification of elastic properties using the Modified Constitutive Relation Error. *Computer Methods in Applied Mechanics and Engineering*, vol.295, 196-218.

[95] W. E, B. Engquist, X. Li, W. Ren and E. Vanden-Eijnden (2007) Heterogeneous multiscale methods: a review. *Communications in Computational Physics*, vol.2(3), 367-450.

[96] A. Brandt (1977) Multi-level adaptive solutions to boundary value problems. *Mathematics of Computation*, vol.31(138), 333-390.

[97] A. Quarteroni and A. Valli (1999) Domain Decomposition Methods for partial differential equations. *Oxford Science Publications.*

[98] I. Daubechies (1992) Ten lectures on Wavelets, CBMS-NSF Regional Conference Series in Applied Mathematics. *SIAM Publications.*

[99] M. Ainsworth and J.T. Oden (2000) A posteriori error estimation in finite element analysis. *Wiley-Interscience*, New York.

[100] L. Greengard and V. Rokhlin (1987) A fast algorithm for particle simulations. *Journal of Computational Physics*, vol.135(2), 280-292.

[101] G.H. Golub and C.F. Van Loan (1983) Matrix computation. *The Johns Hopkins University Press*, Baltimore, Maryland.

[102] R. Car and M. Parrinello (1985) Unified approach for molecular dynamics and density-functional theory. *Physical Review Letters*, vol.55(22), 2471-2474.

[103] E.B. Tadmor, M. Ortiz and R. Phillips (1996) Quasicontinuum analysis of defects in crystals. *Philosophical Magazine A*, vol.73(6), 1529-1563.

[104] A.J. Chorin, O.H. Hald and R. Kupferman (2002) Optimal prediction with memory. *Physica D*, vol.166, 239-257.

[105] W. E and B. Engquist (2003) The heterogeneous multi-scale methods. *Communications in Mathematical Sciences*, vol.1(1), 87-132.

[106] I.G. Kevrekidis, C.W. Gear J.M. Hyman, P.G. Kevrekidis, O. Runborg and C. Theodoropoulos (2003) Equation-free, coarse-grained multiscale computation: Enabling microscopic simulators to perform system-level analysis. *Communications in Mathematical Sciences*, vol.1(4), 715-762.

[107] A.L. Garcia, J.B. Bell, W.Y. Crutchfield and B.J. Alder (1999) Adaptive mesh and algorithm refinement using direct simulation Monte Carlo. *Journal of Computational Physics*, vol.154, 134-155.

[108] F. Feyel, J. Chaboche (2000) FE^2 multiscale approach for modelling the elastoviscoplastic behaviour of long fibre SiC/Ti composite materials. *Computer Methods in Applied Mechanics and Engineering*, vol.183, 309âĂŞ330.

[109] J.Q. Broughton, F.F. Abraham, N. Bernstein and E. Kaxiras (1999) Concurrent coupling of length scales: Methodology and application. *Physical Review B*, vol.60(4), 2391-2402.

[110] J. Rannou, N. Limodin, J. Rethore, A. Gravouil, W. Ludwig, M.C. Baietto-Dubourg, J.Y. Buffière, A. Combescure, F. Hild and S. Roux (2010) Three dimensional experimental and numerical multiscale analysis of a fatigue crack. *Computer Methods in Applied Mechanics and Engineering*, vol.199, 1307-1325.

[111] J.C. Passieux, F. Bugarin, C. David, J.-N. Périé and L. Robert (2015) Multiscale displacement field measurement using digital image correlation: Application to the identification of elastic properties. *Experimental Mechanics*, vol.55(1), 121-137.

[112] C.G. Broyden (1970) The convergence of a class of double-rank minimization algorithms. *Journal of the Institute of Mathematics and its Applications*, vol.6, 76-90.

[113] R. Fletcher (1970) A new approach to variable metric algorithms. *The Computer Journa*, vol.13(3), 317-322.

[114] D. Goldfarb (1970) Family of variable-metric derived by variational means. *Mathematics of Computation*, vol.24, 23-26.

[115] D.F. Shanno (1970) Conditioning of quasi-newton methods for function minimization. *Mathematics of Computation*, vol.24(111), 647-656.

[116] K. Svanberg (1987) The method of moving asymptotes - A new method for structural optimization. *International Journal for Numerical Methods in Engineering*, vol.24, 359-373.

[117] C. Zillober (1993) A globally convergent version of the method of moving asymptotes. *Structural Optimization*, vol.6(3), 166-174.

[118] Q. Ni (2003) A globally convergent method of moving asymptotes with trust region technique. *Optimization Methods and Software*, vol.18, 283-297.

[119] K. Miller (1970) Least squares methods for ill-posed problems with a prescribed bound. *SIAM Journal on Mathematical Analysis*, vol.1, 52-74.

[120] B. Nayroles, G. Touzot and P. Villon. (1992) Generalizing the finite element method: Diffuse approximation and diffuse elements. *Computational Mechanics*, vol.10, 307-318.

[121] P. Breitkopf, H. Naceur, A. Rassineux and P. Villon. (2005) Moving least squares response surface approximation: formulation and metal forming applications. *Computers and Structures*, vol.83(17-18), 1411-1428.

[122] D. Brancherie, P. Villon and A. Ibrahimbegovic. (2008) On a consistent field transfer in non linear inelastic analysis and ultimate load computation. *Computational Mechanics*, vol.42(2), 213-226.

[123] S. Avril, P. Feissel, F. Pierron and P. Villon. (2010) Comparison of two approaches for differentiating full-field data in solid mechanics. *Measurement Science & Technology*. vol.21(1), pp.015703.

[124] A. Zaoui. (1998) Matériaux hétérogènes et composites. École Polytechnique.